Università degli Studi di Cagliari

PHD DEGREE

International PhD in Innovation Science and Technology:

Methods and Systems for Environmental Protection

Cycle XXXI

TITLE OF THE PHD THESIS

On the Prediction of Swash Excursion and the Role of Seagrass Beach-cast Litter: Modelling and Observations

Scientific Disciplinary Sectors

GEO/04 GEO/12

PhD Student:	Marinella Passarella
Coordinator of the PhD Programme	Prof. Roberto Orrù
Supervisor	Prof. Sandro De Muro

Final exam. Academic Year 2017 – 2018
Thesis defence: January-February 2019 Session

To my parents, Tanja and my dearest friends which with their comprehension, support and love made all this possible...

The limits between what is possible and what is not are only located in our mind. They are inversely proportional to the time, dedication and passion we put to overcome them...

ABSTRACT

Criticality in coastal management and environmental protection is intensified by coastal hazards and climate changes which nowadays should not be ignored. Due to ongoing sea level rise and the increase in the severity of wave storms, knowing in advance the effects of storms and human impacts at the coasts becomes fundamental for management and environmental protection purposes. This research deals with the wave runup and swash on the beach which, representing the final expression of wave action at the coast, are often included into hazards management, prediction and mitigation frameworks. Existing swash parametrizations are tested against worldwide-collected field datasets showing that still large errors in wave runup prediction could be made. The original contribution of this work consists of coastal processes knowledge enhancement, providing four new swash predictors: 2 for total and 2 for infragravity swash. Moreover, the innovative machine learning approach adopted (genetic programming) can replicate the functionality and dependencies of previously published formulas, improving predictability (compared to well-established parametrizations derived by classical regression approaches) and providing physical insight into coastal processes. The beach slope emerged as an important parameter when predicting infragravity swash, contributing to clarify the existing discussion in the literature. Novelty in this research also consists of field measurements of wave swash and runup with the presence of seagrass (*Posidonia oceanica*) litter on the beach face and berm. Measurements are performed through an ad-hoc installed easily-reproducible coastal video monitoring station, from which the interaction between wave swash and seagrass berm is studied. Results show that runup process is shifted offshore due to seagrass wrack accumulation and that the swash energy is shifted towards higher frequencies, with the swash peak frequency being located within the incident band, in contrast with a nearby seagrass-free profile under the same wave forcing condition. This behaviour is probably due to the beach slope made steeper by the seagrass beach-cast accumulations. The findings of this research involve implications for coastal protection and management (e.g. seagrass deposits role on coastal protection), hazards mitigation and prediction (e.g. inundation).

ACKNOWLEDGEMENTS

I express my sincere thanks to **my tutor Prof. Sandro De Muro**, Director of the Coastal and Marine Geomorphology Group (CMGG) of the University of Cagliari for his support. I wish to extend my thank to him for believing in me, providing me with resources, funding, infrastructures and instrumentation. Thanks to his effort, availability and planning necessary for executing the field campaigns.

With immense pleasure and a deep sense of gratitude, I wish to express my sincere thanks to **my mentor Prof. Giovanni Coco**, that accepting to support me, resulted in an essential presence for this PhD research. His help in planning, elaborating and coordinating the work, deeply helped me. My thanks are extended in particular to his availability to host me at the University of Auckland where I had the opportunity to learn theory and analysis techniques essential for this PhD thesis. But greatly more important my thanks to him is devoted to having taught me the real deep sense of research. Research which is based primarily on the respect of the individual persons. Research, that exists thanks to the curiosity and passion of people and it is based on collaborations and networking. Thanks for supporting, encouraging, and pushing me to overcome my limits, always and continuously with deep respect.

I am grateful to **my colleagues** of the CMGG, for welcoming and motivating me to carry out this research and also for providing me with infrastructural, facilities and many other resources needed for my work. Thanks to **Angelo Ibba, Dr. Andrea Ruju, Dr. Carla Buosi, Dr. Nicola Pusceddu, Dr. Paolo Frongia, Marco Porta, Dr. Walter Brambilla**. Their daily availability, moral support and suggestions were of great importance and support in several ways throughout my research work. Thanks to Dr. Carla Buosi for her continuous positive encouragement, moral and technical support and her help during the field campaigns. Thanks to Dr. Nicola Pusceddu and Dr. Paolo Frongia for the moral and practical guidance during the preliminary case studies and the fieldwork. Thanks to Marco Porta for his kind availability and collaboration during the planning of the coastal video-monitoring station and for the preliminary case-studies. Thanks to Angelo Ibba for his comprehensive and continuous support and availability. Thanks to Dr. Walter Brambilla for his encouragement, help for the coastal-video monitoring system planning and infrastructure, as well as for his support in geo-

referencing the field data.

Thanks to **Dr. Andrea Ruju**, dear friend and colleague for his help, supervision and support both moral and technical during this research. Thanks to his contribution for part of the data collection and analysis performed in Chapter 6. Without his assistance, this work would not have been the same.

I am grateful to Sardinia Regional Government for the financial support of my PhD scholarship (P.O.R. Sardegna F.S.E. Operational Programme of the Autonomous Region of Sardinia, European Social Fund 2007-2013 Axis IV Human Resources, Objective l.3, Line of Activity l.3.1.), essential to carry out this research activity.

I acknowledge the support and funding rendered by the **NEPTUNE Project**, (Natural Erosion Prevision Through Use of Numerical Environment) L. R. 7.08.2007, N.7: Promozione della ricerca scientifica in Sardegna e dell'Innovazione tecnologica in Sardegna. The support derived by this project allowed the field data-collection campaigns at sea and contributed to my visiting period at the University of Auckland.

I gratefully acknowledges the funding "**GLOBUSDOC** international placement programme" of the University of Cagliari, which allowed my visiting period at the University of Auckland.

With a sense of gratitude I acknowledge the **Marina Militare**, the **ASL 8 Cagliari** and **Gabriele Nardone** engineer of **ISPRA** institution, for their availability in providing me with infrastructural support and the data shared.

I am grateful to **Dr. Evan B. Goldstein** for his suggestions on Machine Learning analysis and to **Prof. Karin Bryan** for her support for coding the image georectification process. I would like to thank **Dr. Umberto Andriolo** for his availability and suggestions about the planning of the video-monitoring station.

Last but not the least, I wish to extend my profound sense of gratitude to **my parents**, my whole **family** and **Tanja** for providing me with their constant encouragement and moral support along with patience and understanding. Thanks to my dearest **friends** for expressing kind words of support and encouragement in the past three years whenever required.

Place: Cagliari

Date: submitted 14/09/2018, reviewed 28/01/2019 **MARINELLA PASSARELLA**

Contents

List of Figures

List of Tables

Chapter 1

INTRODUCTION

Coastal areas host several different type of activities which can be grouped into sectors: defence and national security, marine renewable energy, ports and shipping, marine aggregates and dredging, cabling, fisheries and aquaculture, wastewater disposal, tourism and recreation, marine resource extraction. Those sectors exploite marine areas nearby the coast, and conflicts between them exist introducing potential cumulative impact on the environment, even if a marine conservation sector exists (e.g. marine protected areas and parks).

The complexity of managing coastal areas requires specific marine planning and strategy. The Organisation for Economic Co-operation and Development (OECD), reports in a recent issue paper, that Marine Spatial Planning (MSP) is fundamental for the European integrated maritime policy EU (2007). Furthermore, it could contribute to achieve a good environmental status (EPC, 2008), and the blue growth strategy (EU, 2012) for European Countries (Stephen, 2017). UNESCO (2018) reports that marine spatial planning is the object of projects, discussion and implementation in over 60 countries around the world. It is required to all European members states by 2021 (by the Marine Spatial Planning Directive, adopted in 2014, (EU, 2014)) to set up a national marine spatial plan, but not all the European countries have adopted one yet (e.g. Italy only has regional pilot projects).

Furthermore, following the Climate and Energy Packages targets, the strategy denominated "Blue Growth" (EU, 2012) to enhance the "blue" economy (which has a value of about €500 billion a year and assure roughly 5.4 million jobs), was set in Europe in 2012 (EU, 2012). The Blue Growth is centred on the exploitation of marine resources, rising from one hand the attention of policymakers and investors on coastal areas, but on the other hand, potentially incrementing the impact of human activities on the coasts. Results from this work can have useful applicability to marine environmental protection and strategic coastal planning as required urgently worldwide and specifically in Europe.

Environmental protection is strictly related to coastal management, and criticality in those fields is enhanced by coastal hazards, and climate changes which nowadays should not be ignored.

The last Intergovernmental Panel on Climate Change (IPCC) reports, released in 2013-2014, summarizes the impacts, adaptation, vulnerability and mitigation related to CC, starting from the review of the relevant scientific literature. Compared with previously released IPCC's reports (in 2007) the evidence of the influence of human actions on climate changes has risen (IPCC, 2014). This influence is principally related to anthropic CO_2 emissions, the warming of the ocean and atmosphere, in resulting decrease of ice cover, global mean sea level rise, ocean acidification, habitats and marine ecosystems impact, as well as the water cycle changes (IPCC, 2014).

Special attention is given to coastal systems (Wong et al., 2014), oceans (Hoegh-Guldberg et al., 2014; Rhein et al., 2013), sea level rise (Church et al., 2014) and small islands (Nurse et al., 2014), since the ocean has a fundamental role in regulating the global climate and effects of CC are particularly appreciable at coasts. The Ocean acts as a buffer to CC thanks to its capacity of heat storage immensely higher than the atmosphere about 93% of the energy excess due to human activities is absorbed by the oceans, 3% by the continents and only 1% by the atmosphere (Rhein et al., 2013). Moreover the ocean naturally "recycles" CO_2 through four ocean 'carbon pumps' (Solubility, Biological, Continental Shelf and Carbonate Counter) and stores carbon to the deep ocean reservoir (Reid et al., 2009). At coast consequences of CC (as rising severity of the storms, change in wave climate and storm surge, sea level rise) are translated often into natural hazards as coastal erosion, flooding and they strongly influence coastal processes and morphodynamics.

A parameter often used to assess the effect of storms on the coast and to predict when the sea will potentially reach a certain high and extension towards the coast, is the wave runup. Wave runup, the wave generated vertical excursion of water up a beach slope, is the final expression of processes acting within three connected coastal zones as waves travel from deep to shallow waters: 1) the shoreface, where wave transformation towards the coast occurs; 2) the surf zone, where most of the energy is released by breaking of the waves; and 3) the swash zone, where the water edge runup (uprush) and down (backwash) on the beach face. Wave runup is composed by the swash (vertical water oscillation) and the setup (temporal mean of swash oscillation). Swash calculations have two components: one due to the incident and the other to the infragravity (wave period, T $>$ 20 s) waves (Guza and Thornton, 1982; Komar, 1998).

Understanding runup and its constitutive components is necessary for comprehending the impacts of coastal hazards, managing the coasts and improving the knowledge of swash zone hydrodynamics and sediment transport. Runup is also demonstrated to contribute to about 60% of the total water level in extreme conditions (Serafin and Ruggiero, 2014). The action of extreme runup during storms can reach the dunes, contributing to natural erosion processes (Komar, 1998; Ruggiero et al., 2001), and flooding be-

hind them, extending the water edge to inhabited areas. In regards to coastal hazards, in the last two centuries, humans extended their activities and settling towards the coast, rising human impact and vulnerability of the coast itself (Nordstrom, 2013). Several strategies are proposed to mitigate coastal hazards, including managed retreat strategies (accommodating natural processes), or building of rigid structures (impacting, however, the natural coastal processes). To precisely understand and predict wave runup can contribute to improving mitigation and adaptation strategies. For instance, runup is included in methodologies for evaluating the effective water edge position at the coast, for representing vulnerability to flooding in coastal management maps useful for coastal managers and politicians (Perini et al., 2016), and to managers and practitioners dealing with hazard setbacks, evaluating risk and coastal vulnerability (e.g Bosom and Jiménez (2011); Vousdoukas et al. (2012)).

The utility of accurate runup prediction rises in a changing climate (affecting the wave climate and producing sea level rise) and for coastal areas affected by increasing human impact. Swash processes are also of interest for understanding rates of coastal sediment transport (e.g. Masselink and Puleo (2006)) and developing numerical models of the swash zone morphodynamics (e.g.Karambas and Koutitas (2002)). Understanding and prediction of runup elevations are therefore critical to scientists trying to understand the dynamics of flow motions and sediment transport.

Broad considerations about the future of the coasts worldwide are given by Masselink et al. (2012b) and Nordstrom (2013) where the importance of climate changes in influencing coastal processes appears clearly. Specific coastal systems impacts, from Masselink et al. (2012c); Wong et al. (2014), are listed below:

- Site specific increase/decrease in magnitude and frequency of storms which possibly produce an increase/decrease in wind speed and wave heights with consequent coastal erosion/deposition, geomorphological and sediment supply change.
- Change in wave direction during a storm affecting the longshore transport, determining a modification of beach width of the order of 10 m in few weeks.
- Rise of sea level is likely related to inundation of small islands, coastal flooding and erosion with consequent dryland and wetland loss and change, as well as the saltwater intrusion (in groundwater). Sea level rise also possibly impacts ecosystems mainly affecting animals and plants (corals, mangroves, seagrass) which will suffer changes in light availability, sea water characteristics (e.g temperature and salinity).
- Increase of sea surface temperature is likely related to processes as a decrease of upwelling and seawater oxygen content, increase of hurricane intensity, increase

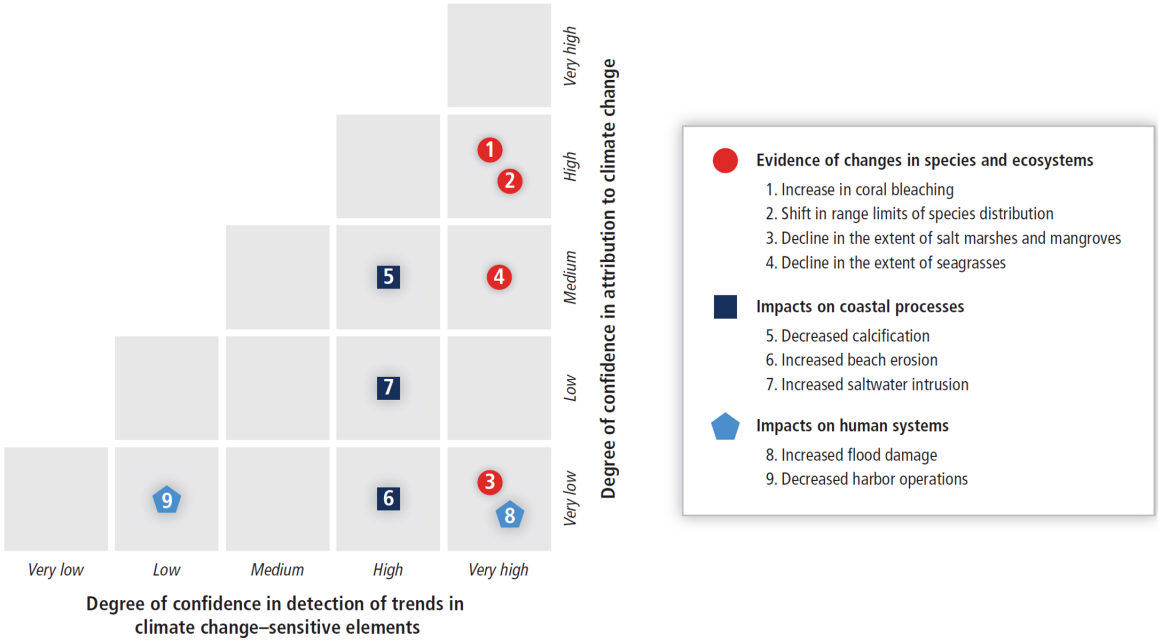

Figure 1.1 Confidence in detecting sensitivity and attribution of coastal systems to climate changes (Wong et al., 2014).

in ocean stratification, coral bleaching enhancing vulnerability to mortality, shifting of marine species towards poles.

- Increase of CO2 in atmosphere likely favour ocean acidification, and reduction of carbonate with serious consequences on marine ecosystems.

The confidence with which those changes in coastal systems are happening and will possibly continue to happen is summarized in Figure 1.1

Coastal areas and ecosystems are subject to cumulative impact (due to both anthropogenic and CC drivers), the highest predicted impacts are concentrated around the coasts because anthropogenic drivers from land and ocean sum up, resulting to largest areas of high predicted impact in North and China seas, Eastern Caribbean, North-east America, Mediterranean, Persian Gulf, Bering Sea, and Sri Lanka (Halpern et al., 2008; Wong et al., 2014). No coast or ecosystem is completely free of anthropogenic impact due mainly to an excessive use of natural resources and threatened ecosystem (Wong et al., 2014; Lotze et al., 2006).

Marine vegetation habitats are recognized to contribute in protecting the coasts (Ondiviela et al., 2014) and mitigating coastal hazards (e.g. coastal erosion), however, is demonstrated that they are deteriorating worldwide (Duarte et al., 2004), due to CC and human pressure (Wong et al., 2014). Seagrass meadows in general (Wong et al., 2014) and *Posidonia oceanica* in particular in the Mediterranean Sea (Duarte et al., 2004),

are under stress and mortality. They furnish several ecosystem services as high productivity acting as a biogenic sediment factory, water oxygenation, fish nursery, reducing wave energy with possible consequent shoreline defence and sediment entrapment (Vassallo et al., 2013). Seagrass deposits on the beach face (beach-cast litter, beach wrack, banquette) likely have an effect of directly protect the coastline from wave action and consequent erosion and flooding during storms (debate in the literature is still open, Gómez-Pujol et al. (2013); Simeone et al. (2013); Vacchi et al. (2017)).

The importance of seagrass ecosystems is largely recognized, and a high economic value is attributed to those ecosystems (e.g. *Posidonia oceanica* is estimated to be worth 172 €m^{-2} a^{-1} (Vassallo et al., 2013)). Seagrass represents fragile ecosystems which are often protected as the *Posidonia oceanica* meadow is safeguarded by EU legislation such as the Habitat Directive (Habitat Type 1120, (EC, 1992)), the Water Framework Directive (EPC, 2000) and the Marine Strategy Framework Directive, (EPC, 2008). Posidonia seagrass is a key element of Australian (various species) and Mediterranean coastal areas (*Posidonia oceanica*). Within the Mediterranean Sea, Sardinia island keeps highly environmentally conserved coastlines, representing a strategic location to perform studies devoted to coastal management and environmental protection which includes the seagrass role (Demuro and De Falco, 2015). Despite the laws dedicated to the protection of seagrass ecosystems, bad practices exist in managing coastal areas in relation to this and other frail ecosystems as ungoverned anchoring and the mechanical removal of seagrass litter from the beach face, berm and backshore (Nordstrom, 2013; Demuro and De Falco, 2010, 2015). The main landforms alterations are due to heavy visitation, deforestation, pedestrian and vehicle trampling, military use, structures and parking building, beach cleaning and beach wrack removal especially by heavy mechanical vehicles on dunes, backshore, berm and beach face (Eastwood and Carter, 1981; Anders and Leatherman, 1987; Demuro and De Falco, 2010, 2015; Wiedemann, 1984).

Good practices for managing and surveying beaches were developed, in order to limit the human impact especially of heavy visitation like the building of elevated boardwalks, fencing sensitive areas, and educating stakeholders or visitors. (Carlson and Godfrey, 1989; Demuro and De Falco, 2010, 2015).

As pointed out by Demuro and De Falco (2010, 2015), an erroneous use of beach systems, with consequent human impact, is probably due to a misunderstanding of the beach morphodynamics. The authors stress that the beach should not be managed as a static element, but indeed as naturally subject to cyclic change and evolution at different time scales, which spread from seconds to millennia.

This work investigates coastal processes, directly connected to coastal management and hazards, which take place in different coastal zones. Coastal areas can be classified

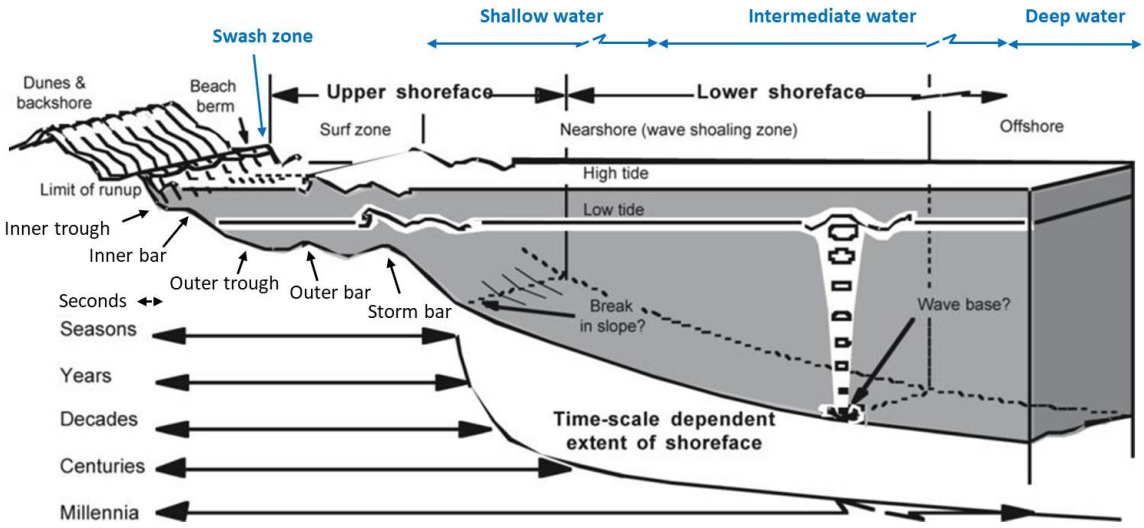

Figure 1.2 Morphological cross-shore elements (modified from Cowell et al. (1999) in Masselink et al. (2012a)). Illustration includes coastal zones according to wave propagation towards the coast (in blue) inserted for this work.

by numerous approaches, based on the phenomena which drive coastal geomorphology, hydrodynamics and morphodynamics as geology, waves, tide, climate, sea-level oscillations (Masselink et al., 2012a). Even though an extensive literature exist on the subject including peer-reviewed papers, books, and treatises (Niedoroda and Swift (1991) in Cowell et al. (1999), Davis Jr and Hayes (1984), Short (1999a), Masselink et al. (2012a), Short and Jackson (2013)), in this thesis the coastal and the spatial/temporal classifications adopted for introducing and contextualize the work, for clarity and consistency, are the one illustrated and reported in Masselink et al. (2012a) or adapted from it.

Coastal zones can be summarized by Figure 1.2: the shoreface (including the nearshore, the surf and the swash zone), the dunes and the backshore.

The shoreface is the landward region of the continental shelf which extends, moving from the sea towards the coast, from the offshore limit of sediment transport induced by wave action to the maximum runup reached by waves on the beach face (Cowell et al., 1999). As reported in Masselink et al. (2012a) the shoreface can be subdivided into Lower (in which morphological changes are influential only during extreme events) and Upper (where sediment transport results in morphological changes yearly), and it includes nearshore, surf and swash zones. The swash zone represents the area in which the sea reach the land, and from the swash zone to the backshore, the human activities are inevitably strongly interconnected with the marine environment.

At the same way in which coastal processes interest different location within the coastal area, they also take place at different time scales. Figure 1.3 shows both spatial and temporal scale frameworks relevant to coastal processes. This work focuses on the

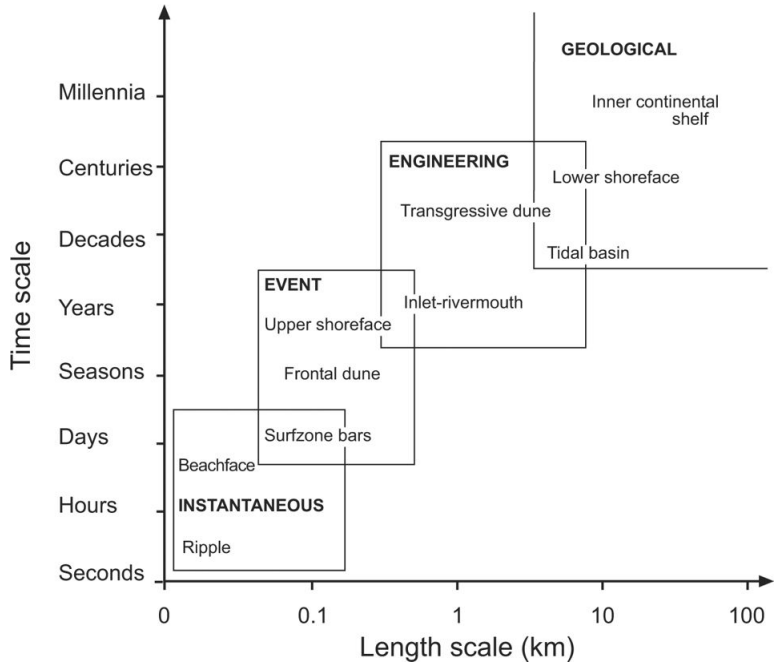

Figure 1.3 Interrelationship between spatial and temporal scale in which coastal processes take place, from Cowell and Thom (1994) in Masselink et al. (2012a).

upper shoreface until the swash zone. Covering phenomena which take place during time scales which spread from seconds (wave runup and swash oscillations) to months (coastal wave recoding). In relations with the definitions adopted by Masselink et al. (2012a) initially proposed by Cowell and Thom (1994) this work is temporally located within the instantaneous and event time scales.

The coastal stretches which are studied in this thesis are mainly composed of wave-dominated sandy beaches, but the results found here, particularly the coastal hazards- and management-related implications, are potentially expandable to other types of coastlines.

For both protecting and managing the coastal environment, it is necessary to know the keys coastal processes driving coastal hydro- and morpho-dynamics. For which is critically important to gather on the field and organize environmental data, which would be utilized: a) to have a baseline knowledge of coastal processes b) as input and validation of models; c) to predict and manage coastal hazards and CC. This work both measures on the field (also retrieving information from remote sensing, as coastal video imagery) and deeply re-analyses previously collected data.

Once the information on the field is gathered, it is fundamental to integrate them with modelling techniques for allowing for prediction (e.g. physics-based models, data-driven models, conceptual models) as well as innovative data-mining methodologies as Machine Learning (ML).

In this context predicting the effect of storms at the coast becomes fundamental

and this work allows to improve the knowledge and predictability of wave runup on sandy beaches. In addition, it proposes to achieve a better understanding of the role of vegetation within the swash zone also in relation to coastal protection with increasing coastal hazards and human pressure. Future development of the present doctoral thesis includes coastal early warning systems, which would allow knowing in advance the coming of a storm and when the sea water may reach critical levels at the coast.

The research performed during this PhD was founded by Sardinia Regional Government which financially supported my PhD scholarship (P.O.R. Sardegna F.S.E. Operational Programme of the Autonomous Region of Sardinia, European Social Fund 2007-2013 Axis IV Human Resources, Objective l.3, Line of Activity l.3.1.). This PhD activity additionally took place within the framework of the NEPTUNE Project, (Natural Erosion Prevision Through Use of Numerical Environment) L. R. 7.08.2007, N.7: Promozione della ricerca scientifica in Sardegna e dell'Innovazione tecnologica in Sardegna. The support and funding rendered by NEPTUNE project allowed the installation of the video-monitoring system and the field data-collection campaigns at sea. Thanks to the international collaborations activated within the project (e.g. University of Auckland, New Zealand and Curtin University, Australia), part of this research activity was performed at the University of Auckland. The visiting period was founded by the BLOGUSDOC scholarship of the University of Cagliari and partially by the NEPTUNE project.

1.1 Aim and Objectives

This work aims to improve the knowledge and the predictability of swash processes useful to the purpose of coastal protection, management, hazards mitigation and prediction. In order to reach this aim the following general objectives are defined:

1. To evaluate existing swash formulas on wide and comprehensive field datasets.
2. To propose new formulations of swash elevation on sandy beaches for improving predictability.
3. To verify the applicability, and highlight the potential of innovative data-driven techniques (Machine Learning) to model coastal processes, such as the swash elevation on sandy beaches.
4. To perform previously missing field measurements of wave swash and runup on sandy beaches, with the presence of underwater vegetation and its litter.
5. To assess the influence that the beach-cast seagrass litter deposited on the beach has on wave runup and swash.

In order to accomplish the main objectives listed above, secondary objectives have been defined for each point. Firstly, the evaluation of existing swash formulas required:

- To identify swash formulas distinguished between total, incident and infragravity swash.
- To gather large field vertical swash datasets comprehending total, incident, infragravity swash recorded on beaches spreading from dissipative to reflective worldwide, under a wide range of environmental conditions, including extreme storms (fundamental for coastal and hazards management).
- To test and compare, the swash formulas performance on the same field dataset.

Secondly, in order to find a new formulation of vertical swash on sandy beaches, which could improve its predictability, the following goals should be reached:

- A methodology for modelling the swash elevation on sandy beaches should be selected between the available data-driven approaches.
- A large dataset including a wide range of beach types, locations and wave conditions should be gathered, for ensuring as much universality of the formulas as possible.
- The formulas found should be strongly tested on field dataset not used for their creation, and verified by a comparison against the most largely accepted and adopted formulas in the literature.

Thirdly, in order to confirm the applicability and enhance the potential of Machine Learning approaches to swash process it is important:

- To select the appropriated Machine Learning technique.
- To evaluate the predictive power of the predictors chosen and their universality.
- To evaluate the interpretation of the results from the physical process point of view and not only from the mere prediction performance of the formulas.

Furthermore, a specific field experiment is necessary to accomplish the fourth and fifth main objectives, which will ensure:

- Contemporary measurements of wave swash, incident wave field, beach morphology, cross-shore beach elevation profiles.
- The setting (planning, installation and calibration) of an ad-hoc coastal video-monitoring station, in a suitable study area.

- The experimental design should ensure the contemporary occurrence of: a) the presence-absence of underwater vegetation litter on the beach, b) wave conditions which will ensure a sufficient wave swash to be observed by the video-monitoring system.

- Time stack images should be created during the condition of presence/absence of seagrass beach-cast litter on the beach face ensuring the comparison on two nearby beach transect.

In Chapter 2 a review of the literature inherent to the topics studied in this doctoral thesis is provided. Chapter 3 explains the methodology adopted for performing this research. Chapter 4 explores the accomplishment of the main objective n° 1, and it has been published recently in Passarella et al. (2018a). Chapter 5 links the main objective n° 2 and 3 proposing a new formulation of swash elevation on sandy beaches, by the use of a Machine Learning technique. The main contents of this chapter have been published in Passarella et al. (2018b). In Chapter 6 is described the field experiment planned and performed for reaching the goal n° 4, and its results (main objective n° 5).

Chapter 2

REVIEW OF LITTERATURE

Wind-generated ocean waves, the perturbation of the sea surface due to wind stress on the free water surface (η), are between the most significant process driving coastal sediment transport and morphodynamics within the shoreface and the swash zone (Huntley, 2013). They represent the highest energy input into coastal systems as microtidal wave-dominated beaches (Wright and Short, 1984). Waves can be generated by local winds, resulting into "wind sea" or by faraway storms, creating waves which have travelled for several km before reaching the coast, defined "swell sea". A number of theories exist for formulating their motion which can be grouped into: linear and nonlinear. The combined action of waves, wave-induced currents and tides force the morphodynamics of the shoreface including the swash zone and the beach. The above-mentioned processes can be monitored by field campaigns and simulated by models.

2.1 Nearshore hydrodynamics

2.1.1 Linear Wave Theory

The linear wave theory or Airy wave theory (Airy, 1845), is based on sinusoidal waves (Figure 2.1) also called small waves, small amplitude waves, infinitesimal waves, or linear wave, of the shape of:

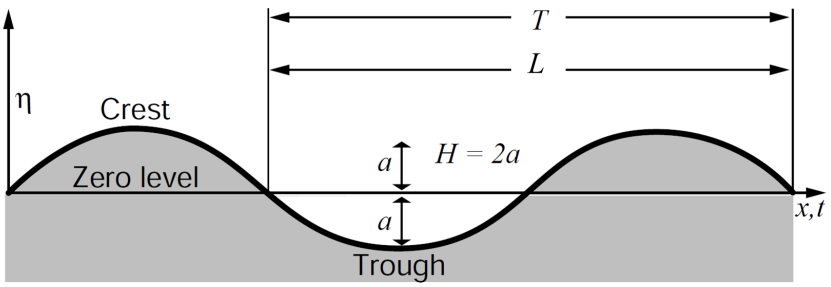

Figure 2.1 Sinusoidal wave (courtesy of WMO (1998)).

$$\eta(x,t) = asin(kx - \omega t) \tag{2.1}$$

where:

η is the free surface elevation, measured from the zero level or mean water level (MWL), it depends on x (wave propagation direction), and t (time),

$a = \frac{H}{2}$, wave amplitude is half of the wave height (H),

$k = \frac{2\pi}{L}$ is the wave number, and L is wave length,

$\omega = \frac{2\pi}{T}$ is the angular frequency, and T the wave period,

The assumptions and approximations for the linear wave theory to be formulated are (WMO, 1998; Svendsen, 2006):

- Work with an ideal fluid (viscous, drag and friction terms can be neglected), for which the only forces acting on it are gravity and pressure.
- Incompressibility of the seawater (constant density) for which a continuity equation can be derived.
- Irrotational fluid assumption (individual particles do not rotate) permits the introduction of the velocity potential.
- The wave amplitude can be considered small in comparison with water depth and length ($H << L$ and nonlinear terms and bottom boundary layer effects are neglected).
- Constant depth.
- 2-dimensional vertical plane; 1-dimensional motion in the horizontal direction of wave propagation (x)
- The periodic motion studied has a wave length (L) defined as the distance between two successive wave crests, and a period T identifying the time interval between to successive crests or troughs passing from a fixed point.

Some other basic wave characteristics and relationships are:

- the wave frequency $f = \frac{1}{T}$;
- the wave propagation speed, or phase speed $c = \frac{L}{T} = \frac{\omega}{k}$;
- the wave steepness $\frac{H}{L}$.

Generally, during wave propagation (from the location of generation) waves with different periods travel at different velocities with longer waves travelling faster. This principle leads to waves to be grouped and to the dispersion relation:

$$\omega^2 = kg\, tanh(kh) \tag{2.2}$$

where h is the water depth,

$tanh$ is the hyperbolic tangent,

g is the acceleration of gravity.

It is possible to rewrite Eq. 2.2, replacing ω and k with their definitions, explicitly for the wave length L:

$$L = \frac{gT^2}{2\pi}\, tanh(\frac{2\pi}{L}h) \tag{2.3}$$

or the wave speed or wave phase c:

$$c = \frac{gT}{2\pi}\, tanh(\frac{2\pi}{L}h) \tag{2.4}$$

The dispersion relation in its three formulations leads to the description of wave characteristics, at varying depth or better at varying relative water depth, the ratio between water depth and wave length ($\frac{h}{L}$ or kh).

The nearshore area can be subdivided into deep ($\frac{h}{L} > \frac{1}{2}$), intermediate ($\frac{1}{20} < \frac{h}{L} < \frac{h}{L} > \frac{1}{2}$) and shallow water ($\frac{h}{L} < \frac{1}{20}$) according to the wave interaction with the seabed (Figure 1.2). In deep water the seabed is irrelevant to the wave motion, at a depth of $h = \frac{L}{2}$ the wave base start to touch the sea bed and the wave to fell its the influence, which becomes more significant in shallow water (notice that deep, intermediate and shallow water are not associated with fixed depths but they are wave-dependent).

From a physical point of view, the wave characteristics change within the three regions. From Equation 2.3 and 2.4 as the water depth decreases also wave length and celerity diminish (while wave period remains constant not depending on water depth). For deep water the $tanh(\frac{2\pi}{L}h) \approx 1$ allowing to the approximations $L_0 = \frac{gT^2}{2\pi}$ and $c_0 = \frac{gT}{2\pi}$ (zero subscript indicates deep water), from which wave length and phase velocity depend only on wave period (water depth is irrelevant). While for shallow water $tanh(\frac{2\pi}{L}h) \approx \frac{2\pi}{L}h$, leading to $L^2 \approx gT^2h$, which becomes $L \approx T\sqrt{gh}$ and the wave phase velocity can be simplified as $c = \sqrt{gh}$. Therefore in shallow water, the wave celerity is depending only on water depth and there is no frequency dispersion.

The airy wave theory also provides the wave particle velocities formulations in which the orbital velocities under the wave (velocities are directed into the wave propagation direction under the crest and opposite backwards under the trough), decrease of intensity with depth and describe a closed circular path in deep water, an oval path in intermediate water and an horizontal movement forwards and backwards in shallow water. In reality the orbital paths are not completely closed, furthermore, the velocity decreases with depth, leading to a certain mass transport associated with waves, with

important consequences in coastal hydrodynamics, as a net drift of water towards the coast (stoke drift). These processes are of high relevance in coastal hydrodynamics especially to sediment transport applications (for details the reader is referred to specialized books (e.g. WMO (1998); Svendsen (2006)).

Another fundamental wave characteristic is the wave power. The wave energy density (sum of potential and kinetic energy of all particles within a wave length) is defined as:

$$E = \frac{1}{8}\rho g H^2 \tag{2.5}$$

Where ρ is the water density.

The velocity at which the energy propagates is named group celerity or group velocity formulated as:

$$C_g = nC \quad where \quad n = \frac{1}{2}(1 + \frac{2kh}{sinh\, 2kh}) \tag{2.6}$$

where c is the phase velocity,

k is the wave number,

h is the water depth,

n varies from $\frac{1}{2}$ in deep water to 1 in shallow water.

$sinh$ is the hyperbolic sine.

The wave power or the wave energy flux (P) is the product of the wave energy times the velocity at which it propagates (C_g):

$$P = EC_g = EnC = \frac{1}{8}\rho g H^2 \frac{c}{2}(1 + \frac{2kh}{sinh\, 2kh}) \tag{2.7}$$

In deep water, $C_g = \frac{c}{2}$ while in shallow water it turns into the same of the wave phase $C_g = C$.

The linear wave theory is still largely used even though a number of limitations exist, mostly because even if the ocean waves are not sinusoidal, it has been successfully demonstrated that real sea states can be represented as a superimposition of an infinite number of sinusoidal waves with different wave characteristics and directions (Huntley, 2013). Barber and Ursell (1948) performed a pioneering experiment measuring swell waves using pressure recorders located underwater (at 33-20 m) and the surface elevation with echo-profiles. From Barber and Ursell (1948) onwards the Fourier's analysis has been applied to wave data, obtaining the wave spectrum describing the wave energy content distributed for frequencies and directions (Huntley, 2013).

2.1.2 Wave Transformation Processes

In intermediate and shallow water, while wave celerity and group velocity are a function of depth (Eq. 2.4), the wave frequency and the period are not, leading to changes in waves during their propagation (Stewart, 2008). As the wave travels towards the coast (starting from intermediate water), because of the seabed influence on their motion, they are subject to five main transformation processes:

- The wave shoaling consists of a change in wave height as waves move from deep to intermediate and shallow waters. Assuming that no energy loss due to bed friction occurs, the conservation of wave energy flux should be verified so that as waves move towards the coast (WMO, 1998):

$$\frac{\mathrm{d}(C_g E)}{\mathrm{d}s} = 0 \tag{2.8}$$

  Where $C_g E$ is the energy flux per unit of crest;

  s is the wave propagation direction.

  For Eq. 2.5 and Eq. 2.6 in Eq. 2.8 at a change in wave celerity, period and water depth it corresponds to a change in wave height. Eq. 2.8 is an approximation which is valid if the assumptions of waves travelling on a constant depth, and negligible wave dissipation (due to friction and breaking) and generation (increase in wave energy for both energy transfer between components of wave spectrum and wave generation) are respected (resulting therefore in Eq. 2.8 being applicable offshore the surf zone) (Huntley, 2013).

  As waves enter into intermediate waters H first diminishes and then increases, particularly right before breaking. This change is due to the modifications of wave group velocity, length and celerity occurring as wave propagate towards the coast. The shoaling coefficient K_s (Eq. 2.9) can be used for quantifying these effects on the wave height:

$$K_s = \frac{H}{H_0} = \sqrt{\frac{C_{g0}}{C_g}} \tag{2.9}$$

  where H_0 is the deep water signification wave height; H is the wave height at the depth of interest; C_{g0} is the deep water wave group velocity; C_g is the wave group velocity at the depth of interest.

- The wave refraction is the result of the wave celerity diminishing with water depth. Considering a regular bathymetry parallel to the coastline, waves along a wave front (defined perpendicular to wave rays and to single wave propagation

direction) approaching the coast with a certain angle, will experience different phase velocities. Resulting into waves in deeper water travelling faster than the waves of the same wave front in shallower water. This affects the wave front which tends to turn parallel to the bathymetry (on regular bathymetry parallel to the coast). Consequently, the waves tend to approach perpendicular to the coast and the wave rays to be spread apart, being the waves refracted. On more complex bathymetry the refraction process can lead to different behaviours, for instance, the wave energy tends to concentrate on headlands and the bays to be more sheltered. In presence of submarines canyons as an example (Figure 2.2) a divergence of wave rays and energy happens, while convergence and focussing arise when waves travel on areas of localized shallower bathymetry. Refraction has important consequences for nearshore currents, sediment transport and morphology (Masselink et al., 2012a).

The wave energy flux should also be conserved between two wave rays at two different locations, and then the ratio $\frac{H}{H_0}$ can also be written as (WMO, 1998):

$$\frac{H}{H_0} = \sqrt{\frac{C_{g0}}{C_g}} \sqrt{\frac{\cos \alpha_0}{\cos \alpha}} = K_s K_r \tag{2.10}$$

where K_r is named wave refraction coefficient; $\cos \alpha_0$ is the distance between two wave rays in deep water; $\cos \alpha$ is the distance between two wave rays at the depth of interest, where α is the angle between the wave rays and the normal to the bathymetric lines (WMO, 1998).

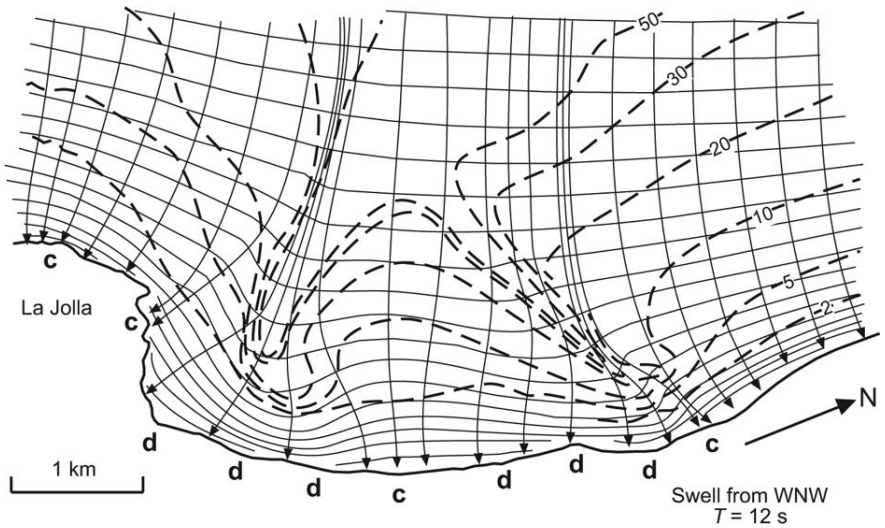

Figure 2.2 Refraction process on complex bathymerty, with zones of convergence (c) and divergence (d) of wave height and energy (courtesy of Munk and Traylor (1947) in Masselink et al. (2012a)).

- The wave diffraction is the consequence of wave energy propagating along the wave front instead of the wave propagation direction. This phenomenon occurs when waves encounter an obstacle during their propagation as an island or an artificial structure. The wave fronts are refracted in the otherwise sheltered area, turning and changing shape becoming curvilinear. Diffraction is the mechanism for which wave energy enters into small entrance bays or harbours (Masselink et al., 2012a).

- When waves reach the coast they can be back reflected offshore when encountering a vertical cliff, artificial structure or a sufficiently steep sloping beach. When the slope is gentle enough another process occurs, which leads to wave energy dissipation into the surf zone: the wave breaking.

  The reflection or breaking of waves depends not only on the slope of the nearshore bathymetry and coastline but also on the wave characteristics, as the steepness ($\frac{H}{L}$). A relationship for distinguishing when one of the two processes prevails was formulated by Iribarren and Nogales (1949), the relationship (Eq.2.11) between wave characteristics and beach gradient was named Iribarren number or similarity parameter:

$$\xi = \frac{tan\beta}{\sqrt{(\frac{H}{L_0})}} \tag{2.11}$$

  Battjes (1975) reviewed their milestone work, highlighting the implications of their discovery in terms of "breaker height-to-depth ratio", "phase difference across the surf zone", "breaker types", "breaking criterion", "reflection" and "run-up and set-up", from which few key points are reported below.

  A value associated to Iribarren number ξ_c (Eq. 2.12) is given for which if $\xi < \xi_c$ breaking will occur.

$$\xi_c = \frac{4}{\sqrt{(\pi)}} \approx 2.3 \tag{2.12}$$

  $\xi_c \approx 2.3$ is considered a value between complete breaking and complete reflection.

  The ration between wave height and depth at breaking, identify the breaking index or breaking criterion γ_b (2.13):

$$\gamma_b = \frac{H_b}{h_b} \tag{2.13}$$

  where H_b and h_b are respectively the wave height and the water depth at breaking.

For values of $\gamma_b = 0.78$ (theoretical maximum height to depth ratio of McCowan (1894)) breaking will typically occur. However, this value increases for steeper beaches reaching $\gamma_b \approx 1.2$ and can decreases for beaches with smaller slope until $\gamma_b \approx 0.6$ Galvin (1972) as reported by (Woodroffe, 2002). When the wave heights within the surf zone are limited by the water depth, the surf zone is defined saturated (usually saturation occurs for incident wave field, while infragravity longer waves can be, in particular cases, partially saturated). Another research investigation field regards how the wave height evolves after the breaking and how the ratio $\frac{H}{h}$ decay within the surf zone (Nelson and Gonsalves, 1992). The authors found, by field measurements on a low sloping beach ($\beta < 0.01$) that it decays $33\% - 48\%$ over the mid to the inner surf zone, suggesting the importance of considering this variation especially when an infragravity wave component is present.

The different type of breaking waves, according to (Battjes, 1975) can be related to the offshore Iribarren number (associated with offshore wave conditions):

- Collapsing waves which arise when $\xi_0 > 3.3$ corresponding to steep beaches and waves with low steepness.
- Plunging if $0.5 < \xi_0 < 3.3$ for waves of intermediate steepness on beaches of intermediate slopes.
- Spilling breakers which occur on a gently sloping beach and steep waves and are associated with $\xi_0 < 0.5$.

- The wave reflection has important implications in the nearshore morphodynamics for the interaction between the incident and reflected waves which can give rise to standing waves, for the influence on cross-shore currents and bars formation (Masselink et al., 2012a).

  The reflection coefficient (Eq. 2.14) is defined as the ratio between the reflected and the incident wave with the method of (Miche, 1951):

$$r = \frac{H_r}{H_i} \tag{2.14}$$

  According to Battjes (1975) the reflection coefficient depends on the type of wave breaker (and is associated mostly with surging breakers (Masselink et al., 2012a)), and therefore on ξ. As Iribarren number increase also r does. Reflection is higher for steeper beaches and lower wave steepness (longer and lower waves), partial reflection occurs for $r < 1$, while $r = 1$ represents the limit condition of total reflection (e.g. vertical wall).

2.1.3 Infragravity Motion

The infragravity motion is a low-frequency motion defined for frequencies lower than the typical incident wind sea and swell waves. The infragravity waves are therefore waves of a fundamentally longer period than the typical peak period of the incident wave spectra (Svendsen, 2006). The definition of the limits of infragravity waves varies in the literature, for instance being defined between 20-200 s period waves by Huntley (2013) and 30-300 s in Masselink et al. (2012a). The frequency threshold assumed for subdividing the infragravity motion from the incident waves is not univocal, however, the majority of the studies assumed $f = 0.05Hz$ (Guza and Thornton, 1982; Holman and Sallenger, 1985; Raubenheimer and Guza, 1996; Ruessink et al., 1998; Senechal et al., 2011; Stockdon et al., 2006; Hughes et al., 2014) with some exceptions adopting $f = 0.04Hz$ (Nelson and Gonsalves, 1992).

Low frequency motion in the field was firstly studied by Munk (1949) and Tucker (1950) (Symonds et al., 1982). The former recorded wave motion with the period of the order of minutes by the use of a new tsunami recorder during high wind waves. The author attributed the formation of long waves to the changing in wave height of incoming waves there, where the wave groups are destroyed (at breaking). A free long wave is released seawards and it is named surf beat (Svendsen, 2006). The latter found a correlation (Fig. 2.3) between an envelope of the incoming waves and a long wave (with a time difference proportional to the needed time for the swell to travel within the surf zone and the one necessary to the long wave to be back reflected offshore). Longuet-Higgins and Stewart (1964) found a long wave π out of phase with the incident wave group, and this was re-interpreted by Symonds et al. (1982) as a signal of the possibility that the long wave of Longuet-Higgins and Stewart (1964) would be released during breaking and that it would travel back offshore as a free wave.

Figure 2.3 shows wave groups of incident waves the related envelope and the bound infragravity wave. Compared with the still water level (SWL), a set-down (set-up) of the infragravity waves occurs in correspondence of the maximum (minimum) of the wave envelope (Huntley, 2013) as shown by the means of the radiation stress by Longuet-Higgins and Stewart (1964).

A comprehensive review and a deep mathematical analysis of the infragravity motion is given by the book of Svendsen (2006), few key concepts form this book are reported below. Different mechanisms of infragravity wave generation have been proposed in the literature, however, the dominant stream in research is to attribute the formation of infragravity waves to the variation in location and height of wave breaking (Fig. 2.4), firstly studied by Symonds et al. (1982).

Waves in groups have different wave heights and considering that the breaking will

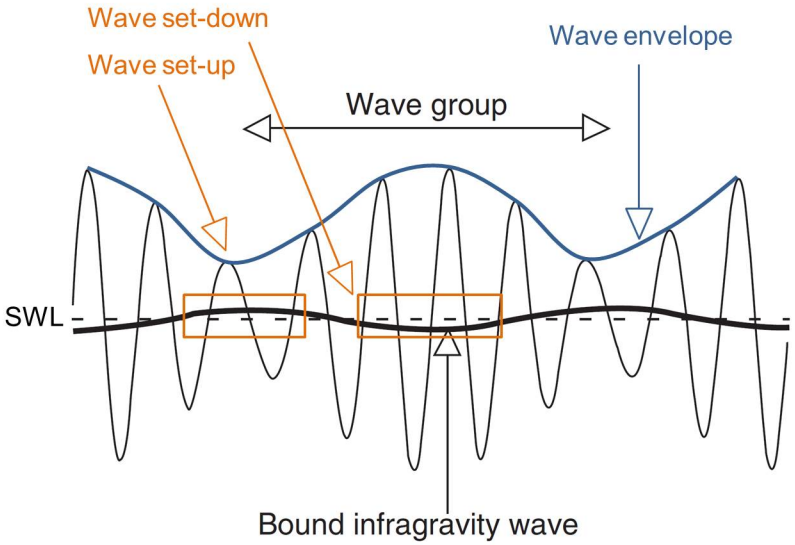

Figure 2.3 Short waves and group (thin black line), bound infragravity wave (thick black line), wave envelope (blue line). Modified from and courtesy of PhD thesis of Gerben Ruessink in Huntley (2013).

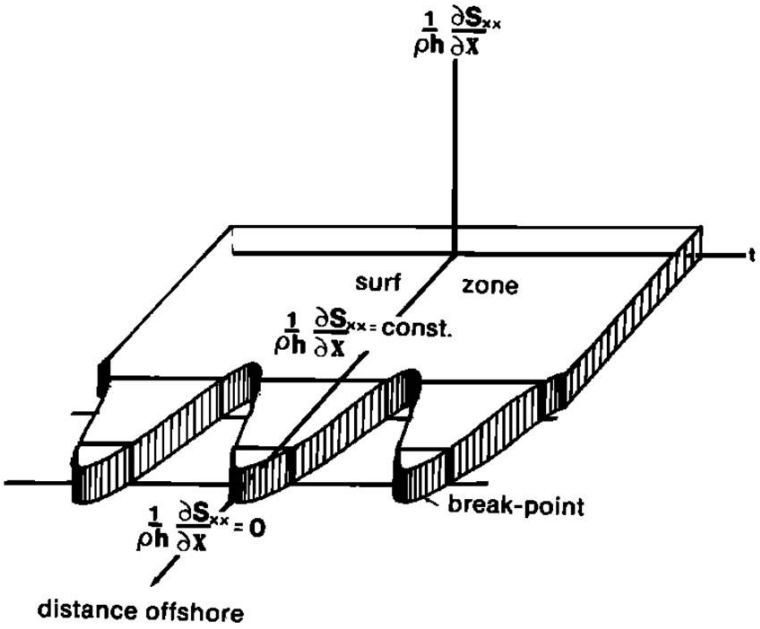

Figure 2.4 Changing location of the breaking point (and therefore of the strong decrease in radiation stress $\frac{1}{\rho h}\frac{\partial S_{xx}}{\partial X}$) due to incident regular wave groups which forces infragravity motion, courtesy of Symonds et al. (1982).

occur at different breaking depths according to the heights, the breaking point will change position in time. Symonds et al. (1982) in their study assumed shallow water waves, and that the breaking will occur always at the same breaking criterion value, so that according to Eq. 2.13 after breaking all waves will have the same height. This implies that the radiation stress will be constant after breaking (Fig. 2.4 $\frac{1}{\rho h}\frac{\partial S_{xx}}{\partial X} = const$). As a consequence, the infragravity energy will be produced only outside the surf zone and in the portion of the surf zone comprehended between the start and end point of breaking (Fig. 2.4). This because a changing wave breaking location implies a temporal variation in the starting point of strong decrease in radiation stress (S_{xx}) and set-up beginning (which occurs mostly at the start of the surf zone). In Figure 2.4 $\frac{1}{\rho h}\frac{\partial S_{xx}}{\partial X}$ represents the cross-shore radiation stress gradient, where x is the cross-shore direction, ρ the water density, S_{xx} is the radiation stress.

Also, nonlinear interactions between short waves (even monochromatic wave train studied by Bowen and Guza (1978)) have been demonstrated to transfer energy towards longer frequencies (an early study of the interaction between different spectral components of incident wave spectra was performed by Gallagher (1971)). This energy transfer from incident short waves to longer waves was considered responsible for the forcing of infragravity waves.

However, the mechanism of changing location of wave breaking has been shown to be dominant (in formation of infragravity waves) compared with the forcing process due to the non-linear resonant interaction between short waves. The consequent basic concept is to consider the set-up/set-down variation in time (with related currents) being a proper long wave. The forcing of infragravity waves is therefore essentially due to the change in radiation stress, which takes place in the surf zone, in relation to the breaking (Fig. 2.4).

The infragravity motion becomes more relevant in the surf and swash zone, mainly in relation with three aspects:

1) The relevance of infragravity motion is shown to be high within the surf zone (Fig. 2.5), which increases moving onshore (due to shoaling of infragravity waves) where on contrast, the incident energy decays, by means of breaking (Masselink et al., 2012a; Aagaard and Masselink, 1999). According with Huntley (2013) this arises especially during storms (when the surf zone becomes wider allowing breaking of higher incident waves) while incident waves break the infragravity motion (mostly) do not, and the inner surf zone total wave energy can be dominated ($\approx 80\%$ reported by Russell (1993)) by infragravity band (Guza and Thornton, 1985; Holman et al., 1978). As a consequence, the shoreline seems to be dominated by infragravity motion (mostly on dissipative beaches).

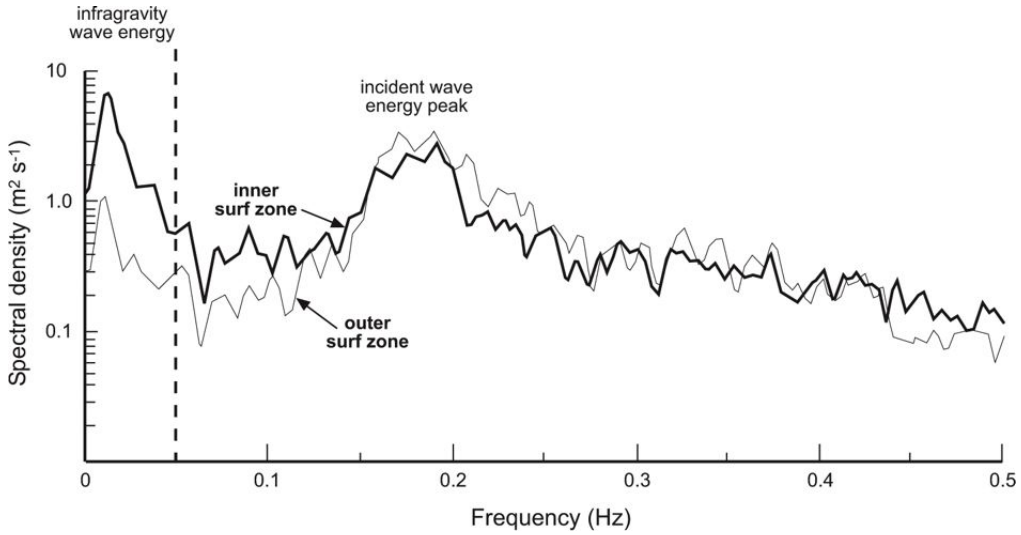

Figure 2.5 Cross-shore velocity measurements within the surf zone show considerable contribution of energy in the infragravity band ($f < 0.05Hz$), which is higher in the inner surf zone compared with the outer surf zone (in contrast with the incident wave energy). Courtesy of Aagaard and Masselink (1999) in Masselink et al. (2012a).

2) The shoreline oscillation has been shown to occur at frequencies lower than those of incident waves, apart for very steep beaches (Huntley, 2013), suggesting that in some way the energy of incident waves, which then possibly break, would be transferred into lower frequency energy within the surf and the swash zone (Svendsen, 2006). The wave runup and swash on the beachface have demonstrated to be strongly forced by infragravity motion, especially on dissipative beaches, when saturation is extended to the infragravity band (Ruessink et al., 1998; Ruggiero et al., 2004; Senechal et al., 2011; Guedes et al., 2013).

3) The interest in the infragravity motion was initially connected with the link attributed between long waves and the formation of many morphological features within the shoreface (multiple bars, rip channels, beach cups etc). In fact, the spatial scale of such features seems to not be ascribable directly to the incident wave field (Huntley, 2013; Masselink et al., 2012a). Furthermore, according to Huntley (2013), recent studies (Werner and Fink, 1993; Coco et al., 1999, 2001) do not attribute the formation of these morphological features directly to long waves but instead to processes of feedback and self-organization between hydrodynamics and sediment response. Nowadays, it seems most possible that the long waves motion responds to these features, instead of being responsible for their formation (Huntley, 2013). Some of the concepts mentioned in this section will be expanded in the next sections and chapters.

2.1.4 Wave Runup, Set-up and Swash Processes

The surf and the swash zone are connected and the residual wave energy after breaking in the surf zone is responsible for the up and down oscillation of the shoreline. The waves run on the beachface, between the runup and the run-down limits. The water motion named uprush and backwash indicates, therefore, the water moving up and down the beachface. Figure 2.6 indicates the vertical water level reached by the waves (wave runup), as results of two distinguished components: the wave set-up and the swash.

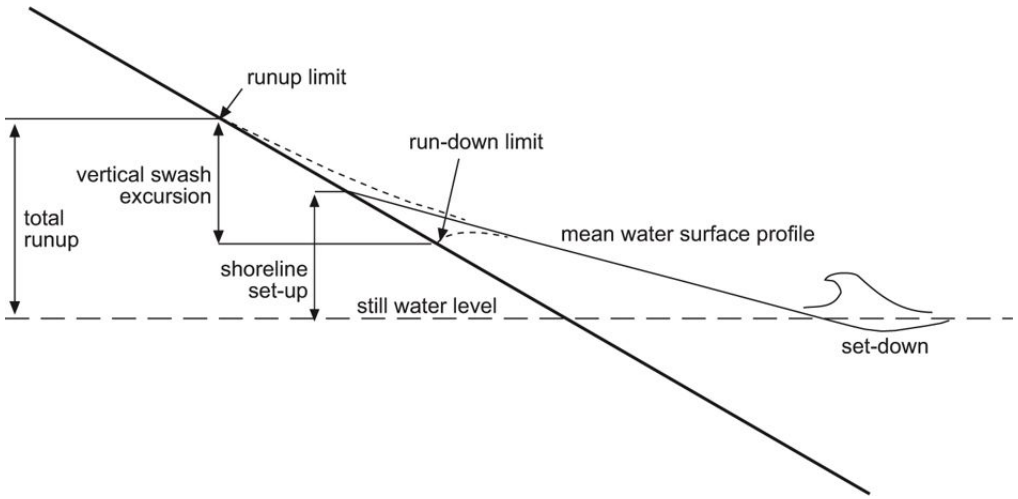

Figure 2.6 Wave runup, set-up and vertical swash excursion schematics. Courtesy of Komar (1998) in Masselink et al. (2012a).

The wave set-up was theoretically formulated by the milestones works of Longuet-Higgins and Stewart (1962, 1964) using the concept of radiation stress (S_{xx}). The radiation stress is defined as the force exerted on a section of water by the action of waves only (subtracting the hydrostatic pressure), or equivalently as the mean wave momentum flux. The cross-shore component of the radiation stress is proportional to the wave energy (E) and thus to the square of the wave height (H) (as ascribed by Eq. 2.15), for a long sinusoidal wave which is not breaking the relationship is given by (Svendsen, 2006):

$$S_{xx} = \frac{3}{2}E = \frac{3}{16}\rho g H^2 \tag{2.15}$$

where E is the wave energy, ρ is the water density, g the acceleration of gravity and H the wave height. The authors found that there is a balance (Eq. 2.16) between the cross-shore gradient of the radiation stress and the variation of the water surface elevation (ζ) along x (cross-shore direction).

$$\frac{\partial S_{xx}}{\partial x} = -\rho g h \frac{\partial \zeta}{\partial x} \tag{2.16}$$

where S_{xx} is the radiation stress, h is the water depth, ρ is the water density, g the acceleration of gravity, and ζ is the water surface elevation.

Eq. 2.16 expresses that at an increase of the radiation stress in the cross-shore direction it corresponds a decrease in the water surface elevation gradient along x. This implies that outside the surf zone, where S_{xx} increases (due to shoaling H increases and thus S_{xx} for Eq. 2.15), the term $\frac{\partial \zeta}{\partial x}$ should diminish. This results in a lowering of the water surface elevation, and it drives the wave set-down phenomenon. On the contrary, after breaking where $\frac{\partial S_{xx}}{\partial x}$ decreases due to wave breaking, a balance should arise with an increase in the term on the right of Eq. 2.16, determining the wave set-up.

The motion of the wave swash is composed by an onshore decelerating component (up-rush) and once the maximum swash is reached on the beachface, the backwash flows offshore-directed accelerating with a magnitude smaller than the previous uprush. This difference in magnitude of swash motion is called swash asymmetry and it is of high relevance for sediment transport. The swash motion time scale can vary between seconds and minutes depending on the relative wave and beach conditions, with longer (shorter) period oscillation associated to energetic low sloping dissipative (low energy steep reflective) beaches (Masselink and Puleo, 2006). The swash flow is turbulent, aerated, very shallow and varies rapidly, which makes challenging its measurement in the field (Masselink and Puleo, 2006), furthermore, its intermittent nature makes difficult the data analysis phase as well (e.g. inhibition of classical time series analysis), (Hughes and Baldock, 2004).

The swash motion can be thought as developing in cycles, one cycle can be defined between the approach of a bore on the beachface and the arrival of the next bore, and can be represented into different phases (Osborne and Rooker, 1997). In the first phase, a strong onshore directed flow is present in the upper part of the bore, while an intense offshore directed flow is located near the bed. High level of turbulence characterize the bore arrival and collapse on the beachface. In the second phase the uprush can accelerate as a consequence of bore collapse, can infiltrate, and velocities are all onshore directed. In the third phase, once the maximum uprush is reached the backwash start to accelerate offshore and the swash lens becomes thicker. In the last phase, the seaward part of the backwash starts to decelerate because of encountering the next bore, and ex-filtration can occur.

According to Svendsen (2006) the swash zone mechanics is an active area of research with still open questions. The classical wave theories existing are not applicable to the swash motion, because the main assumptions for them are not valid in the swash zone. For instance, the wave height is not small when compared with the water depth. Also, the slope change is not small compared with the horizontal scale of the motion, in the swash zone. Although theories exist for swash motion formulation (specific ap-

plication of the Nonlinear Shallow Water Equations, or a ballistic model), it is hard to relate the offshore wave conditions to the swash motion itself. This possibly encouraged empirical swash elevation formulations.

Another approach, as reviewed by Ruggiero et al. (2004), consists in relating the wave swash amplitude to the reflected waves at the shoreline, found proportional to the amplitude of the standing component of the incident wave field by Miche (1951), through laboratory experiments. It has been shown that saturation can occur for wave runup by laboratory tests (Guza and Bowen, 1976) and extensively by field measurements (Guza and Thornton, 1982; Holman and Sallenger, 1985; Raubenheimer and Guza, 1996; Holland et al., 1995; Ruggiero et al., 2004; Guedes et al., 2013). Between the results of Guza and Bowen (1976), it stands out that the swash (considered as the fluctuation component of the runup) is confirmed to be linked to the reflected incident wave height (as hypothesized by Miche (1951)) and that once a maximum value is reached, a greater rise in incident wave energy results in increased dissipation only and not in a further increase in the swash itself. This leads to the idea of a saturation of the surf zone and its link with the swash zone hydrodynamics, which has received large research interest in the last decades. Therefore during saturation, the swash should not depend on offshore wave height. In order to understand if saturation occurs or not a surf similarity parameter can be used ϵ_s (for a value of $\epsilon_s \approx 1$ the breaking initiates):

$$\epsilon_s = \frac{\alpha_s \omega^2}{g\beta^2} \tag{2.17}$$

where α_s is the swash amplitude, ω^2 the wave angular frequency, g the acceleration of gravity, and β the beach slope. Guza and Thornton (1982) looking at the results of breaking waves in Battjes (1975) reported ϵ_s being $= 1.25$ and independent from breaking wave height as well as α_s. Therefore they clarified that the swash amplitude reaches a saturated level where it does not increase with incident waves.

When $\epsilon_s \leq 1$ Carrier and Greenspan (1958) found that solution of the equations of the non-linear inviscid shallow-water theory exists, for non-breaking monochromatic standing waves. Runup grows until ϵ_s reaches a critical value which has been estimated between 1.25 and 3 (Guza and Bowen, 1976; Guza and Thornton, 1982).

When the findings of Miche (1951) and Carrier and Greenspan (1958) are merged the vertical wave runup (here represented by S) can be expressed by the following:

$$\frac{S}{H_s} = \begin{cases} \sqrt{(\frac{\pi}{2\beta})} & : \xi_0 \geq \xi_c^* \quad reflective \\ \frac{\xi_0^2}{\pi} & : \xi_0 < \xi_c^* \quad saturated \end{cases} \tag{2.18}$$

where $\xi_c^* = (\frac{\pi^3}{2\beta})^{\frac{1}{4}}$. When the condition of saturation is verified, substituting Eq. 2.11 in Eq. 2.18, the runup elevation does not depend upon the significant wave height

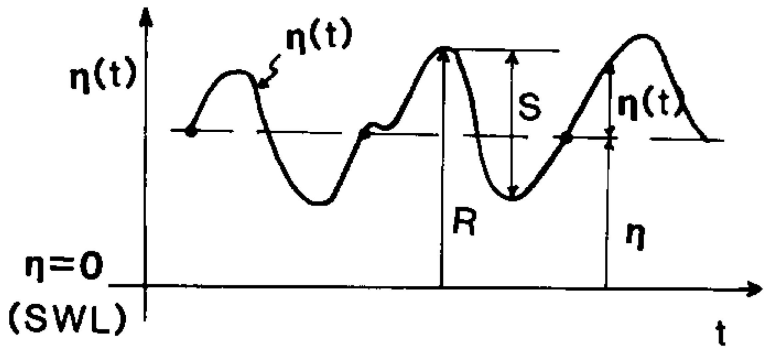

Figure 2.7 Schematics representing the wave swash (S), set-up and runup (R), in relation to the time series of shoreline elevation ($\eta(t)$). Courtesy of Holman (1986).

but on the offshore wave length (L_0) and the cube of the slope (β) only.

2.1.4.1 Empirical Runup and Swash Formulation

The swash zone hydrodynamics and particularly the wave swash and runup prediction were intensely studied in the last decades. Strong effort was put for finding the connections of the runup and swash height with the environmental parameters, from field measurements, as the beach slope (β), the offshore significant wave height (H_0) and length (L_0), their ratio and combinations expressed by wave steepness ($\frac{H_0}{L_0}$) and by Iribarren number (Eq. 2.11) (Guza and Thornton, 1982; Holman, 1986; Holland et al., 1995; Ruessink et al., 1998; Ruggiero et al., 2004; Stockdon et al., 2006; Senechal et al., 2011; Guedes et al., 2012). The wave runup and swash measures can be represented well by the diagram (Fig. 2.7) form the milestone work of Holman (1986). From which the definition of the components of wave runup is formulated, in relation to time series of shoreline elevation ($\eta(t)$) which are usually measured in the field.

The shoreline elevation $\eta(t)$ is the instantaneous elevation of the water on the beachface (referred to the offshore measured SWL). The wave runup (R) is defined as a local maximum of the shoreline elevation. The wave swash (S) is defined between two $\eta(t)$ zero up-crossing, as a vertical range. The wave set-up ($\overline{\eta}$) is the time mean of $\eta(t)$ and the fluctuations around the mean define the swash ($\eta'(t)$).

The first predictors of these phenomena were developed in the context of coastal structures (Miche, 1951; Hunt, 1959) and the formulas proposed, usually developed for steep slopes and under the assumption that runup motions reflect the standing component of the incident wave field. Overall these formulas suggested a dependence of the uprush elevation on wave steepness and structure slope.

Hunt (1959) using data from laboratories experiments found that the non-dimensional

runup ($\frac{R}{H}$) is give by:

$$\frac{R}{H} = 2.3\frac{\tan\beta}{\sqrt{\frac{H}{T^2}}} \tag{2.19}$$

where H is the wave height, T the wave period and $\tan\beta$ is the plan slope.

Battjes (1975) rearranged Eq. 2.19 in terms of Iribarren number (Eq. 2.11) obtaining that:

$$R = H\xi \tag{2.20}$$

where H is the wave height and ξ the Iribarren number (Eq. 2.11).

A variety of predictors have since then been developed for vertical runup (R) and swash (S) on sandy beaches (e.g. Guza and Thornton (1982); Holman and Sallenger (1985); Holman (1986); Ruessink et al. (1998); Stockdon et al. (2006)), with details of the parametrizations depending on different combinations of deep water significant wave height (H_0), deep water wave length (L_0) and beach slope (β).

Guza and Thornton (1982) proposed a linear relationship between the significant vertical swash (R_s) and the significant wave height (H_s):

$$R_s = \mathrm{c}\ H_s, \tag{2.21}$$

where $c = 0.7$. Guza and Thornton (1982) also first distinguished between infragravity and incident swash components, through spectral analysis of the runup records. They indicate that the swash energy spectra related to incident waves (R_{in}) do not depend on incident waves (incident significant swash excursions represented by circled numbers in Fig. 2.8 stay constant as H_s grows), suggesting saturation. In fact, during their experiment they found the inner surf zone saturated, the height of the bore depth limited, and that changes in offshore wave height do not correspond to changes in the bore height. However, the swash component associated with a longer period (infragravity, R_{Ig}), increases with increasing wave height (uncircled numbers in Fig. 2.8).

They also highlighted that the infragravity swash component depends only on significant wave height (therefore excluding the beach slope) while the incident component can saturate as a result of the dissipative processes occurring in the surf zone.

Their findings were later confirmed by several other studies although different dependencies on environmental parameters were suggested (e.g. Holman and Sallenger (1985); Ruessink et al. (1998)).

Holman and Sallenger (1985) studying an intermediate to reflective beach (Duck, North Carolina, USA) described R_s as:

$$R_s = c\ \xi_0\ H_0, \tag{2.22}$$

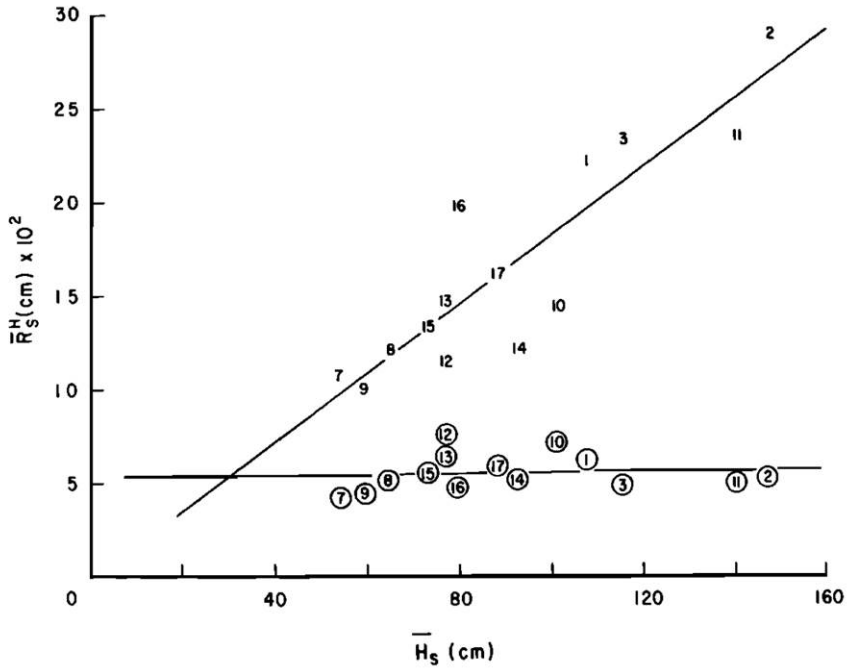

Figure 2.8 Significant wave swash excursion measurements versus significant wave heights in Guza and Thornton (1982).Incident (circled numbers) and infragravity (uncircled numbers) band associated measurements. Courtesy of Guza and Thornton (1982).

where c is a constant, $\frac{H_0}{L_0}$ is the wave steepness and ξ_0 is the surf similarity index,or Iribarren number (Eq.2.11).

Holman (1986) re-analysed the data from Holman and Sallenger (1985) for obtaining the extreme value statistics. The data they analysed contained two stormy events reaching 4 m H_s and an Iribarren number ranging about $0.5 < \xi_0 < 3.5$. They found that for $\xi_0 > 1.5$ the incident wave band motion dominates the swash. Smaller ξ_0 are instead related to infragravity motion. The importance of further studying the infragravity motion considering that storms are usually related to small Iribarren numbers stood out.

The relationship for the 2% exceedance level of swash height, for stormy conditions determined by $\xi_{0:\,storm} = 6.3\beta$, was proposed as:

$$R_2 = (5.2\beta + 0.2)H_s, \tag{2.23}$$

where β is the beach slope and H_s the significant wave height.

Ruessink et al. (1998)studied a low sloping beach (Terschelling) under dissipative conditions where the infragravity swash is dominant. Through linear regression, they found that R_{Ig} is independent of the beach slope and that R_{Ig}/H_0 depends on ξ_0 (and therefore on wave steepness) only under highly dissipative conditions, while for more reflective conditions R_{Ig} seems to depend solely on H_0. The constant of proportionality

between R_{Ig}/H_0 and ξ_0 was found lager than what found previously on stepper beaches and the authors related this with the saturation of the high infragravity band. Ruggiero et al. (2004) analysing a subset of data of Ruggiero et al. (2001), on a highly dissipative infragravity-dominated beach (Agate), found R_{Ig} depending on β in contrast with the previous Ruessink et al. (1998) study on dissipative beaches. However, when a wider runup dataset of Oregon beaches was considered the correlation between β and R_{Ig} results to be only weak (Ruggiero et al., 2004).

The question about if and when the wave swash depends on the beach slope in the case of infragravity motion remained open in the literature.

The subject was debated again by recent studies as in the work of Stockdon et al. (2006), which also provided the most largely accepted and used formulation for wave runup and swash on natural beaches.

Stockdon et al., (2006), aimed to improve the work of Holman (1986) using 10 experiments from different locations to generate new parameterizations of wave runup on natural beaches. The 2% exceedance value of wave runup R_2 was defined as:

$$R_2 = 1.1 \left(\langle \eta \rangle + \frac{S_{Tot}}{2} \right), \tag{2.24}$$

where $\langle \eta \rangle$ is the maximum setup elevation and S_{Tot} is the total swash defined as:

$$S_{Tot} = \sqrt{(S_{in})^2 + (S_{Ig})^2}, \tag{2.25}$$

where S_{in} and S_{Ig} are the incident and infragravity components of the swash. Stockdon et al. (2006) used regression techniques to obtain relationships for S_{in} and S_{Ig}:

$$S_{in} = 0.75\beta\sqrt{H_0 L_0}, \tag{2.26}$$

and

$$S_{Ig} = 0.06\sqrt{H_0 L_0}. \tag{2.27}$$

A number of predictors have been also developed including the effect of other variables, arguing that solely the wave height, length, and the beach slope might be reductive for the runup the swash process formulation. A number of studies can be mentioned proposing other predictors which account for the cross-shore wind component and the tidal range (Vousdoukas et al., 2012), the presence of nearshore sandbars (Cox et al., 2013) or the sediment mean grain size for the case of gravel beaches (Poate et al., 2016), the influence of the wave directional spread (Guza and Feddersen, 2012).

However, the simplicity of relating the runup and swash elevation to the offshore significant wave height and length and the beach slope seems to prevail in the literature. Furthermore, the problem of a spread and consistent data availability of other environ-

mental parameters makes difficult the application of more articulated formulas. Since its publication the formulations of vertical wave runup and swash proposed by Stockdon et al. (2006) are between the most accepted and applied in the literature.

The above-mentioned empirical runup and swash formulas have been based primarily on classic regression approaches starting from field measured data (e.g. Ruessink et al. (1998), Ruggiero et al. (2001), Stockdon et al. (2006), Vousdoukas et al. (2012)). However, the existing predictors still result in significant error in runup elevation (Atkinson et al., 2017). For example, Stockdon et al. (2006) runup formula has been tested by Vousdoukas et al. (2012) on an intermediate to reflective beach, by Cohn and Ruggiero (2016) on dissipative beaches and by Atkinson et al. (2017), along with others formulas, on intermediated beaches. Vousdoukas et al. (2012) collected measurements of swash over more than a year and found that Eq. 2.24 by Stockdon et al. (2006) tends to underestimate observed runup, with a root mean square error RMSE=0.46 m, higher than the formulas elaborated by the authors for the specific beach of the experiment. (Atkinson et al., 2017) used swash data from experiments on 11 beaches ranging from dissipative to reflective, under moderate waves. They confirmed what found by Vousdoukas et al. (2012), that Eq. 2.24 by Stockdon et al. (2006) tends to underestimate the runup measurements with RMSE=0.32 m. Cohn and Ruggiero (2016) found that generally 1D Xbeach simulations better agree with field data than Stockdon et al. (2006) formulation for both S_Ig and $\langle\eta\rangle$. For one of the experiments reported by the authors, the root mean squared difference between Stockdon et al. (2006) formulas and field data for R_2, $S_Ig/2$ and $\langle\eta\rangle$ was equal to 0.2 m, 0.19 m and 0.28 m.

Even though accepted empirical formulation of wave swash and runup elevation are largely used, the error which can be committed, even under stormy condition (critical for natural hazards as flooding and erosion), is not clear. Furthermore, if on one hand wave runup formulations performances have been received interest in the literature to be tested, the same was not for swash predictors. The universality of the empirical formulations derived on one or more field studies (on one or more beaches) is also questionable. Still, gaps in the literature exist in regards to fileld of validity and performance of existing wave runup and swash formulations, which makes of this topic an active area of research.

2.1.5 Coastal Currents

Apart from waves in coastal regions and within the shoreface, other water motions are extremely relevant to sediment transport and therefore to beach morphodynamics, the coastal currents. The currents driven by the wind and tides are usually located more offshore of the surf zone. However, the most interesting currents related to the beach and swash morphodynamics in wave-dominated coastal systems are the current induced

by waves. The main currents which act within the surf zone (Fig. 2.9) are the wave-driven longshore currents, the rip currents and the bed return flow (undertow). The three currents are likely to coexist, if the incident wave field is oblique to the bathymetry, longshore and rip currents can be present as well as return flow (even if of less intensity).

A recent summary of these phenomena is given by Masselink et al. (2012a), from which the key points below are reported. Those flows are deeply linked with the breaking of the waves. They are essentially due to the gradients in water surface elevations which can appear both longshore and cross-shore, as a consequence of varying breaker heights. They are proportional to the incident wave energy so that during storms they will be more intense, contributing more to sediment transport (which is proportional to the flow velocity). All the three currents can be defined quasi-steady as they have a constant velocity for given forcing and environmental conditions (waves, tide, etc.).

Longshore currents are due to oblique incident wave field, in relations with the bathymetric lines and in simplified beaches with the shoreline. They are proportional to the angle of incidence and to the wave breaking height and can exceed $1m/s$ velocity. They may be located in different areas of the shoreface, depending on the presence or not of morphological features as sand bars. For instance, if a sand bar is present, the longshore currents will usually be confined between the bar and the swash zone (within the trough). Other nearshore phenomena can influence the longshore currents, as the tides and the winds, In case of longshore wind with the same direction of the currents, the flow velocity may be greatly increased.

The bed return flow occurring most intensely in the mid surf zone or in presence of bars landward of the bar crest is related to the set-up gradient within the surf zone. Due to wave energy dissipation at breaking, a decrease of the cross-shore radiation stress gradient induces a set up in the water surface elevation ((Longuet-Higgins and Stewart, 1962) Eq. 2.16). As a consequence of wave set-up, a water pressure gradient is directed offshore. This gradient is balanced overall by the onshore wave momentum but, near the bed, the pressure gradient is still imbalanced. This lead at the seabed to a net force which will be offshore directed, producing the return flow current also named undertow. The return flow is part of varying vertical distribution of water flow velocities. In the upper part of the water column, the flow is onshore directed (linked to the onshore directed wave mass transport) and a return flow directed offshore characteristic instead of the near-bed flow. This cross-shore current is less intense than the alongshore current and is of the order of magnitude of $0.1-0.5m/s$ ($0.5m/s$ can be reached under extreme storms).

The rip currents are other types of cross-shore currents, and they can extend farther offshore than the other two type named above, overpassing also the surf zone. They are intense currents ($0.5m/s$) which flow on channels in the surf zone usually between transverse bars and are associated with hazard as mortality for people swimming in their

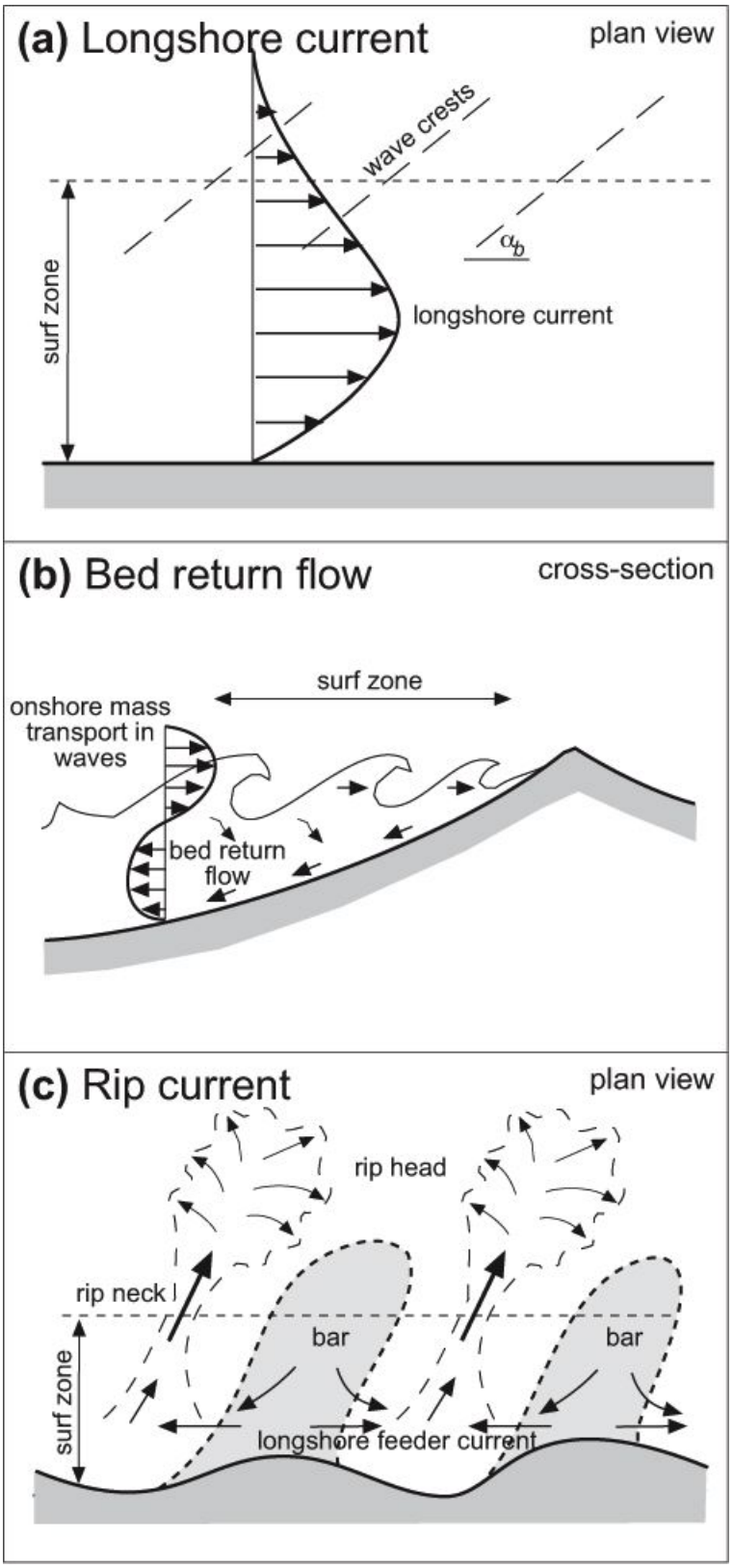

Figure 2.9 Coastal currents within the surf zone, lonshore current (a), bed return flow (b), rip current (c). Courtesy of Masselink et al. (2012a).

presence. In case of extreme storms, mega-rips can originate in their necks velocities up to $2m/s$. Maximum current velocities occur in the rip neck and may reach up to $2m/s$ under extreme storm conditions when mega-rips form (Short, 1985). Figure 2.9c represents the entire circulation system characterizing the nearshore when rip currents are formed. Within the surf zone, nearer to the coast, a longshore feeder current bring water to the rip necks which are located between transverse bars. This because of the enhanced breaking on the bar compared with the rip channel, an alongshore pressure gradient is formed which leads water between the bars. Intense and narrow offshore directed currents pass through the surf zone, called rip necks. Then once the flow velocity decreases outside the surf zone, the rip neck expand forming the rip head. Between single rip currents, there is an onshore-directed flow which closes the coastal circulation cell associated with the presence of rip currents.

A recent field study (Austin et al., 2010), by the means of lagrangian drifters, found that a greater eddy within the surf zone characterizes the rip currents system.

2.2 Beach and Swash Zone Morphodynamics

The hydrodynamics covered by the previous section is connected to sediment transport and to the formation and evolution of forms (from which is in turn influenced) within the entire shoreface and beach. Coastal hydrodynamics is therefore intrinsically connected with beach and shoreface morphology. Wright and Thom (1977) coined the term "coastal morphodynamics" for their approach to study coastal environments defining it as "the mutual adjustment of topography and fluid dynamics involving sediment transport". This approach considered time scales from instantaneous to the Quaternary and spatial scale of the order O(cm) to O$(1000)km$ (Fig. 1.3), covering an extensive range of coastal processes. They applied a system approach to coasts, considering the coast and its morphology as a geomorphic system, connected with external factors and environmental conditions as well as having an input and output of both energy and material (Masselink et al., 2012a).

The mechanics of the systems can be applied to coasts with the main features summarized recently by Masselink et al. (2012a). Coastal systems represent typical open systems since the fluxes of matter and energy is freely exchanged between components of the system and with factors external to the system itself. In coastal areas, the system can manifest as a geomorphological process which models landforms within the shoreface, the beach and the back beach. Changes in the systems occur through coastal processes. A system can be defined in quasi or dynamic-equilibrium when over time the components of a system tend to remain stable.

According to Sterman (2000), the complexity of a system is due to the interactions (feedback) between its components more than by the complexity of the components

themselves. In the book, is highlighted the importance of identifying the feedback process in a system, because two feedback processes determine the entire dynamic of the system itself (along with other factors, such as time delays, the nonlinearities and the flow structures). The positive feedback loop is defined self-reinforcing since it tends to amplify what is happening in the system leading to change (Fig. 2.10, B to C) while the negative feedback opposes instead to the change, tending to maintain a quasi-equilibrium (Fig. 2.10, D to E). The positive feedbacks reinforce their own growth, while the negative feedbacks are self-limiting, tending to a balance and an equilibrium. A self-reinforcing process would grow infinitely, but in nature, no such process usually occurs, so that a limiting factor to the growth is represented by the negative feedback. Between positive and negative feedback processes a relaxation time occurs (Fig. 2.10, C to D). Reversing feedback points out thresholds in morphodynamic behaviour (Cowell and Thom, 1994).

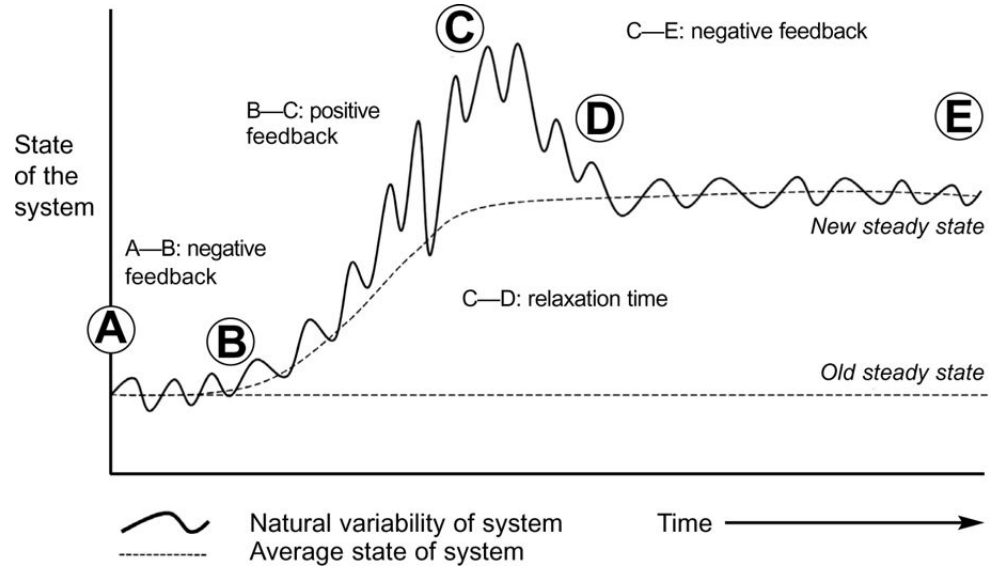

Figure 2.10 System mechanics states for coastal systems. The stages between A and B, D and E represent negative feedback, between B and C positive feedback, and between C and D relaxation time between positive and negative feedback. Courtesy of Masselink et al. (2012a).

Cowell and Thom (1994) identified feedback loops between topography and fluid dynamics which lead to sediment transport and morphology changes. They also reported as positive feedback produces the growth of an instability resulting in a new mode of operation of the system thanks to self-organization process (which is also defined as adaptive) (Waldrop, 1993). While negative feedback in response to minor perturbation can be associated with properties of self-regulation (Wright and Thom, 1977). Werner and Fink (1993) highlighted the importance of considering complex system research when studying coastal morphodynamics. Coco and Murray (2007)

review explore the vision of the sand rhythmic patterns formation theories, from the original approaches attributing patterns formation to imprinting of hydrodynamical or geological templates, to the self-organization theory.

2.2.1 Beach States and Morphodynamics

Coastal morphodynamics and particularly shoreface and beach morphodynamics are extensively reviewed and treated in several textbooks and treatises (Short, 1999a; Cowell and Thom, 1994; Masselink et al., 2012a; Short and Jackson, 2013).

A fundamental element of beach morphodynamics studies is the beach profile. The measure of cross-shore beach profile, permit the view of several morphological elements characterizing a beach (Fig. 1.2). Furthermore, the relative easy technique used for acquiring measurements of cross-shore beach elevations, in comparison with areal measurements, made this method spread worldwide.

The main morphological elements characterizing a cross-shore beach profile, moving offshore from the back shore are the dunes, the berm, the sand bars and the troughs (Fig. 1.2). The complexity of the beach systems, focussing on wave dominated beaches, can then be extended including a large number of different combinations of these basic morphological elements adding as well new elements as: beach cusps, mega cusps, ripples, mega ripples, different kind of bars (transverse bars), runnels, terraces, scarps, etc. The relative hydro/morphological conditions determining one or another configuration of the beach system have been largely studied (Gourlay, 1968; Wright and Short, 1984; Short, 2006) and subdivided into different type of beaches as dissipative, intermediate, reflective and states (Fig. 2.12, 2.13, 2.14).

The repetition in time of the same beach profile can reveal changes into the morphological asset of the beach in the cross-shore direction while, surveying more beach transects in the same beach along the shore, furnish information about the beach longshore morphology (e.g (Farris and List, 2007; Larson and Kraus, 1994)). Repeating measurements of beach profiles during the year, a seasonal variability in the beach profile was initially identified (Hayes and Boothroyd, 1969). Later, researchers noted that the seasonal variability more than being linked to standard seasons is strictly dependent on the wave climate of the year (Nordstrom, 1980). They investigated on the field the changes in beach profiles, finding that a cyclic change of more exposed beaches occurs, in contrast with more sheltered beaches (bayside) which follows instead a seasonal response.

However simplifying, a ”summer” and ”winter” beach behaviour can be schematically distinguished 2.11.

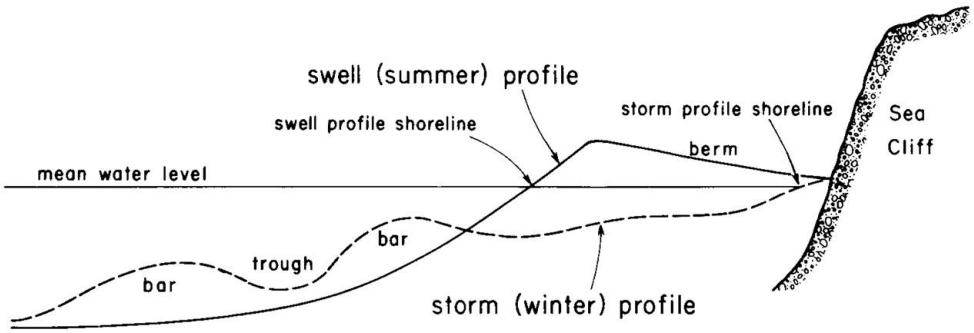

Figure 2.11 Beach profile morphology and seasonal changes. Courtesy of Komar (2018).

During winter when the severity of the storms is higher, the beach assumes a profile with the sand being moved from the berm to submerged sand bars, which in turn works for wave energy dissipation (breaking) farther offshore. In summer, when the storms are less intense and frequent, the sand is re-deposited on the beach berm. As a consequence, the part of the beach emerged, results wider during summer than winter.

Among the morphodynamic processes occurring in the coastal areas, the beach morphodynamics has received larger interest. The morphodynamic approach has been applied on beaches since the late 1960s, starting with the Coastal Studies Institute of Louisiana State University and then extensively spread in Australia in the last decades by the Coastal Studies Unit at the University of Sydney (Short and Jackson, 2013). These studies based primarily on field observation brought to an understanding and classification of the different type of beaches.

In order to distinguish between the different type of beaches and their characteristics, several empirical relationships have been used. Relationships which permit to predict the beach conditions based on environmental parameters as beachface slope, offshore wave height, and period, breaking wave height and sediments properties.

Wright and Short (1984) formalized the subdivision of beaches in morphodynamic states, in their milestone work on Australian wave-dominated beaches. The beach morphodynamic state was defined by the author as the group of possible depositional forms and related hydrodynamical process. They summarized the results of their research during three years 1978-1982 based on field observations of beaches around the Australian coast, mostly located in south-east Australia. According to the authors, the high variability of beach type studied permitted to generalize their results and to predict the modal (most recurrent) beach states.

They based their classification and modal beach state prediction on the dimensionless fall velocity Ω (Gourlay, 1968):

$$\Omega = \frac{H_b}{TW_s} \tag{2.28}$$

Where H_b is the breaker height, T the wave period, and W_s is mean sediment fall velocity.

They extended the work of Gourlay (1968) on laboratory beaches to natural beaches based on their observations. They linked values of $\Omega < 1$ to reflective beaches (steeper without bars), $\Omega > 6$ to dissipative beaches (smaller beach slope and presence of multi-bar system) and for value between the two, the intermediate beaches are defined (moderate slope with 1 or 2 bars).

The authors stress that the hydrodynamics/sediment transport relative forcing, the morphologies and their changes, vary greatly with beach modes, which in turn depend on surf and swash zone regimes: dissipative, intermediate, reflective. They confirmed on the field, previous findings regarding dissipative beaches being dominated by longer period motion (e.g. infragravity, as well as the shoreward decay of incident waves with a contextual increase of infragravity energy on the onshore direction) when compared with the incident wave-dominated reflective beaches.

The long-term observations of beaches, with varying forcing conditions, permitted to Wright and Short (1984) to report in which case a certain morphology would form and which is the connection with sediments type and hydrodynamic conditions associated, such as the formation of rip currents. For instance, the dissipative beaches (Fig. 2.12, a) with fine and very fine sand exposed to high energy condition tended to exhibit little change. On the other hand intermediated beaches, lacking sediments (medium grained sediments) and exposed to highly variable wave conditions showed the largest mobility, leading to the formation of several beach states (Fig. 2.12-2.13, b-e). For reflective beaches (Fig. 2.13, f) instead, only a modest mobility was reported occurring on beaches with coarse-grained sand, exposed to waves with low steepness.

Successively, the work of Wright and Short (1984) was extended and re-analysed in several ways Short (1999b, 2006) and the wave-dominated, updated micro-tidal beach systems states representation by Short and Woodroffe (2009); Short and Jackson (2013) are here illustrated in Fig. 2.14.

The intermediate beach states are therefore the most variables and comprehend the longshore bar and trough (LBT), the rhythmic bar and beach (RBB), the transverse bar and rip (later modified into the transverse bar and beach (TBB) (Short, 1999b, 2006)) and the low tide terrace (LTB) (or ridge-runnel). Those beach states occur roughly at given Ω values: reflective beach ($\Omega < 1.5$), low tide terrace beach ($\Omega \approx 2$), transverse bar and rip beach ($\Omega \approx 3$), rhythmic bar and beach ($\Omega \approx 4$), longshore bar-trough beach ($\Omega \approx 5$), dissipative beach ($\Omega > 5.5$).

The influence of tides was later formalized by (Masselink and Short, 1993) extend-

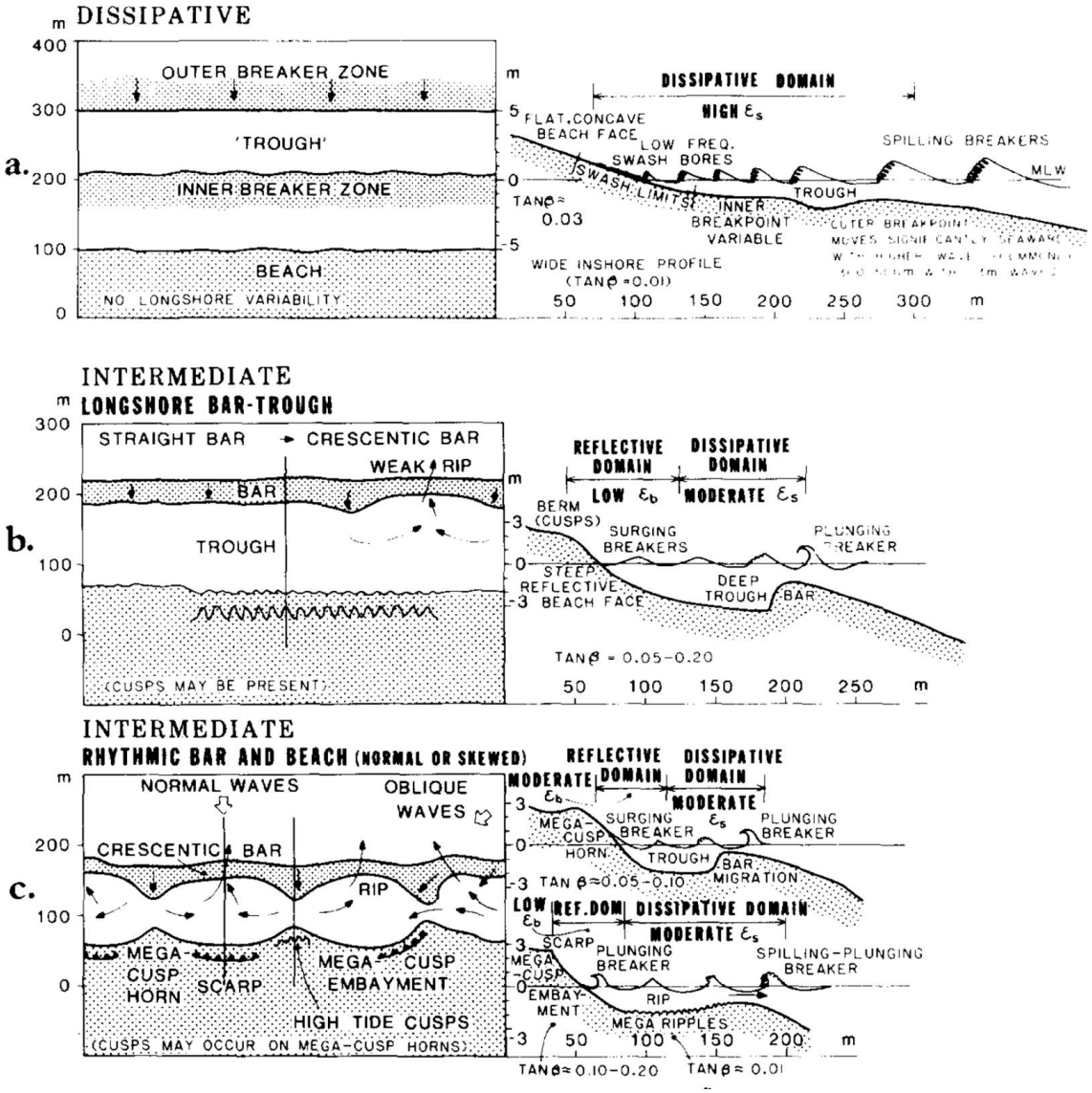

Figure 2.12 Six major Wave-dominate micro-tidal beach states. Courtesy of Wright and Short (1984).

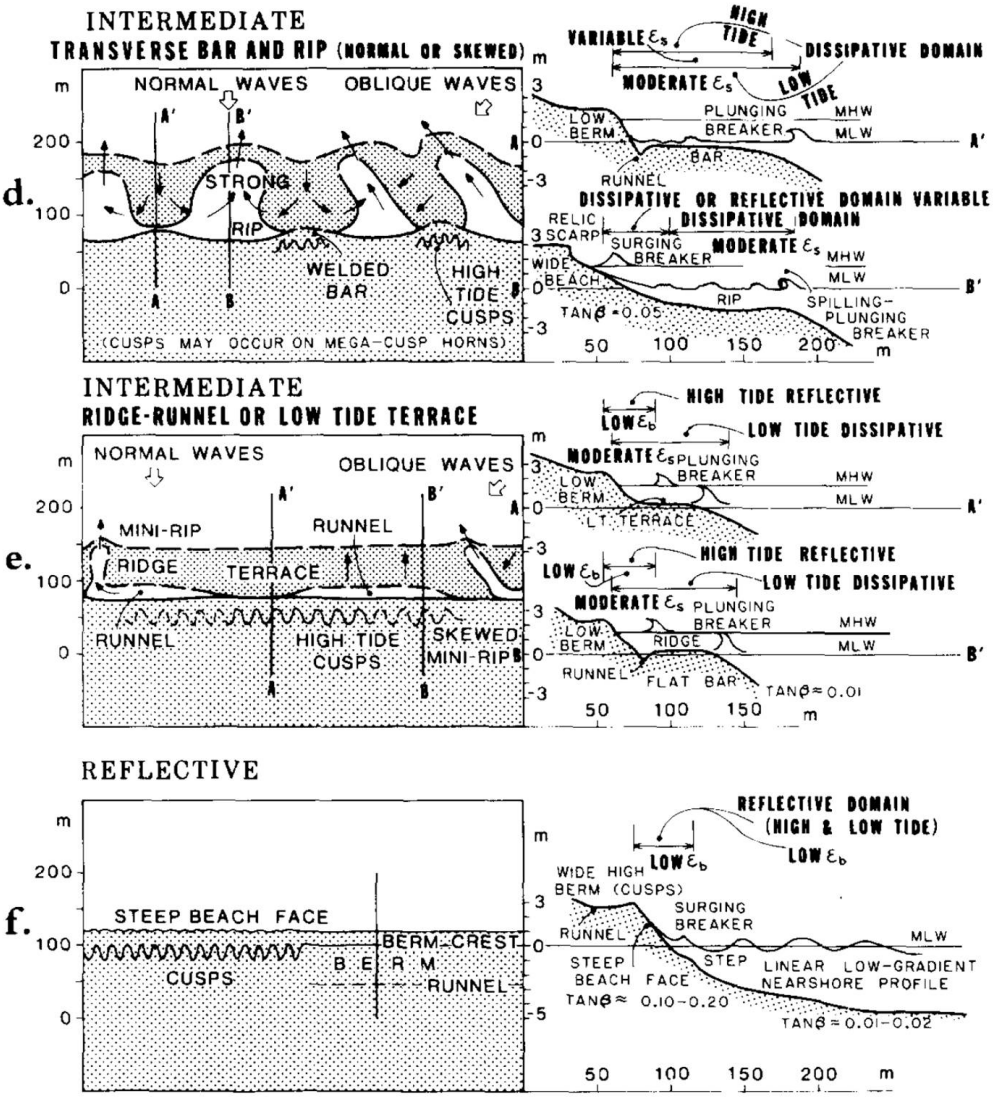

Figure 2.13 Six major Wave-dominate micro-tidal beach states. Courtesy of Wright and Short (1984) continued.

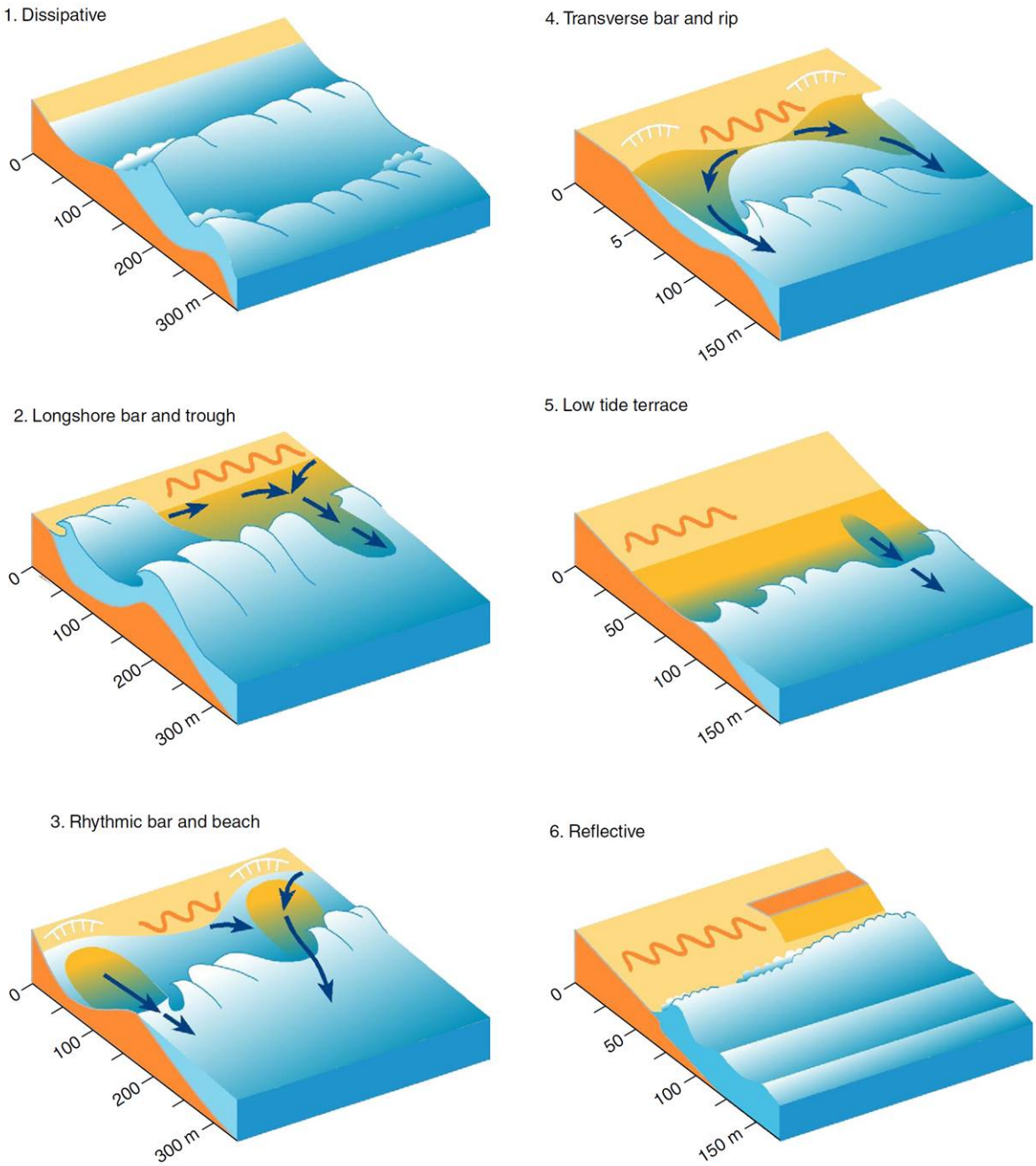

Figure 2.14 Wave-dominate micro-tidal beach states. Courtesy of Short and Woodroffe (2009) in Short and Jackson (2013).

ing the type of beaches using the nondimensional relative tide range parameter (RTR) along with Ω. The type of beaches became therefore 13, 6 wave-dominated (in the micro-tidal environment), 3 tide-modified and 4 tide-dominated (for meso-, macro-, and mega-tides) as summarized in the work of Short (2006). This classification is of high relevance in the literature because it links the hydrodynamic conditions, the sediment type, with the morphology occurrence and its evolution. Even if those states are elaborated mainly for Australian beaches, is likely that the beach states identified in Wright and Short (1984); Masselink and Short (1993); Short (2006) are representative of beach conditions around the global coastline, as they have already being used to classify beaches worldwide (Komar, 1998).

Other empirical relationships as the surf scaling index or the Iribarren number (also called surf similarity index) have been used for beach classification, and to understand whether waves would break and how, and if the reflection is dominant on wave breaking or vice versa. The surf scaling index of Guza and Inman (1975) was largely applied.

$$\epsilon = \frac{a_b \omega^2}{g\, tan^2 \beta} \tag{2.29}$$

where a_b is the breaker amplitude, ω the wave radian frequency, g the acceleration of gravity, and β is the swash/surf zone gradient respectively for the beach/surf zone classification. Short (1999b) reported from previous works (Wright and Short, 1984; Guza and Inman, 1975), that complete reflection is expected for $\epsilon < 1.0$, reflective beaches are attributed at values of $0.1 < \epsilon < 2.5$, dissipative conditions at $20 < \epsilon < 200$, with the range in between representing intermediate beaches. Furthermore, plunging waves are associated to $\epsilon > 2.5$, while spilling breaker type are connected to value of $\epsilon > 20$ (Galvin, 1972). Substituting the definition of angular frequency ($\omega = \frac{2\pi}{T}$, where T is the wave period) and breaker wave heigh ($H_b = 2a_b$) into Eq. 2.29, the surf scaling index can be rewritten as:

$$\epsilon = \frac{2\pi^2 H_b}{g\, T^2\, tan^2 \beta} \tag{2.30}$$

directly related to the significant wave height at breaking (H_b) and to the wave period T.

The Iribarren number (Eq. 2.11) is also often used for beach classification — beaches are classified as dissipative for values of $\xi_0 < 0.23$, reflective for $\xi_0 > 1$ and intermediate between the two (Short, 1999b). Those alternative empirical indices resulted useful for beach classification since they related directly the beach slope (swash and/or surf zone) and the offshore or at breaking wave parameters, without needing direct measurements of sediment diameter (that is not always available from field campaigns).

2.2.2 Swash Zone Morphodynamics

An extensive review of the swash zone morphodynamics is given by Masselink and Puleo (2006), from which few key points are reported below. According to the authors the definition of the swash zone is not univocal in the literature, some refers to the zone between the maximum uprush and the minimum backwash, others between the uprush limit and the point of bore collapse on the beachface (Michael and Ian, 1999) or where the bore starts to affect the seabed by its turbulence (Puleo et al., 2000; Masselink and Puleo, 2006). The morphodynamical zone corresponding to the swash zone is named beachface and extends on the beach profile from the berm to the low tide level (Masselink and Puleo, 2006). The shoreface is easily identifiable on micro-tidal environments, being dominated by swash process only and because of its marked unique steep slope. Its definition becomes more complex on macro-tidal systems, where for the alternation of wave processes the beach steepness diminishes.

The swash zone morphodynamics is relevant to the cross-shore exchange of sediments between the sub-aerial and the sub-aqueous marine zones (Masselink and Hughes, 1998) and it is responsible for deposition and erosion there, where the shoreline is located and is therefore directly connected to the coastal erosion hazard. Furthermore, longshore transport on the beachface was demonstrated to accounts for a significant part of the total transport and of the littoral drift by laboratory experiments (Bodge and Dean, 1987; Kamphuis, 1991; Smith et al., 2003) as reviewed by in Masselink and Puleo (2006).

The slope of the beachface was connected since early studies to the asymmetry in the swash flow (Bagnold, 1940). In the literature is found that an equilibrium exists between swash asymmetry and the component of the gravity directed downslope, which drives the beachface gradient (Hardisty, 1986).

Apart from the beachface, some other morphological elements which characterize the swash zone are berm, beach step and beach cusps, as summarized by Masselink et al. (2012a). The beach berm represents an accumulation features located shoreward than the beachface and it is separated from it by the berm crest, which is the highest part of the morphology before the slope of the beachface starts seaward. This slope would be more marked on gravel and coarse sand beaches, making the beach crest easily distinguishable. However, on fine sediment beaches, it may be not easily identifiable because of the milder beachface slopes. Berm and shoreface adapt rapidly to changing wave conditions so that the beach asset can transform rapidly. The profile under storm conditions assumes a concave beach shape (possibly presenting a scarp) due to the erosion of the berm and beachface. In contrast, as a response to low-energy wave conditions, the beach presents a convex profile characterized by accumulation and berm formation. Both accretion and erosion of beach berm require the wave overtopping of the berm

itself.

The beach step may form due to a back wash vortex nearby the end of the beachface seaward, leading to an accumulation of coarser material. The step is a small scarp submerged characterized by a vertical scale length of $\approx 0.01m - 1m$ and is more appreciable on gravel and coarse sand beaches. The interaction of the backwash with the incoming incident bore may lead to step formation by erosion of the beachface and deposition of coarse material.

The beach cusps are rhythmic patterns appearing on the shoreface composed by alternating embayments and horns. The embayments are low-sloping, oriented seaward while, the horns are characterized by steep slopes. The spacing between to consecutive horns varies and is generally $\approx 10 - 50cm$ (Masselink et al., 2012a). The uprush has been shown to be divergent at the horns (Coco et al., 2000). The circulation within the beach cusps consists therefore of the uprush, divergent at the horns and of the backwash forming a mini-rip at the centre of the embayments (Masselink et al., 2012a).

The formation of some rhythmic features on the beachface and shoreface have been historically linked to long wave motion such as edge waves. The subject has been largely debated in the literature, and it still receives large interest. However, a more recent emerging theory based on self-organisation attribute to a positive feedback between sediments and swash flow the formation of beach cusps (Werner and Fink, 1993; Coco et al., 2001). The positive feedback is self-reinforcing as it acts as enhancement of the existing small perturbation in the beachface topography, leading to a change in the system (the formation of rhythmic features). In addition, a negative feedback in the system impedes that once developed the cusps would be dismantled. Usually, a strong change in hydrodynamic conditions as a storm could induce a change in the systems which will lead to cusps disappearance.

In general two main research paths attribute to two different mechanisms the formation of rhythmic features and in generally propose two different views of coastal morphodynamics and its leading mechanisms (Fig. 2.15).

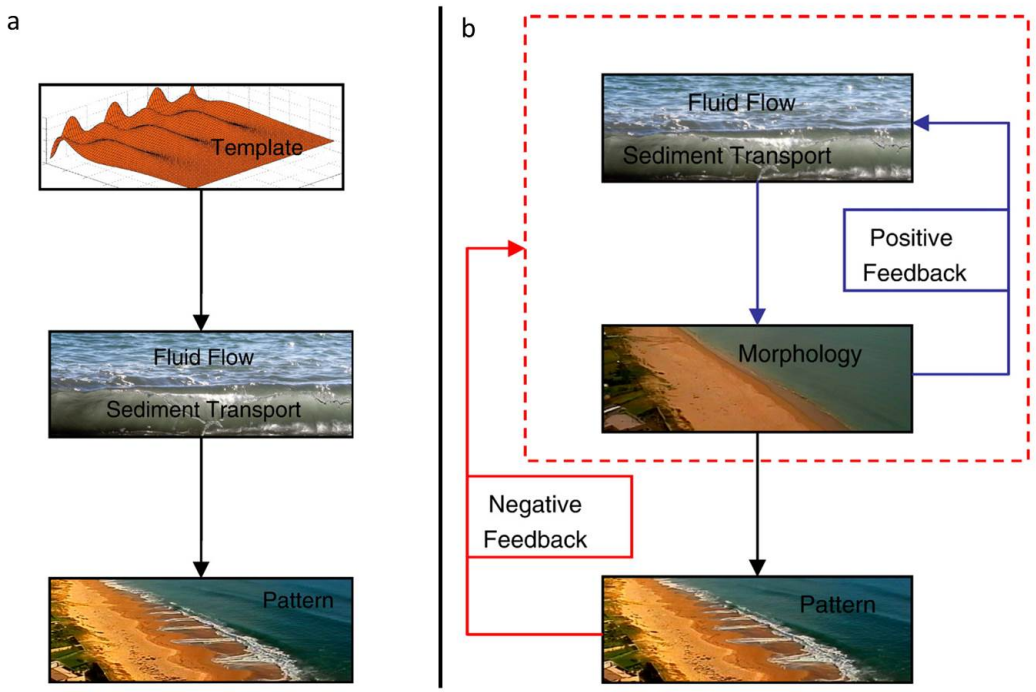

Figure 2.15 Pattern-template (a) Vs Self-organization (b) theories of pattern formation within swash zone and shoreface. Courtesy and modified from Coco and Murray (2007).

One is the template-forcing principle and the other the self-organization mechanism. A recent review (Coco and Murray, 2007) discuss the differences between the two approaches through the analysis of several morphological elements as beach cusps, and crescentic sandbars. The first working principle attribute to spatial structures in the forcing (such as in the hydrodynamics or geology) the imprinting of the templates in the sand, forming a given shaped pattern. This forming mechanism is based on the idea that the template unidirectionally impresses the forcing template on the sediments, which appears passively subject to the change in morphology.

The second theory explains the formation of rhythmic features in the sand with a mutual response and adaptation between fluid and sentiment process, between swash motion and changing topography following a self-organization process. In this perspective, therefore, fluid and sentiments interact influencing each other. The changes are due to initial perturbations in the sand. This self-organization process has been successfully modelled, finding general agreement with field measurements (Werner and Fink, 1993; Coco et al., 1999, 2000, 2001).

A recent review of waves in relation to geomorphological processes, states that nowadays, seems to be more likely that long period waves are responding to the morphology they find more than the other way around (Huntley, 2013).

2.2.3 Seagrass Beach-cast Litter

Coastlines and shoreface worldwide can be characterized by the presence of vegetation, and seagrass meadow extending for thousands of kilometres being reported in temperate and tropical bioregions (Short et al., 2007).

The seagrass meadow located within the shoreface, due to the natural cycle in plant life can produce a particularly large amount of seagrass litter. Those wracks often deposit on the coastlines worldwide, creating in some cases enormous accumulation on the shoreface, berm and backshore, named beach-cast litter, banquette, beach wrack or seagrass berm. The mean yearly volume of banquette can exceed $1800\ m^3$ (Simeone, 2008) with recorded peaks of accumulation (in the case of Western Mediterranean) of $9000\ m^3$ (Simeone and De Falco, 2012) reaching and influencing also the dune development (De Falco et al., 2003; Vacchi et al., 2017). The high of deposits can exceed $2m$ and $500\,kg$ of dry $wt\,m^{-1}$ (Mateo et al., 2003) and within the banquettes over $60\,kg/m^3$ of sediments can remain trapped (Vacchi et al., 2017).

These considerable deposits are regulated by seasonality in seagrass life cycles. For instance, *Posidonia oceanica* (L), the most abundant species in the Mediterranean Sea, is reported to shed its leaves and to disconnect the rhizomes mainly between September and October (Mateo et al., 2003).

The reproductive phases (germination, flowering and fruiting) of seagrass vary depending on the species, even within the same settling site (Buia and Mazzella, 1991). Buia and Mazzella (1991) analysed the three most spread seagrass species in the Mediterranean Sea over almost a decade. They observed that flowering occurs for *Cymodocea nodosa* in April-May (following the minimum water temperature), for *Zostera noltii* in July, while for *Posidonia oceanica* in September or November depending if the meadow is located respectively at water depths shallower or deeper than 15 m. For *Cymodocea nodosa* germination was observed after 2 months of anthesis (flower expansion), 2 of fruit growing and 8-10 of dormancy, while it occurred for *Posidonia oceanica* after 8 months subdivided into anthesis and fruit maturing. *Zostera noltii* showed fruiting in August, and *Posidonia oceanica* did not show dormancy.

Seagrass can be defined as clonal rhizomatous plants, which are composed of modules as rhizomes, leaves and roots (Hemminga and Duarte, 2000). According to Hemminga and Duarte (2000) these modules are repeated for several units which compose the meadow. Each unit called ramet also hosts fruits and flowers, depending on the moment of the plant life cycle. In the seagrass architecture the rhizomes can extend below the sediments and be horizontal and vertical, their function is of connecting extending and integrating the clones. The rhizomes can have a different level of flexibility which decreases with the size of seagrass species and increases with longevity. For instance, *Posidonia oceanica* is characterized by ligneous almost woody rhizomes. The leaves

of most seagrass species are long, thin and narrow, and their size varies among species. For instance, *Halophila* is formed by leaves shorter than 1 cm while species as *Zostera asiatica* present leaves longer than 1 m. Leaf fibres of *Posidonia oceanica* can form balls rolled by waves that deposit on Mediterranean beaches.

The necromass associated with seagrass decomposition can stay within the plant meadow itself or interact with other marine and dune ecosystems (Boudouresque et al., 2015). Part of the necromass once released by the meadow can stay on the seafloor nearby the meadow and floating can be transported by coastal hydrodynamics due to wave storms and currents (Simeone and De Falco, 2012). When these deposits reach the shore can form large seagrass berms. The edification of banquette was reported to be higher successively to storm events, generally in winter (Mateo et al., 2003) and to be greater for exposed beaches with respect to the sheltered coastlines (Simeone and De Falco, 2012). Using samples collected at two locations along the beach profiles, on three Mediterranean wave-dominated beaches, Simeone and De Falco (2012) found that on the shoreface the banquette is mostly composed by leaves, while on the backshore by a mixture of sediments and leaves. The authors also report that the contribution of the rhizomes to the banquette composition is restricted and limited to the exposed (more energetic) study sites. The seagrass wrack can represent 50.7 % and 70 % of the yearly meadow production of biomass and carbon respectively (Mateo et al., 2003).

2.2.4 Seagrass and Coastal Hydrodynamics

The marine vegetation and their beach-cast litter, therefore, interact with the hydrodynamic and morphodynamic processes treated herein. Although several studies were conducted on seagrass interaction with coastal hydrodynamics, the influence of seagrass beach litter on the swash process is mostly neglected (only qualitatively described or suggested) and the debate on how and in which terms the seagrass contributes in protecting the coastline from erosion remains open. Contrasting opinions still exist.

Firstly, an aspect largely investigated is the influence of vegetation on coastal hydrodynamics particularly on wave reduction while propagating on marine vegetation like seagrass meadows or mangrove forests. Several studies were performed in laboratory (Fonseca and Cahalan, 1992; Luhar et al., 2010; Maza et al., 2015; John et al., 2016) in the field (Luhar et al., 2013; Infantes et al., 2012) and by modelling approaches (Guannel et al., 2015; Van Rooijen et al., 2016). Useful parametrizations of wave dumping attributed to different vegetation types and different hydrodynamics/vegetation interaction conditions were found. Formulations of vegetation effect on the incident and infragravity waves as well as wave set up were also included in storm impact models as XBeach (Van Rooijen et al., 2016). An approach for the quantification of hazard reduction services provided by vegetation was also proposed (Guannel et al., 2015). The

submergence ratio of the seagrass, the width of the meadows, the vegetation density distribution and the biomass resulted between the main factors influencing wave attenuation, which increases with meadow width and strongly decreases with submergence ratio (Maza et al., 2015; John et al., 2016). The closer the vegetation is to the water surface the greater the wave dumping, the wider and the denser the meadow is, over which wave propagates, the higher the wave reduction. Preliminary laboratory studies on the influence of such parameters on the wave runup were also realized, resulting with wider meadow inducing a higher reduction of wave runup (John et al., 2016), and an increase in relative plant height resulting in a diminishing of relative runup for emergent vegetation models (John et al., 2018). An integrated modelling approach was proposed by Guannel et al. (2015) for quantifying the effect of vegetation on coastal hazards reduction. Using two case studies (seagrass meadow and mangrove forest) they demonstrated that the vegetation can lower the total water level and reduce the beach erosion. Furthermore, the authors proposed to include the effect of vegetation on wave set up and incident swash by modifying the runup formulation of Stockdon et al. (2006), assuming that the influence of vegetation has a limited impact on the infragravity swash component.

The second aspect concerning the interaction between coastal hydrodynamics and seagrass meadow regards the effect of the flow on the plant settling within the shoreface. The relationship between hydrodynamics and seagrass meadow spatial distribution on the shoreface was therefore studied (Infantes et al., 2009; Vacchi et al., 2010; Ruju et al., 2018). The limiting factors for the lower limit of the seagrass meadow are mainly attributable to the light availability (Duarte, 1991). In the case of *Posidonia oceanica* it was shown to be located at depths between $15 - 23\ m$ for high turbidity levels and at $45 - 48\ m$ for high water transparency (Boudouresque et al., 2012). In contrast, the upper limit (the one towards the coast) is related in the literature to several factors including substratum type and hydrodynamic constraints. Both field and numerical modelling experiments were performed, indicating that some thresholds in the wave-particle orbital velocities at the bottom during storms ($0.4m/s$, $0.8m/s$), and current velocities, can be related to the installation or not of the meadow (Infantes et al., 2009; Ruju et al., 2018).

A third aspect relating coastal hydrodynamics with seagrass investigates the beach-cast seagrass litter, which can become of interest considering the large amount of deposition which can occur on beach face, berm, and backshore. Even though the beach-cast seagrass litter received large interest (Jeudy de Grissac, 1984; Jeudy de Grissac and Audoly, 1985) in Simeone (2008), and morphological, physical features were largely investigated (Simeone and De Falco, 2012; Oldham et al., 2014; Mateo et al., 2003), the attempts to relate this morphology to the coastal hydrodynamics are still limited (Mateo et al., 2003; Simeone, 2008; Simeone and De Falco, 2012; Simeone et al., 2013;

Gómez-Pujol et al., 2013). Mateo et al. (2003) propose a first schematics describing formation-destruction of banquette. The authors describe that wave action at the base of banquette produces erosion until collapse occurs. Oldham et al. (2014) suggests that erosion of beach wrack is in addition possibly due to an increase in floating material from the banquette after a period of drying.

Focusing on this third aspect, in the literature, there are contrasting opinions, on the role of deposited beach wrack in beach protection. On one hand, it is clearly stated that it protects the beach from erosional processes (Boudouresque and Jeudy de Grissac, 1983; Simeone, 2008; Green, 2003). The World Atlas of seagrasses reports, from a study in Kenya, that beach-cast can influence the erosional processes associated with wave action and swash, contributing to beach stability (Green, 2003). The same concept is found in Nordstrom and Jackson (2012), where it is suggested that beach wrack can influence wave runup, however, quantitative studies are still missing. On the other hand, other studies state that vegetation berm does not largely influence the eventual erosional process in case of storms and that its role in beach protection should be re-considered (Gómez-Pujol et al., 2013).

From a review of the literature, it seems that the behaviour of beach-cast efficiency in reducing wave action is differentiated between low and high energy conditions, between exposed and sheltered beaches (Nordstrom and Jackson, 2012; Simeone, 2008; Simeone and De Falco, 2012). In Nordstrom and Jackson (2012) low energy beaches seems to be more highly responsive to the protection function of beach-cast litter, due to the mild wave conditions. Other studies reviewed that in less sheltered beaches the banquette plays a role in reducing wave energy during storm (Vacchi et al., 2017). In fact, also a large amount of wrack material was reported to be removed from the shoreface of a Mediterranean beach by waves, also during winter/spring storms (Simeone and De Falco, 2012). However, the definition of low and high energy beaches is not unequivocal and clear, so that a high level of uncertainty remains.

From the literature review (e.g. Gómez-Pujol et al. (2013); Vacchi et al. (2017)) it appears that still, gaps exist on 1) the dynamics of deposition and erosion of banquettes (beach wrack morphodynamics) and 2) on its role of beach protection. Furthermore, it appeared that not many studies were performed (Jeudy de Grissac, 1984; Jeudy de Grissac and Audoly, 1985; Mateo et al., 2003) in Gómez-Pujol et al. (2013) and they were mainly of qualitative nature. These gaps in the literature might be connected to the lack of studies on the interaction of seagrass beach-cast and waves, more precisely with the swash hydrodynamics. The morphodynamics of banquette was connected with storms events and their timing in a limited number of attempts (Gómez-Pujol et al., 2013; Simeone et al., 2013). However, the influence that seagrass beach-cast litter has on wave runup and its quantification are completely ignored in the literature. Moreover, an

overall view of including these morphodynamical process in a more comprehensive vision of feedbacks between wrack and swash fluid as representative of a self-organization process has not considered and discussed yet. It is clear that a number of gaps exist in the literature of morphodynamics of seagrass beach-cast litter and its interaction with the swash zone process.

2.3 Coastal Monitoring, Modelling and Managing

Knowledge-based management strategies can induce a more correct management of the coast. Application driven investigations lead scientists to influence policy from the local to the international level (Wainwright and Mulligan, 2012). Researchers can collaborate with practitioners contributing to enhancing the coastal processes comprehension where gaps in the literature are still present. The knowledge of coastal processes can be reinforced by linking observations of the natural processes in the field with advanced modelling techniques, devoted to a correct and environmentally respectful management of marine and coastal areas.

2.3.1 Field Observations of Swash Excursion

The swash-zone hydrodynamics and particularly the swash excursion has been largely studied firstly by the means of resistance wires (Guza and Thornton, 1982) and later by the observation of shoreline motion through video systems (Holman and Guza, 1984; Holman and Sallenger, 1985; Holman, 1986). The two method were compared in several works (Holman and Guza, 1984; Holland et al., 1995), with Holland et al. (1995) findings correspondence between the video−based estimates and measurement obtained by wires located very close to the bed.

More recently the proliferation of runup measurements exist as a result of video monitoring experiments (Ruessink et al., 1998; Ruggiero et al., 2001, 2004; Stockdon et al., 2006; Guedes et al., 2011; Senechal et al., 2011; Guedes et al., 2012; Vousdoukas et al., 2009, 2012; Poate et al., 2016). Even though most measurements of swash excursion are obtained on oceanic sandy beaches with large incoming waves, exceptions exist. For instance gravel beaches were investigated by Poate et al. (2016) obtaining also a new formulation of wave runup for gravel beaches, as well as field experiments were performed in the Mediterranean Sea where Vousdoukas et al. (2009) instigated three sediment-starved pocket beaches, under ordinary wave conditions (not focussing on storm events).

Swash excursion field experiments mainly include video observations of swash oscillations, coupled with wave and beach surveys data. Additionally contextual current, sediment transport and meteorological data along with other environmental observations can be collected, however, measurements of wave swash in correspondence of

underwater vegetation or its deposits on the beach seems still missing in the literature. This type of field experiments is highly needed for management applications in relation to coastal hazards and climate change. In fact, Guannel et al. (2015) in their modelling framework for quantifying the effect (for coastal communities) of hazards reduction produced by vegetation, express the urgency of field measurement of runup with the presence of vegetation. In fact they found that field datasets are missing for validating their modified version of Stockdon et al. (2006) runup formula which include the vegetation effect.

2.3.2 Machine Learning for Wave Swash Modelling

The field data represents valuable information essential also for modelling coastal processes, depicting the reality which the models attempt to reproduce with an approximation. Their utility is both related to the validation of existing models and to the creation of new one. However, the observations on the field present a number of limitations. Firstly, they are limited both in time and space, since the field campaigns can be programmed for a limited time and a restricted area. Secondly, the hostility of the marine environment makes difficult and expensive to operate at sea, introducing a resource limitation to the research campaigns. Furthermore, researchers have to rely on natural events without having control of the boundary conditions. The models can fulfil to those limitations, however introducing other uncertainties, due to their attempt to reproduce a real process without being able to represent its entire complexity (Roelvink, 2011). Models can be applied for the purpose of environmental protection when ensuring a critical and precise interpretations of their results (Wainwright and Mulligan, 2012), also testing them against field measurements.

The modelling of the environmental processes in general can be differentiated into several types: mathematical (physics-based), data-driven, conceptual, explanatory (simulation) and physical models. Once data are collected in the field, the information contained in the data can be further explored to gain knowledge and to model the observed phenomenon. The techniques used for these purposes are defined data-driven approaches. Between the data-driven approach available, Machine Learning (ML) has demonstrated extraordinary potential. Many different data-driven techniques fall under the purview of ML (e.g., decision trees, artificial neural networks, Bayesian networks, and evolutionary computation), all of which have shown applicability in coastal settings (e.g., Pape et al. (2007); Knaapen and Hulscher (2002); Dickson and Perry (2016); Yates and Cozannet (2012)). Previous Machine Learning work has focused on predicting runup and swash, but only for engineered structures, impermeable slopes, and/or for laboratory experiments (e.g., Kazeminezhad and Etemad-Shahidi (2015); Bonakdar and Etemad-Shahidi (2011); Bakhtyar et al. (2008); Abolfathi et al. (2016) and not on

natural beaches. Only Vousdoukas et al. (2011) used artificial neural network (ANNs) for shoreline contour elevation (which includes the wave runup), on a natural beach in Portugal.

Between the ML existing techniques Genetic Programming (GP) is a population-based approach based on evolutionary computation (Koza, 1994). GP has been largely adopted showing good results in coastal applications (Goldstein et al., 2013; Goldstein and Coco, 2014; Tinoco et al., 2015). The predictors produced by GP techniques showed overall to reduce the errors compared with classical-regression-based predictors. Even though ML has shown high potential as a data-driven techniques for modelling coastal process, it has not being used for obtaining predictors of wave swash on natural beaches before Passarella et al. (2018b).

2.3.3 Coastal Management and Good Practices

Several actions have been taken for trying to modify coastal morphology according to human needs (Masselink et al., 2012a), with the consequent modifications or destruction of natural landforms (Nordstrom, 2013). Even though coastal erosion is a natural geological process fundamental of the formation and maintenance of the beaches (Short, 2012) humans largely focussed their actions at the coast for fighting coastal erosion. In the 90s coastal management was mostly devoted to "hard engineering" (e.g. breakwaters) interventions, recently shifting towards "soft" intervention (e.g. beach nourishment) Masselink et al. (2012a).

Furthermore, a number of bad practices can be identified attributed to ignorance or economic interests in the exploitation of the natural beach resource. In fact, coastal areas represent a rising economic sector in the global economy with a incoming of about 2 billion of dollars per day (Silva et al., 2007). The carrying capacity of a beach system can be overcome (Da Silva, 2002) and coastal tourism can be responsible for severe coastal issues and environmental impact (Silva et al., 2007). Coastal landforms alterations are often a consequence of heavy visitation, tourism, deforestation, pedestrian and vehicle trampling, military use, structures and parking building, beach cleaning and beach wrack removal (especially by heavy mechanical vehicles) on dunes, backshore, berm and beach face (Eastwood and Carter, 1981; Anders and Leatherman, 1987; Demuro and De Falco, 2010, 2015; Wiedemann, 1984). Beach wrack removal resulted highly impacting as it is a spread practice (Duarte, 2004; Nordstrom, 2013). The beachcast removal was analysed in the Mediterranean, for instance as exemplification case study in Sardinia Island for the year 2004 resulting in a total of $106,180\ m^3$ being removed from 44 beaches, generally using heavy vehicles (Simeone, 2008).

However, these structures, actions and bad practices excite a strong impact on coastal morphodynamics, and alternative coastal management procedures exist. In order to

limit the human impact, especially due to heavy visitation, new management actions and good practices were suggested. For instance, the building of elevated boardwalks, fencing sensitive areas, avoid beach cleaning with seagrass beach-cast litter removal especially with heavy vehicles, realignment of beach use and educating stakeholders or visitors. (Carlson and Godfrey, 1989; Demuro and De Falco, 2010, 2015). The beach is also equated by the authors, to a living organism of which the single constitutive parts play functions essential for the correct working of the whole beach system. In this vision, all the element from lagoons to the underwater seagrass meadows require the same safeguard and protection in a systemic coastal management view (Demuro and De Falco, 2010, 2015; De Muro et al., 2017b). Good practices should also be sustained by the scientific knowledge based on field measurements, of morphodynamical processes as well as accompanied by information and participation of stakeholders (Carlson and Godfrey, 1989; Demuro and De Falco, 2015).

Recent studies show that managing strategies should include the peculiarity of the presence and role of ecosystems and habitats as lagoons, seagrass, mangroves and salt marshes (Duarte, 2004; De Falco et al., 2008; Barbier et al., 2008; Demuro and De Falco, 2010; Simeone et al., 2013; Möller et al., 2014; De Muro et al., 2017b). Cartography can supplement monitoring and management practices representing coastal hazard vulnerability (Perini et al., 2016) and taking into account the presence of seagrass as proposed for the Mediterranean Sea and Australian case studies (Tecchiato et al., 2016; De Muro et al., 2018, 2017b). Furthermore, the idea that conservation and human use of coastal habitats could not coexist should be re-evaluated (Barbier et al., 2008). In fact, it was recently shown how the use of ecosystem-based management could result in an excellent compromise (Barbier et al., 2008).

Seagrass meadow in the shoreface was shown to decrease globally, with a rate of $110km/yr$ since 1980 (Waycott et al., 2009). Seagrass meadow and vegetation beach-cast litter (banquette) deposited on the beachface, beach, and backshore have been largely studied also for management purpose, being often artificially removed (Gómez-Pujol et al., 2013; Simeone et al., 2013; Simeone and De Falco, 2013). However, the debate about its role in shoreline protection from erosion is still open. Furthermore, a lack of field quantitative studies on seagrass litter influence on swash process seems to arise. This lack of knowledge may be fundamental for supporting knowledge-based, ad hoc-planned coastal management strategies.

2.4 Gaps in the literature

In this section the gaps identified in the literature are listed below:

- Although a number of parametrizations of swash excursion exist, depending on

different combinations of beach and wave characteristics, their universality has not been extensively assessed. It is not clear if existing swash formulas are applicable to a wide range of wave conditions and beach types.

- The most largely adopted empirical parametrization of wave runup still predict with large errors and important underestimations, especially during extreme storms, raising the interest in proposing new formulations of wave swash.
- Although machine learning techniques have demonstrated to have a high potential in modelling nearshore processes, they are not yet being used for finding predictors of wave swash on sandy beaches.
- The influence of the beach slope on the infragravity component of the swash is still an open question discussed controversially by several authors.
- Even though the importance of seagrass in protecting the coast from hazards such as erosion or flooding is largely stated in the literature (even if the debate is still open), the influence that seagrass beach-cast, deposited on the beachface has on the swash process and wave runup has not been measured and quantified yet.
- The dynamics of deposition and erosion of banquettes (beach wrack morphodynamics) in relation with swash process, beach type, storm intensity and timing is not clear.
- Which could be the implications of the lack of knowledge related to the seagrass beach-cast litter/swash process interaction for coastal management?

Chapter 3

METHODOLOGY

In order to facilitate coastal protection, management and hazards mitigation, coastal hydrodynamic and morphological factors are investigated by a multidisciplinary approach which combines field experiments and data-driven techniques.

3.1 Preparatory Case Studies

Part of the focus of this PhD investigation was reached by the literary review treated in Chapter 2 and additionally by two preliminary case studies. The preliminary case studies highlighted some gaps in the literature and suggested the field location for the experimental part of the present work.

The two preparatory case studies, performed within the framework of the NEPTUNE project, investigated two counterpoised beach systems in the Western Mediterranean Sea (Fig. 3.1). One more naturally preserved (case 1) and the other strongly subject to anthropic pressure (case 2).

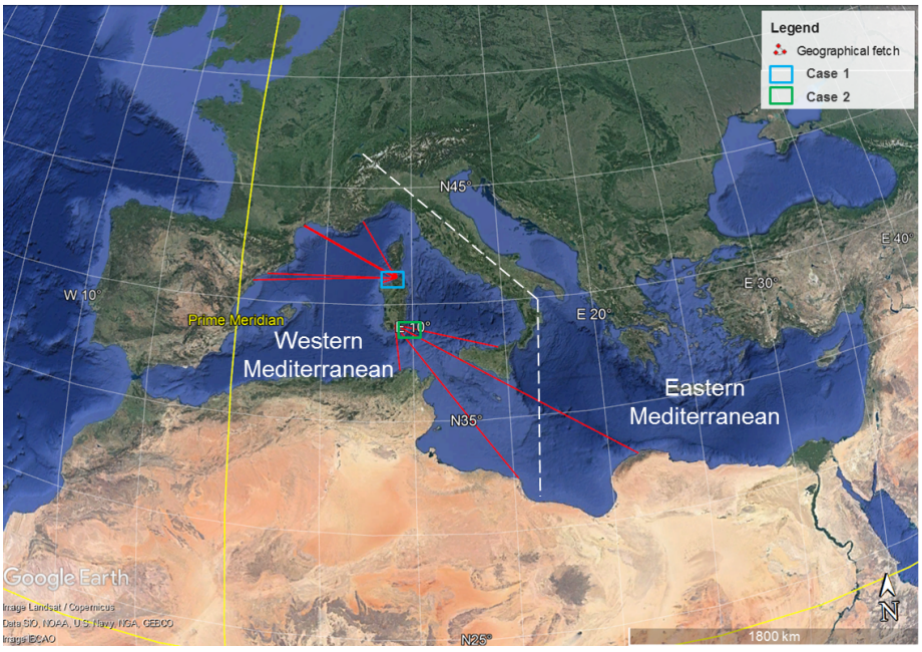

Figure 3.1 Location of two preparatory case studies in the Western Mediterranean Sea.

The studied areas can be classified as microtidal wave-dominated environments because the dominance of waves, which represents the main input of energy in the coastal systems according to the classification adopted by Masselink et al. (2012a) from the works of Davies (1977) and Davis Jr and Hayes (1984). Both areas of study are characterized by a large *Posidonia oceanica* meadow within the shoreface, in one case more intact (case 1) and in the other more degraded (case 2). The works, which integrated morphological, sedimentological, bathymetric, facies, ecological and hydrodynamic data, furnished geomorphological maps, also applicable to coastal management which were published in De Muro et al. (2016, 2018). Both cases are located in Sardinia Island, but with two highly different expositions to storm events (e.g. geographical fetch in Fig. 3.1) and human pressures. While the first (case 1) is located in the north of the island exposed to high northwesterly stormy conditions and low density of population, the second is part of the beach system of the Gulf of Cagliari, surrounded by strong industrial and human activity, with ≈ 500000 inhabitants and exposed to generally lower and less frequent southeasterly wave storms.

The studies reported interesting links between the meadow of a particular species of seagrass (*Posidonia oceanica*) and the hydrodynamics, the human activity and the coastal management, which inspired part of this PhD research. Furthermore, during the field campaigns performed for case study 2, high quantities of banquette (seagrass beach wrack) was reported to be deposited in Giorgino beach (Fig. 3.2), suggesting that the Gulf of Cagliari may be an appropriate area for studying this phenomenon.

Figure 3.2 Seagrass beach-cast (mainly *Posidonia oceanica*) deposition on Giorgino Beach, Gulf of Cagliari, Western Mediterranean, during the field campaigns of preparatory case study 2. Picture courtesy of the Coastal and Marine Geomorphology Group of the University of Cagliari.

A review of the literature was therefore performed on the subject (Chapter 2), finding interesting gaps, regarding the role of seagrass wrack in protecting the coast from erosion and its interaction with wave swash phenomenon (Section 2.2.3 and 2.2.4).

3.2 Comparison of Existing Wave Swash Formulas

Another aspect investigated in this PhD thesis regards the wave swash process and its formulation, being extensively included in coastal hazard and vulnerability assessment framework (Stockdon et al., 2007; Serafin and Ruggiero, 2014).

In Chapter 4 existing vertical swash formulas (total, incident and infragravity) are tested for evaluating their universality on a wide range of forcing and environmental conditions. The dataset used for testing the formulas is a newly compiled dataset from 13 published swash experiments worldwide, 10 experiments from Stockdon et al. (2006), the others from Guedes et al. (2011, 2012), Guedes et al. (2013) and Senechal et al. (2011). Section 4.2 provides details on data and methods adopted, the new compiled dataset includes swash excursion from video observations (S_{Tot}, S_{inc}, S_{Ig}) coupled with offshore wave data (H_0 and T_p) and beach slope (β) from beach surveys. This dataset contains the most extreme conditions recorded for a runup experiment (Senechal et al., 2011) and includes beaches ranging from dissipative to reflective. Two total, 3 incident and 8 infragravity empirical published formulas are tested using different error metrics, details are reported in Section 4.2.1. The literary review (Section 2.1.4.1) and the results of Chapter 4 inspired the research performed in Chapter 5. In fact, it was found that existing swash formulas still result in big errors with scatters which increase for large swash excursion. The need for more accurate prediction of wave runup becomes critical, especially for coastal management and hazards applications when large swash events are more significant.

3.3 New Formulation of Wave Swash by Machine Learning

Between the available modelling approaches, in this work, a data-driven machine learning (ML) technique was selected for the problem of formulating swash elevations on natural beaches, reducing the prediction errors while maintaining a physical mean. The use of ML has rapidly escalated for its ability to automatically learn from the dataset provided (Domingos, 2012). The ML computer science techniques, with origins in artificial intelligence, are able to model complex processes from an empirical dataset. ML has found large applicability to natural science such as ecology (Olden et al., 2008) and specifically to coastal processes studies (Pape et al., 2007; Knaapen and Hulscher, 2002; Dickson and Perry, 2016; Yates and Cozannet, 2012; Goldstein et al., 2013; Goldstein and Coco, 2014; Tinoco et al., 2015) overcoming traditional methods.

ML consists of a number of statistical techniques including supervised learning approaches which from a given set of input and output, act to model complex phenomena searching for relationships between the variables (Olden et al., 2008). For instance, classification and regression trees have found large applicability in case of hierarchical interaction between variables, in which parent and child nodes alternate by recursive partitioning (Olden et al., 2008). Artificial neural network is a modelling approach based on the biological nervous system approach to solving a complex problem. Its innovative structure is composed of numerous elements (neurons) interconnected for working together for solving a problem. The input and output consist of the independent and dependent variables respectively (Olden et al., 2008). Evolutionary computation includes several stochastic optimization methods which find their origins in the evolution process of natural systems, such as genetic algorithm, genetic programming (GP), evolutionary programming and simulated annealing (Olden et al., 2008).

In Chapter 5, among the existing supervised learning approaches, GP (Section 2.3.2 and 5.3.1) was chosen for proposing new formulations of vertical swash. The use of this evolutionary computation technique also permitted to enhance the knowledge of the physical process of wave swash itself. The evolutionary technique of GP allows computers to find insightful relationships between variables involved in a natural process, such as wave swash, learning at each iteration from an experimental dataset. The process of GP can generally be divided into four steps: 1) an initial population of solutions for the problem is produced. For regression tasks such as developing a predictor for swash, the initial population of candidate solutions is in the form of equations (encoded as a tree or graph with a predefined mix of variables, operators and coefficients). For step 2 of the routine the solutions are all compared to the training data to determine 'fitness' using a predefined error metrics; 3) the best solutions that minimise the error are proposed and the worst solutions are discarded; 4) new solutions created through 'evolutionary' rules (crossover via reproduction and mutation) and are added to the population of retained solutions. Steps 2 through 4 are repeated until the algorithm is stopped. The method adopted here has successfully demonstrated to be able to automatically reproduce, form the only input of measured experimental data, Lagrangians and other laws regulating different physical processes as oscillators and pendula (Schmidt and Lipson, 2009), finding large recognition from the scientific community. The ability of the algorithm to discover analytic relations without any information regarding the physics or the geometry of the problem has suggested the adoption of the software based on this method (Schmidt and Lipson, 2018) for the application necessary to this chapter, of retrieving swash formulas from a collected dataset. Only the meaningful information in the dataset should be retained from the algorithm which is based on a principle for identifying nontriviality (Schmidt and Lipson, 2009).

The data (Section 5.2) and method (Section 5.3) adopted for deriving two new pre-

dictors of total and infragravity swash is illustrated in Chapter 5. While details on the training, validation and testing phases are given in Section 5.3.2. Literary review and findings of this chapter also highlight that the parameters used for swash formulation are still limited and that neither experimental data nor modelling approaches exist to consider wave runup in case of seagrass beach-cast litter. This gap identified in the literature is investigated in Chapter 6.

3.4 Wave Swash and Beach-cast Litter Field Experiment

Chapter 6 illustrates a field experiment performed for studying the interaction between the waves moving uprush and backwash on the beach face and the deposition of seagrass beach-cast litter. The field experiment was designed for measuring swash oscillations, coastal waves and environmental conditions with the contrasting conditions of presence/absence of seagrass deposition on a wave-dominated urban beach in the Western Mediterranean Sea (Cagliari, Sardinia, Italy).

The experimental design is reported in Section 6.3.1. The details on the methodology adopted for the new video-monitoring station setting, image calibration and rectification are given in section 6.3.1.1, while the information about how the environmental conditions were monitored during the experiment (e.g. wave, beach morphology and cross-shore elevation) can be found in Section 6.3.1.2. The method adopted for recording the wave swash is explained in Section 6.3.2. The wave swash was obtained manually digitalizing the shoreline oscillations from time stacks images. The ad hoc programmed Matlab routine then converted the horizontal swash time series obtained into vertical swash thanks to the measured foreshore slope. Spectral analysis is finally applied to calculate from the energy spectrum the vertical wave swash, including a frequency partition for the incident and infragravity components. The methodology adopted (from the video-monitoring station installation, calibration, geo-rectification to the wave swash measurements from image analysis) follows approaches largely adopted in the literature (Holman, 1986; Holland et al., 1997; Ruessink et al., 1998; Ruggiero et al., 2004; Stockdon et al., 2006; Archetti and Zanuttigh, 2010; Vousdoukas et al., 2011; Senechal et al., 2011; Taborda and Silva, 2012).

Chapter 4

AN ASSESSMENT OF SWASH EXCURSION PREDICTORS USING FIELD OBSERVATIONS

The main findings of this chapter have been published in Passarella et al. (2018a).

4.1 Introduction

Wave-induced swash is the oscillation of the water edge up (uprush) and down (backswash) on the beach face. The oscillation occurs around the mean of the water level time series (induced by wave action and measured above the still water level), defined as wave setup. The sum of vertical swash and setup determinates the wave runup (Holman, 1986; Stockdon et al., 2006). Since the pioneering work of Guza and Thornton (1982) the contribution of incident (high frequency, $f > 0.05$) and infragravity (low frequency, $f < 0.05$) motion is often considered separately when studying swash (e.g. Ruessink et al. (1998); Ruggiero et al. (2004)).

Chardón-Maldonado et al. (2016), in their recent review paper on swash hydrodynamics, highlighted the importance of studying the swash zone because it represents a buffer region for hydrodynamic forcing where energy is released and sediment transport (accretion and erosion) occurs. During swash oscillations, the rapid flow sets a large amount of sediments in motion so that understanding and prediction of swash excursions is critical for sediment transport studies. Furthermore, the interest in studying this zone increased over the last decades since it often hosts infrastructure, private properties and recreational activities.

Wave swash is a critical parameter when trying to study or manage coastal hazards, in fact waves contribute extensively to storm, hurricanes-induced extreme water levels, which may end in inundation, beach and dune erosion (Bosom and Jiménez (2011); Stockdon et al. (2007); Serafin et al. (2017)). Swash excursion parametrizations (as component of wave runup) are usually included in costal hazard and vulnerability assessment framework (e.g. Stockdon et al. (2007); Serafin and Ruggiero (2014)).

Although a number of parametrizations of swash excursion exists, depending on different combinations of beach and wave characteristics, their universality has not been extensively assessed. This is possibly related with the few tests of the formulas per-

formed on conditions other than those for which they were developed.

Despite recent studies show that the spectral signature of swash (infragravity and incident) is different for beach type (Hughes et al., 2014) it is not clear if swash formulas are applicable to a wide range of wave conditions and beach types. A parameter summarizing the relative beach-wave conditions is the Iribarren Number:

$$\xi_0 = \frac{tan\beta}{\sqrt{(\frac{H_0}{L_0})}} \tag{4.1}$$

where β is the beach slope, H_{S0} is the deep water significant wave height and L_0 the wavelength. The Iribarren parameter is also used to classify beaches according to the following scheme: dissipative (D) for $\xi_0 < 0.23$, reflective (R) for $\xi_0 > 1$ and intermediate (I) for $0.23 < \xi_0 < 1$ (Short, 1999a). The following question is therefore still open: it is possible to use parametric swash formulas for predicting swash excursion, knowing the error which is likely to be committed?

While existing wave runup formulations were recently extensively tested, swash formulas received relatively less interest (e.g. Ruggiero et al. (2004)). Several works focused on the evaluation of existing runup formulas (e.g. Atkinson et al. (2017); Vousdoukas et al. (2012); Cohn and Ruggiero (2016)). For instance, Atkinson et al. (2017) used swash data from 11 intermediate beaches in Australia, for assessing wave runup predictor as the one from Stockdon et al. (2006), highlighting the criticality of formulas performance for coastal hazards and management applications. They verify the accuracy of 11 runup predictors obtained from both field and laboratory data finding that the models retrieved from field data are more accurate. They also found a high variability among models predictions with a MSE of the order of 25%. Among the tested models Holman (1986) and Vousdoukas et al. (2012) resulted in the most accurate. They conclude that for coastal management applications it is recommended to calibrate the runup models on the studied beach, especially if not tested on a dataset including extreme events as in their case. The test of swash or runup predictors on a dataset which includes field measurements of extreme events is therefore highly valuable and recommended when studying environmental protection hazards and management of the coasts.

Overall, an extensive assessment of swash formulas using multiple field datasets is still missing. This chapter aims to test 13 published swash formulas to assess the reliability of each predictor on a wide range of beach types and wave conditions including extreme storms.

4.2 Data and Methods

Shoreline motion monitoring is a largely accepted method for studying the swash-zone hydrodynamics (Holman and Sallenger, 1985). The data used in this chapter are obtained mainly from video observations of swash excursions, coupled with wave data and beach surveys (for details on the methodology the reader is referred to the original works in which the data were collected or analysed: Stockdon et al. (2006); Guedes et al. (2011, 2012, 2013); Senechal et al. (2011).

4.2.1 Swash Formulas and Testing Data

The test of 13 vertical swash formulas from the existing literature (2 for total swash, 3 for incident and 8 for infragravity swash, Table 4.1) is performed against 13 published field experiments (636 swash measurements). The data used in this chapter includes a wide range of environmental conditions, in Figure 4.1 (foreshore slopes 0.01-0.16, offshore significant wave heights 0.4-6.4 m, peak periods 3.7-16.4 s, total swash 0.24-3.3 m, infragravity swash 0.24-2.37 m and incident swash 0.04-2.86 m) on beaches spreading from dissipative to reflective. The above-mentioned dataset includes extreme events, which ensure a test of formulas performance in the most critical cases for coastal hazards and management applications (e.g. flooding).

Table 4.1 Swash formulas tested, total (S_{Tot}), incident (S_{inc}), infragravity (S_{Ig}). Interval of environmental parameters during experiment

Swash Formula (reference)	ξ (Beach Type)	β	Hs (m)	Tp (s)
$S_{Tot\_St} = \sqrt{(S_{in\_St})^2 + (S_{Ig\_St})^2}$ (Stockdon et al., 2006)	0.07-3.22 (D,I,R)	0.01-0.16	0.4-4.1	3.7-17
$S_{Tot_{GT}}(cm) = 3.48\,(cm) + 0.71H_S(cm)$ (Guza and Thornton 1982)	0.3-1.4 (D)	0.03- 0.051	0.5-1.5	-
$S_{in\_St} = 0.75\beta\sqrt{H_S L}$ (Stockdon et al., 2006)	0.07-3.22 (D,I,R)	0.01-0.16	0.4-4.1	3.7-17
$S_{in\_Rg01} = 11.4\beta - 0.01$ (Ruggiero et al., 2004)*	(D)	0.005-0.047	1.4-4.6	5-17
$S_{in\_Rg02} = 0.11H_S - 0.03$ (Ruggiero et al., 2004)*	(D)	0.005-0.047	1.4-4.6	5-17
$S_{Ig\_St} = 0.06\sqrt{H_S L}$ (Stockdon et al., 2006)	0.07-3.22 (D,I,R)	0.01-0.16	0.4-4.1	3.7-17
$S_{Ig\_Rs} = 0.18\,H_S + 0.17$ (Ruessink et al., 1998)	0.068-0.341 (D**)	0.009-0.032	0.3-4.8	4.8-10.8
$S_{Ig\_Ho} = H_S(0.5\xi + 0.34)$ (Holland, 1995)	(D)	0.03-0.043	0.59- 0.87	-
$S_{Ig\_RG} = H_S(0.07\,\xi + 0.65)$ (Raubenheimer and Guza, 1996)	(D,I)	0.02-0.11	0.45-1.34	-
$S_{Ig\_HS} = H_S(0.53\,\xi + 0.09)$ (Holman and Sallenger, 1985)	0.5-3.5 (I,R)	0.1	0.4-4	6-16
$S_{IgRg01} = 9.7\,\beta\, + 1$ (Ruggiero et al., 2004)*	(D)	0.005-0.047	1.4-4.6	5-17
$S_{IgRg02} = 0.33\,H_S + 0.33$ (Ruggiero et al., 2004)*	(D)	0.005-0.047	1.4-4.6	5-17
$S_{Ig\_Sn} = 0.05\sqrt{H_S L}$ (Senechal et al., 2011)***	0.49-0.9 (I)	0.05-0.08	1.1-6.4	11.2-16.4

** field data used for retrieve the formulas are presented in Ruggiero et al. (2001).**mainly dissipative only one exception of $\xi > 0.23$.****referred to the swash zone slope (peculiar case of Senechal et al. (2011) recorded dissipative conditions of the surf zone and intermediate of the swash zone.

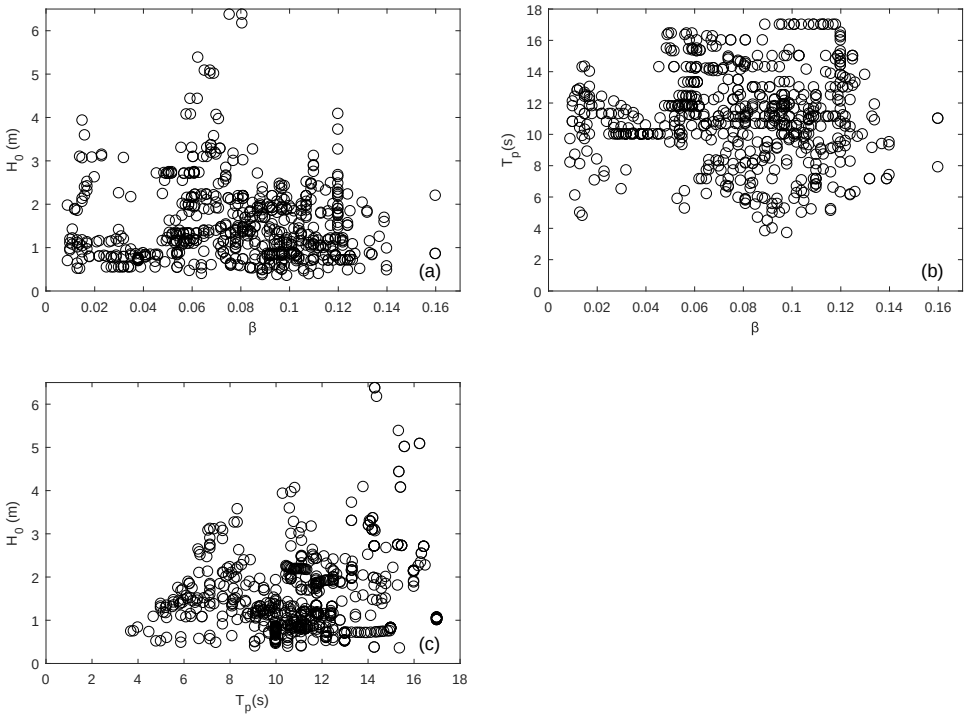

Figure 4.1 Environmental forcing conditions: (a) significant wave height versus beach slope; (b) wave peak period versus beach slope; (c) significant wave height versus wave peak period.

The formulas assessed here in some cases have a similar shape (with the only differences found in the coefficients), especially for infragravity swash. For instance, the formulas S_{IgSt} and S_{IgSn} are exactly the same with a slight difference in the coefficient respectively equal to 0.06 and 0.05, for which$\sqrt{H_0 L_0}$ is multiplied. S_{IgHo}, S_{IgRG},

S_{IgHS} are also similar depending upon H_s and ξ which are proportional to the infragravity swash excursion. S_{IgRs} and S_{IgRg02} are both directly proportional to H_0 with coefficients of proportionality and constants which varies: 0.17, 0.18 for the former and 0.33, 0.33 for the latter.

4.2.2 Error Metrics

Three error metrics are used for evaluating the discrepancy between predicted and observed swash excursions: the Mean Squared Error (MSE, Eq.(4.2)), the Root Mean Square Error (RMSE, Eq.(4.3)), and the Maximum Error (MaxE, Eq.(4.4)).

$$MSE = \frac{1}{N}\sum_{i=1}^{N}(y_i - x_i)^2 \tag{4.2}$$

$$RMSE = \sqrt{\frac{1}{N}\sum_{i=1}^{N}(y_i - x_i)^2} \tag{4.3}$$

$$MaxE = max_{i=1...N}(y_i - x_i) \tag{4.4}$$

Where N is the number of measurements in the dataset, y_i is observed and x_i the predicted value.

4.3 Results

Results show that the formulas both under and over predict the observations depending from the formulation.

4.3.1 Total Swash

Figure 4.2 shows the scatter of predicted versus observed vertical swash. The total swash predicted by Stockdon et al. (2006) has generally less scatter than the one predicted by Guza and Thornton (1982) which tends mostly to under predict the observed data (with local high over predictions). For both formulas, the highest scatters are found for large swash ($> 2m$) in which case remarkable under and over prediction occurs.

4.3.2 Incident Swash

The formulas for incident swash from Stockdon et al. (2006) and from Ruggiero et al. (2004) (one dependent on slope, S_{inRg01} and another on H_s, S_{inRg02} are plotted against the data in Fig. 4.3. S_{in_Rg01} performs better than S_{in_Rg02} suggesting the importance of the beach slope on incident swash process. This behaviour seems to be described correctly by the Stockdon et al. (2006) formula, even if larger scatter is present. The

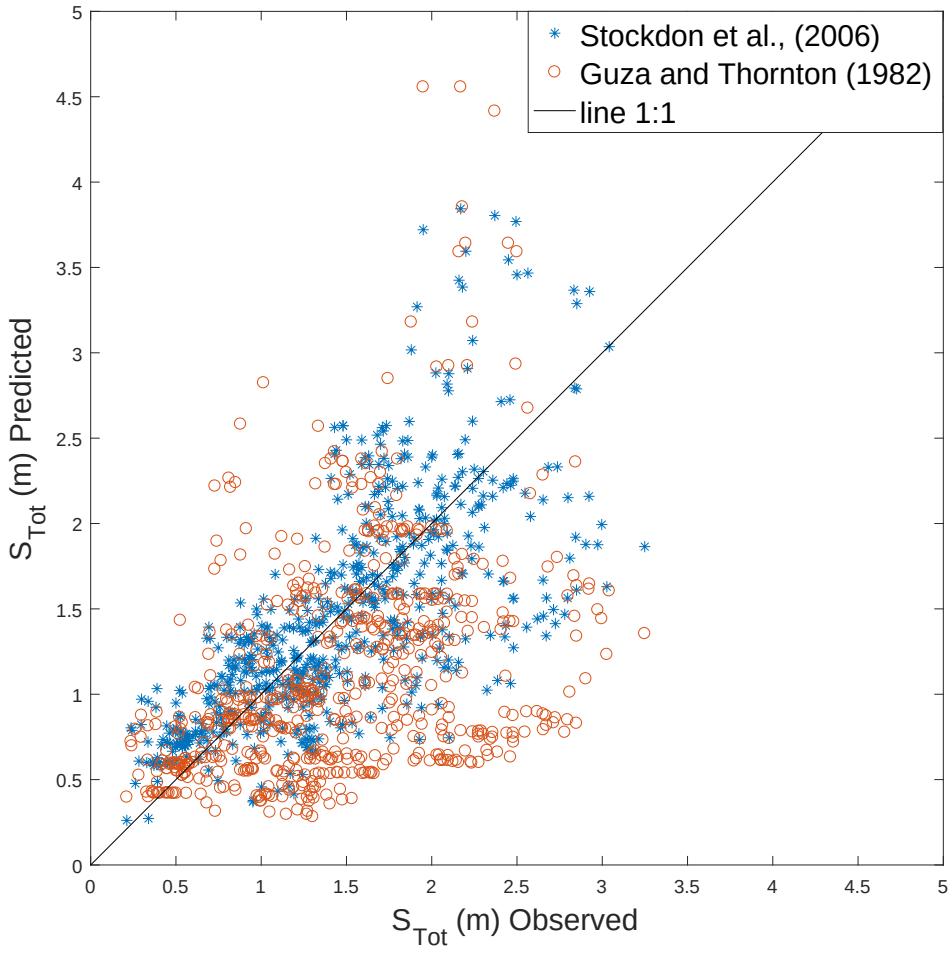

Figure 4.2 Observed versus predicted total swash using the formulas of Stockdon et al. (2006) and Guza and Thornton (1982).

scatter between observations and predictions increases for all formulas for rising incident swash excursion highlighting criticalities of the predictors for storm induced swash. Specifically, Ruggiero et al. (2004) formulas underestimates while Stockdon et al. (2006) both under and over predicts the observations.

4.3.3 Ifragravity Swash

Between the infragravity swash formulas plotted in Fig. 4.4, Ruessink et al. (1998) and Ruggiero et al. (2004) S_{IgRg01} seem to diverge the most from the field data (the former consistently under- and the latter over- predicts). The other formulas generally reproduce the trend in the observed data in some cases with some large over prediction (Raubenheimer and Guza, 1996; Holland, 1995) and underestimation (by Ruggiero et al. (2004) S_{IgRg02}, mostly for large swash excursions ($> 1.5m$). Stockdon et al. (2006), Holman and Sallenger (1985) and Senechal et al. (2011) better reproduce infragravity swash observations.

4.3.4 Errors

The errors in swash formulas are summarized in Fig. 4.5. All error metrics resulted in larger errors in the formula of Guza and Thornton (1982) compared to the Stockdon et al. (2006) total swash formula (Fig.4.5a) (respectively $MSE = 0.2, 0.6\ m^2$, RMSE=0.5, 0.8 m); both maximum errors indicate over prediction of the field observations (the former of 1.8 m and the latter of 2.6 m). Error metrics for incident swash formulas (Fig.4.5b) indicate, consistently with Fig.4.3, that the Ruggiero et al. (2004) formula including beach slope ($S_{in_{Rg}01}$) has smaller errors than the others, while the Ruggiero et al. (2004) formula including H_s (S_{inRg02}) has the largest (respectively $MSE = 0.1$, 1 m^2, $RMSE = 0.3$, 1 m, $MaxE = -1.6$, -2.7 m. $S_{in_{St}}$ errors are intermediate between the two: $MSE = 0.3\ m^2$, $RMSE = 0.5\ m$, $MaxE = 1.9\ m$. $S_{in_{St}}$ appears to overestimate the data measured while the other formulas underestimate observations.

The smallest errors for infragravity swash formulas resulted from the S_{IgSn} formula of Senechal et al. (2011) in Fig.4.5c. Similar results were obtained using S_{IgRg02} and S_{IgHS} while S_{IgRg01} resulted in the highest MSE (0.8 m^2) and RMSE (0.9 m) and S_{IgRG} in the largest MaxE of 2.6 m.

4.4 Discussion

Results show that formulas behave differently with under and over prediction of the field data depending on the details of the formulation. However some trends can be recognized. Generally for large swash events (swash $> 1.5m$) large scatter are found for

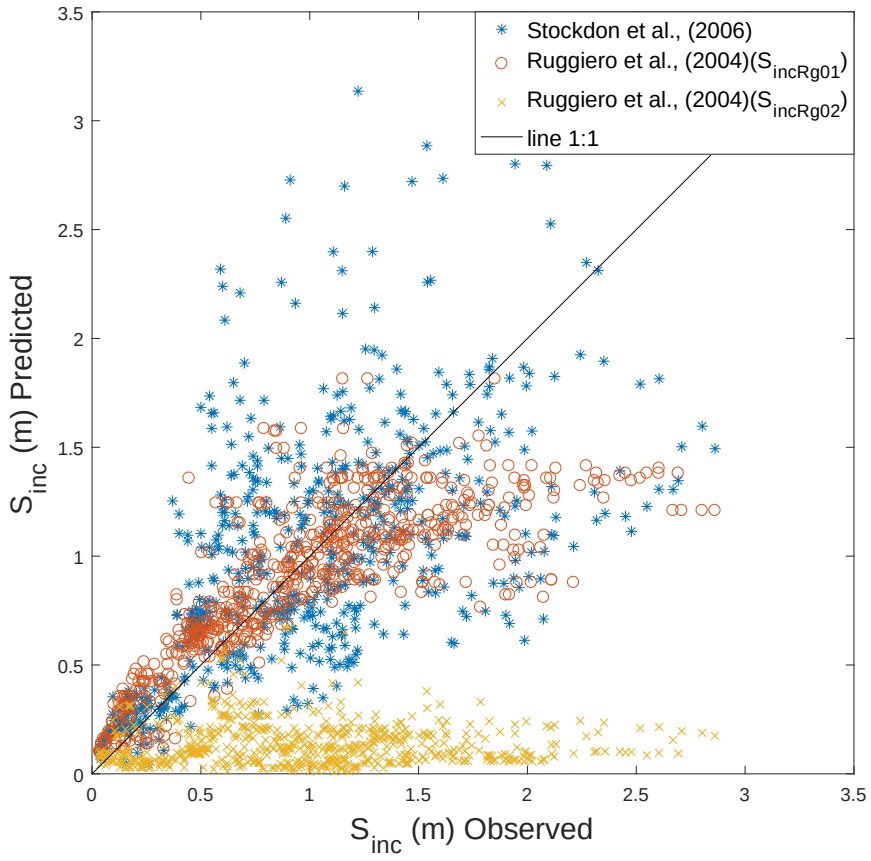

Figure 4.3 Observed versus predicted incident swash using the formulas of Stockdon et al. (2006) and Ruggiero et al. (2004).

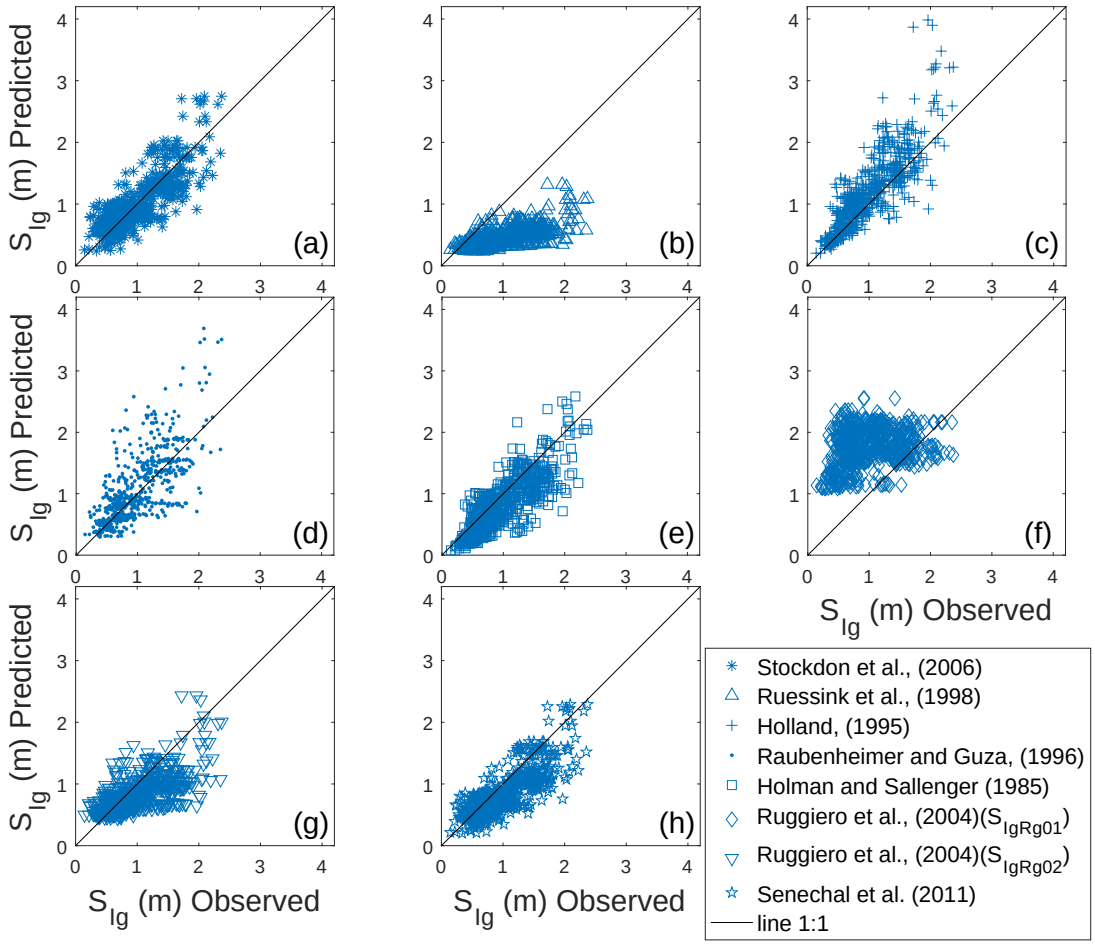

Figure 4.4 Observed versus predicted infragravity swash using the formulas of Stockdon et al. (2006) (a), Ruessink et al. (1998) (b), Holland (1995) (c), Raubenheimer and Guza (1996) (d), Holman and Sallenger (1985) (e), Ruggiero et al. (2004) (f,g), Senechal et al. (2011) (h).

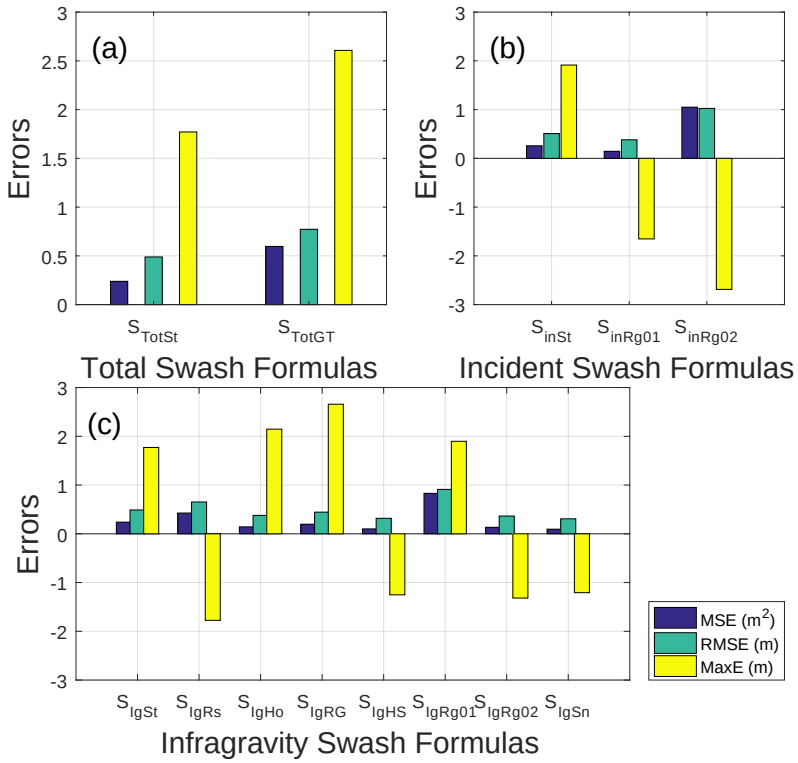

Figure 4.5 The Mean Squared Error (MSE, blue), the Root Mean Square Error (RMSE, green), and the Maximum Error (MaxE, yellow) of 13 published swash formulas tested: a) total swash, b) incident swash, c) infragravity swash.

all formulas (total and infragravity swash is both under- and over- predicted while incident swash is mainly under-predicted). However when looking at extreme conditions (swash $> 2.5m$) total and incident swash are strongly underestimated, while infragravity swash predictions vary for each formulas. The different behavior of the formulas tested in this chapter could be the direct result of the conditions under which the formulas were developed, in other words from the data from which they were initially tested. For instance a formula developed for a dissipative beach under mild wave conditions could easily not work well for a reflective beach during storms. It is surprising that formulas developed using experiments on intermediate to reflective beaches (e.g. S_{Ig_HS}, Holman and Sallenger (1985)) predict better the infragravity swash elevation than formulas with similar shape, obtained by experiment performed on a dissipative beach (S_{Ig_Ho}, Holland (1995)) or under conditions spreading from dissipative to intermediate (S_{Ig_RG}, Raubenheimer and Guza (1996)).

The reader should also note that some predictors were already obtained from part of the dataset used in this chapter (e.g. Stockdon et al. (2006) from 10 of the 13 experiments; Senechal et al. (2011) from the most extreme waves present in the dataset). This aspect reduces confidence and increases uncertainty concerning the universality of the formulas tested and further investigation discriminating data on which the formula were developed, is suggested.

The results of the present chapter are based on the use of three error metrics, in the future test of the formulas, using more advanced techniques as a sensitivity analysis is also suggested. The finding here obtained that S_{in_Rg01} and S_{IgRg02} result in smaller errors than S_{in_Rg02} and S_{IgRg01}, respectively, is in agreement with Ruggiero et al. (2004). In their study the formula for incident swash with slope dependence (S_{in_Rg01}) showed a better correlation with the observations $r = 0.92$ than the formula dependent on H_0 (S_{in_Rg02}) $r = 0.56$. Similarly S_{IgRg02} correlated better ($r = 0.67$) with their field data than S_{IgRg01} ($r = 0.34$). Surprisingly, Ruggiero et al. (2004) formulas for both incident and infragravity swash developed under a limited range of environmental conditions, typically with a fully saturated incident band, perform better than Stockdon et al. (2006) predictors, obtained from a dataset of 10 intrinsically different experiments (in terms of beach characteristics and wave forcing). However, Ruggiero et al. (2004) formulas still has a strong bias for high swash values, which are of critical importance for coastal management and hazard applications. The importance of testing formulas on large datasets not used for obtaining the predictor itself stands out. The fact that one single predictor is retrieved from a wide range of environmental conditions, does not necessarily implicate that it also will perform well on other beaches with likewise variegate environmental conditions.

This chapter highlights that uncertainty related to the prediction swash excursion remains and the universality of swash formulas can be questioned. This is relevant

for swash zone hydrodynamics, sediment transport, coastal management and hazards-related applications (e.g. flooding and erosion).

Parametric formulas of wave runup (and therefore swash) are often used for assessing coastal vulnerability and hazards (Bosom and Jiménez, 2011; Stockdon et al., 2007). This work indicates that some predictors perform better than others under almost all conditions but particularly during storms and extreme conditions, which are the most relevant for planning and management purposes. However, it remains unclear why a certain predictor outperforms another but this work indicates that swash excursion prediction can still result in extremely high errors (maximum errors were almost of $3m$). Caution is needed when applying parametric swash formulas and further investigation on the applicability of parametric swash formulas for extreme conditions is recommended.

4.5 Conclusions

This study tests 13 existing swash (total, incident and infragravity) formulations, using 13 published experiments (636 swash measurements) carried out on beaches worldwide, with the purpose of improving understanding about the universality of those formulas. Formulas behave differently over and under-predicting the field observations. Generally total swash formulas both over and under estimate the field data, with Stockdon et al. (2006) predictor resulting in smaller errors than Guza and Thornton (1982). Incident swash formulas mainly under predict, with Ruggiero et al. (2004) S_{in_Rg01} formula (including beach slope) resulting in smaller errors. Infragravity swash formulas behave differently both over and underestimating the measurements, with Stockdon et al. (2006), Holman and Sallenger (1985), Ruggiero et al. (2004) and Senechal et al. (2011) better reproducing infragravity swash.

Two aspects stands out: a) the importance of considering the kind of data used for developing the formula (and how it might limit) their universality and b) that the scatter between observations and predictions for large swash excursion increases for all formulas. Even though several swash formulas have been developed in the literature, still errors are found (highly relevant to coastal and hazard management applications) when tested in this chapter. An open question seems to persist: is it possible to create new formulas of vertical swash, which could be applicable to a wide range of beach type and environmental conditions, improving predictability?

This and other questions will be addressed in the next chapter (Chapter 5).

Chapter 5

NEW FORMULATION OF WAVE SWASH BY THE USE OF MACHINE LEARNING

The main findings of this chapter have been published in Passarella et al. (2018b).

5.1 Introduction

Wave runup, is the final expression of waves travelling from deep to shallow water and is directly associated with coastal hazards like flooding or erosion. Wave runup height can be defined from water level elevation time series at the shoreline η(t) as the sum of two distinguished components: the wave set up (the temporal mean of the time series $\langle\eta\rangle$ relative to the still water level) and the swash η'(t) (the vertical fluctuation of the water level around the wave set up).

Understanding and predicting swash characteristics is critical for researchers seeking to understand the dynamics of fluid motions and sediment transport in the swash zone (e.g., Elfrink and Baldock (2002); Masselink and Puleo (2006)), and for managers and practitioners addressing hazard setbacks, risk and coastal vulnerability (e.g., Bosom and Jiménez (2011); Vousdoukas et al. (2012)). Wave runup, (and therefore swash excursion) is a key component to evaluate inundation hazards and vulnerability to storm impacts (e.g., Bosom and Jiménez (2011); Stockdon et al. (2007); Serafin et al. (2017)). Stockdon et al. (2007) found that the wave action counted for about 48 % of the maximum total water level during two hurricanes along the USA coast. The problem of accurate predictions of wave runup and swash on sandy beaches has been a research topic for over 50 years but today we still struggle to provide reliable quantitative predictions.

A number of predictors have been developed depending on different combinations of wave and environmental parameters (Section 2.1.4.1). Stockdon et al. (2006) is the most commonly used empirical parametrization of runup but, as can be noted comparing Eq. 2.26 and 2.27, the beach slope is missing from the predictor of the infragravity component of the swash. The dependency (or not) of S_{Ig} on beach slope is a topic that has been debated but not solved (Section 2.1.4.1) and some authors (e.g. Ruessink et al. (1998)) have indicated that infragravity swash is independent from the beach slope

while a weak dependence on beach slope has instead been reported by others (e.g., Ruggiero et al. (2004)). Cohn and Ruggiero (2016) suggested a bathymetric control of the infragravity swash component through 1D and 2D numerical simulations performed using Xbeach (where incident swash contribution is excluded) and compared them with previous formulas (Ruggiero et al., 2001; Stockdon et al., 2006) and field data on dissipative beaches. They suggested that beach morphology ($>$ -2 m MSL) influences the infragravity component of runup more than the nearshore morphology ($<$ -2 m MSL) and indicated that including the foreshore beach slope in the formulation of S_{Ig} improves predictability. Overall, it remains unclear if and when S_{Ig} depends on beach slope.

The empirical runup formulas mentioned in Section 2.1.4.1 were obtained primarily by classic regression approaches (e.g., Ruessink et al. (1998); Ruggiero et al. (2001); Stockdon et al. (2006); Vousdoukas et al. (2012)). Stockdon et al. (2006) predictors have been tested by various authors on beaches ranging from reflective to dissipative (e.g., Vousdoukas et al. (2012); Cohn and Ruggiero (2016); Atkinson et al. (2017)). Predictions using Stockdon et al. (2006) are certainly sound (especially considering the task of generating a universal formula for vertical swash excursion) even though differences between measurements and predictions, possibly associated to local conditions, are inevitably found. More importantly, the regression approach of multiple datasets first proposed by Stockdon et al. (2006) paves the way for this chapter working hypothesis: can powerful data-driven techniques be used to provide robust, reliable and realistic predictions of swash excursion?

When enough data exists, Machine Learning (ML) is a viable approach to regression problems (Section 2.3.2). ML is a sub-discipline of computer science focused on techniques that allow computers to find insightful relationships between variables involved in swash processes, learning at each iteration (algorithm training and validation) from the provided dataset. A key goal of ML is to develop predictors that are generalizable (able to describe the physical process beyond the training dataset itself). Even though ML in general and GP, in particular, were demonstrated to be able to produce predictors which improve predictability of coastal process (e.g. Goldstein et al. (2013); Goldstein and Coco (2014); Tinoco et al. (2015)) they have not being used for obtaining predictors of wave swash on natural beaches yet.

In this study, the focus is on the use of an evolutionary technique, Genetic Programming (GP), to solve the symbolic regression problem of developing new, optimized swash predictors. This chapter contributes to coastal protection and hazards mitigation as well as to enhance the knowledge of swash processes. Particularly, in addition to the total swash, the infragravity component of the swash is investigated, in relation to its dependence on the foreshore slope, as it resulted still an open discussion in the

literature.

In this contribution firstly swash excursion predictors are developed using the original dataset of Stockdon et al. (2006), one of the most comprehensive studies in this area of research. In addition, data from Guedes et al. (2011, 2012), Guedes et al. (2013) and Senechal et al. (2011) is used to broaden the parameter space and to test the new swash equations. The data used in this work cover a broad range of swash excursion including extreme wave conditions (maximum H_0= 6.4 m in Senechal, et al., 2011). High swash excursions, generated by extreme storms, are of particular interest when studying coastal hazards and protection because they relate to flooding, beach and dune erosion (Bosom and Jiménez, 2011; Stockdon et al., 2007). The new ML derived results are also compared to the most widely used predictors from Stockdon et al. (2006). Finally, the physical interpretation of the GP predictors and how ML can be used to gain knowledge of the physical process related to the infragravity swash component is discussed.

Section 5.2 describes and plot the data used. Section 5.3 explores the machine learning data-driven methodology of Genetic Programming adopted to retrieve the swash total and infragravity formulas. Section 5.3.1, the supervised ML approach is presented. In Section 5.3.2 the data pre-processing technique used to decide what data is shown to the ML algorithm is described along with the techniques used to test the results from the ML algorithm against the testing data. Results are presented in Section 5.4, results regarding the GP experiments in Section 5.4.1, the total swash in Section 5.4.2, the infragravity swash in Section 5.4.3. The results are discussed in Section 5.5 and conclusions drawn in Section 5.6.

5.2 Data

This work is based on two published video image-derived runup datasets — 13 field experiments in total. The first dataset (referred to here as the "original dataset" and displayed in blue circles in Fig. 5.1-5.3) is composed by 491 swash measurements from 10 experiments aggregated by Stockdon et al. (2006). The second dataset (referred to here as the "new dataset" and represented by red crosses in Fig. 5.1-5.3) consists of 145 swash measurements compiled for this work from three experiments performed by Guedes et al. (2011, 2013) and Senechal et al. (2011).

The compiled dataset of total and infragravity swash is plotted in Fig. 5.2 and Fig. 5.3. The compilation of a large dataset deriving from 13 different experiments requires merging data collected using different techniques and equipment. Details of each experiment can be found in the original references. Looking at the environmental forcing conditions, Figure 5.1 shows that the original and new dataset cover similar ranges of beach slope, while they differ in significant wave height (the new dataset

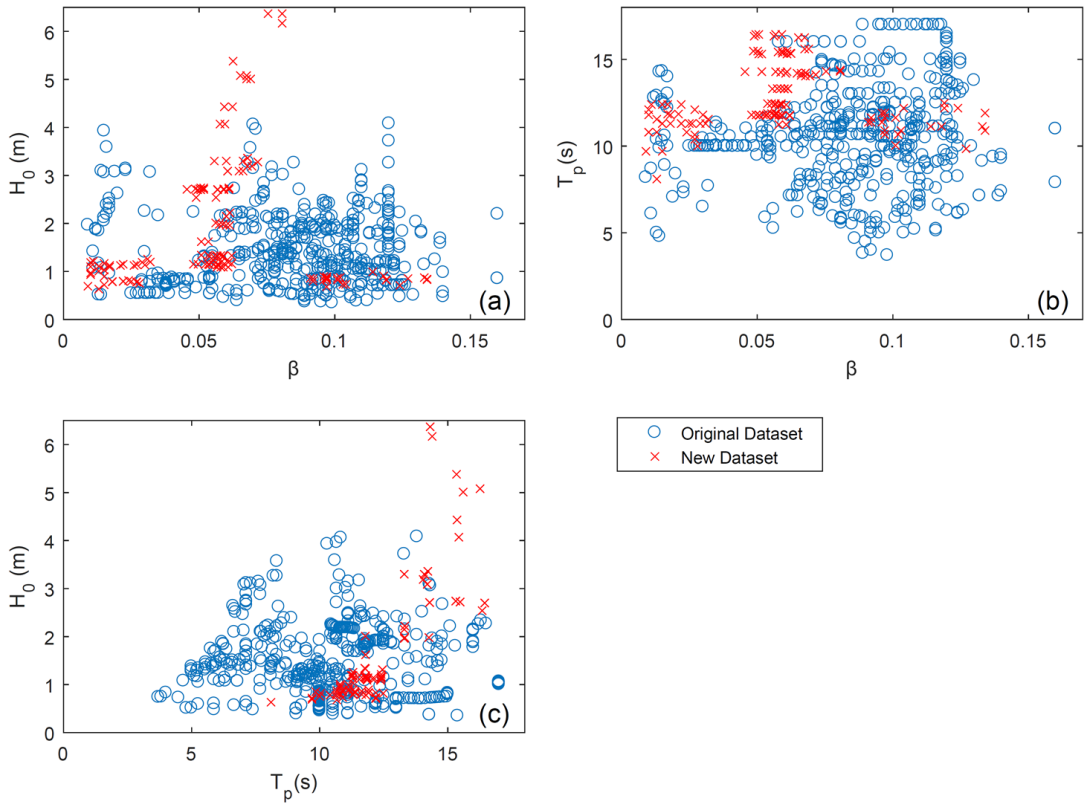

Figure 5.1 Environmental forcing conditions (blue circles: original dataset, red crosses: new dataset): (a) significant wave height versus beach slope; (b) wave peak period versus beach slope; (c) significant wave height versus wave peak period.

includes wave heights over 6 m) and peak period (the original dataset includes more short period waves).

Both datasets include recordings of infragravity swash (S_{Ig}; m), total swash (S_{Tot}; m), beach slope (β) and associated offshore wave characteristics: significant wave height (H_0; m) and peak period (T_p; s). From these measurements the offshore significant wave length (L_0; m), wave steepness (H_0/L_0), and Iribarren number (ξ_0) are calculated. Experiments are located in North America, Europe and Oceania and cover a large range of the environmental condition (see Table 5.1 and Fig. 5.1).

Both datasets include all beach types, from dissipative to reflective. The two datasets also have a similar range of S_{Tot} (although the original dataset records a larger swash, 0.2-3.3 m vs. 0.24-2.5 m of the new dataset), S_{Ig} (about 0.2-2.4 m for both), and β (about 0.01-0.1 for both). The two datasets differ in the range of offshore wave conditions — in the original dataset H_0 and T_p range over 0.4-4.1 (m) and 3.7-17 (s), respectively, while in the new dataset the ranges are 0.6-6.4 (m) and 8.1-16.4 (s).

The dissipative beaches of the original dataset (Fig. 5.4 d, h) are Terschelling (Netherlands) and Agate (USA), and for the new dataset Ngarunui in New Zealand

Table 5.1 Summary of wave and beach parameters for the original and the new datasets, beach name and type (following the classification of Short (1999a) based on Iribarren number (D stands for dissipative, I intermediate and R reflective); the last two rows indicate the range of parameters of the entire two datasets. Each experiment is associated with the citation where the measurements have been originally presented. If no reference is given, the citation to consider is Stockdon et al. (2006).

Experiment	Data set (data points)	H_s (m)	T_p (s)	β	ξ_0	Beach type	S_{Tot}	S_{Ig}
Duck 94 (Holland and Holman, 1996)	Original (52)	0.7–4.1	3.8–14.8	0.06–0.1	0.33–1.43	I, R	0.8–2.9	0.5–2.2
Gleneden	Original (42)	1.8–2.2	10.5–16	0.03–0.11	0.26–1.2	I, R	1.1–2.3	0.9–1.9
Sandy Duck	Original (95)	0.4–3.6	3.7–15.4	0.05–0.14	0.34–3.22	I, R	0.7–2.3	0.3–1.8
San Onofre	Original (59)	0.5–1.1	13–17	0.07–0.13	1.6–2.62	R	0.9–2.6	0.5–1.8
Terschelling (Ruessink et al., 1998)	Original (14)	0.5–3.9	4.8–10.6	0.01–0.03	0.07–0.22	D	0.2–1	0.2–0.9
Scripps Beach (Holland et al., 1995)	Original (41)	0.5–0.8	10–10	0.03–0.06	0.4–0.92	I	0.3–0.7	0.3–0.7
Delilah (Holland and Holman, 1993)	Original (138)	0.5–2.5	4.7–14.8	0.03–0.14	0.44–1.70	I, R	0.7–3.3	0.4–1.7
Duck 82 (Holman, 1986)	Original (36)	0.5–4.1	6.3–16.5	0.09–0.16	0.68–2.38	I, R	0.7–3	0.4–2.4
Agate (Ruggiero et al., 2001)	Original (14)	1.8–3.1	7.1–14.3	0.01–0.02	0.1–0.19	D	0.7–1.5	0.7–1.5
Ngarunui (Guedes et al., 2013)	New (32)	0.6–1.26	8.1–12.4	0.01–0.03	0.13–0.42	D	0.24–0.9	0.24–0.9
Tairua (Guedes et al., 2011)	New (25)	0.7–1	9.9–12.5	0.09–0.13	1.4–2.25	R	1.2–2.2	0.6–0.95
Truc Vert (Senechal et al., 2011).	New (88)	1.1–6.4	11.2–16.4	0.05–0.08	0.49–0.9	I	0.81–2.5	0.63–2.37
All beaches	Entire original (491) (Stockdon et al., 2006)	0.4–4.1	3.7–17	0.01–0.16	0.07–3.22	D, I, R	0.2–3.3	0.2–2.4
All beaches	Entire new (145)	0.6–6.4	8.1–16.4	0.01–0.13	0.13–2.25	D, I, R	0.24–2.5	0.24–2.37

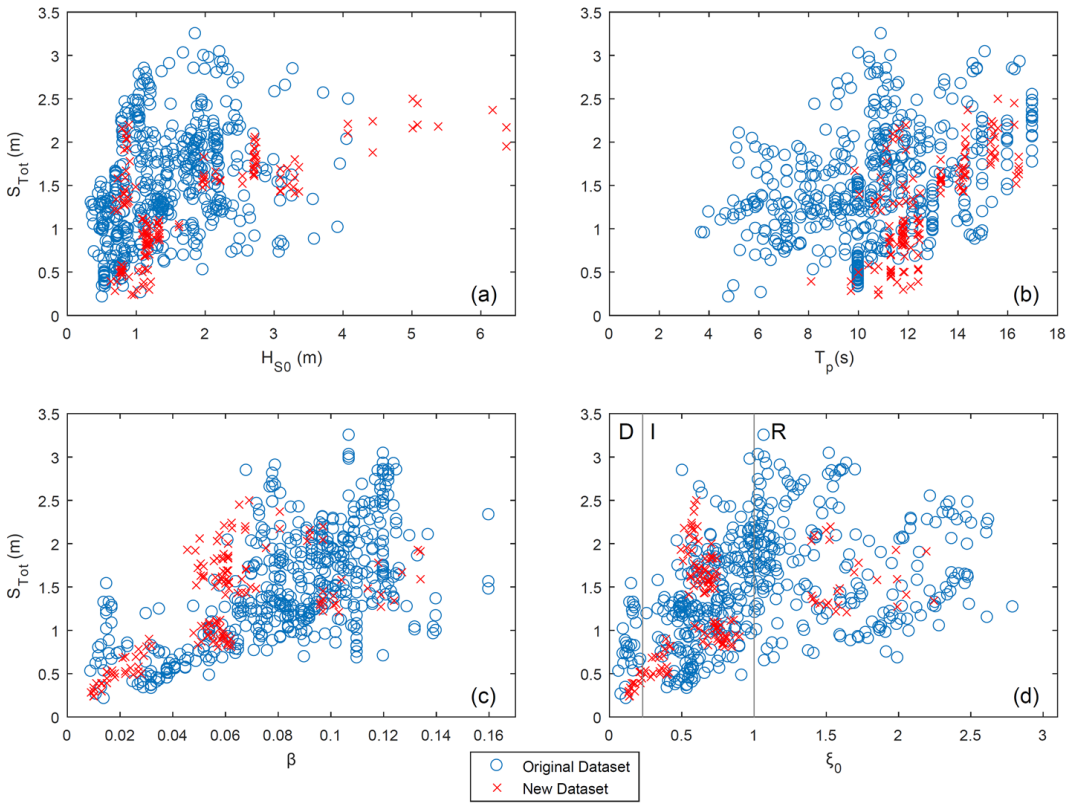

Figure 5.2 Compiled Total swash data (blue circles: original dataset, red crosses: new dataset) against the environmental variables: significant wave height (a), wave peak period (b), beach slope (c) and Iribarren number (d), for which beaches are classified as dissipative (D) for values of $\xi_0 < 0.23$, reflective (R) for ξ_0 <1 and intermediate (I) between the two Short (1999a).

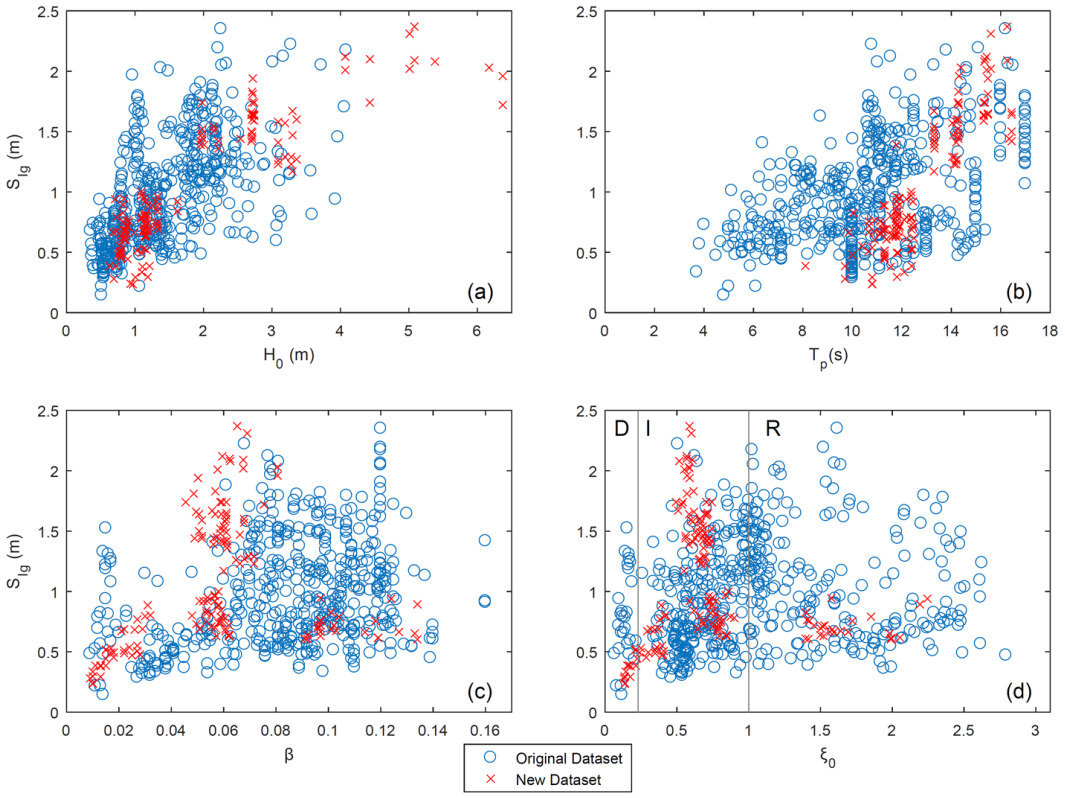

Figure 5.3 Compiled Infragravity swash data (blue circles: original dataset, red crosses: new dataset) against the environmental variables: significant wave height (a), wave peak period (b), beach slope (c) and Iribarren number (d), for which beaches are classified as dissipative (D) for values of $\xi_0 < 0.23$, reflective (R) for $\xi_0 < 1$ and intermediate (I) between the two Short (1999a).

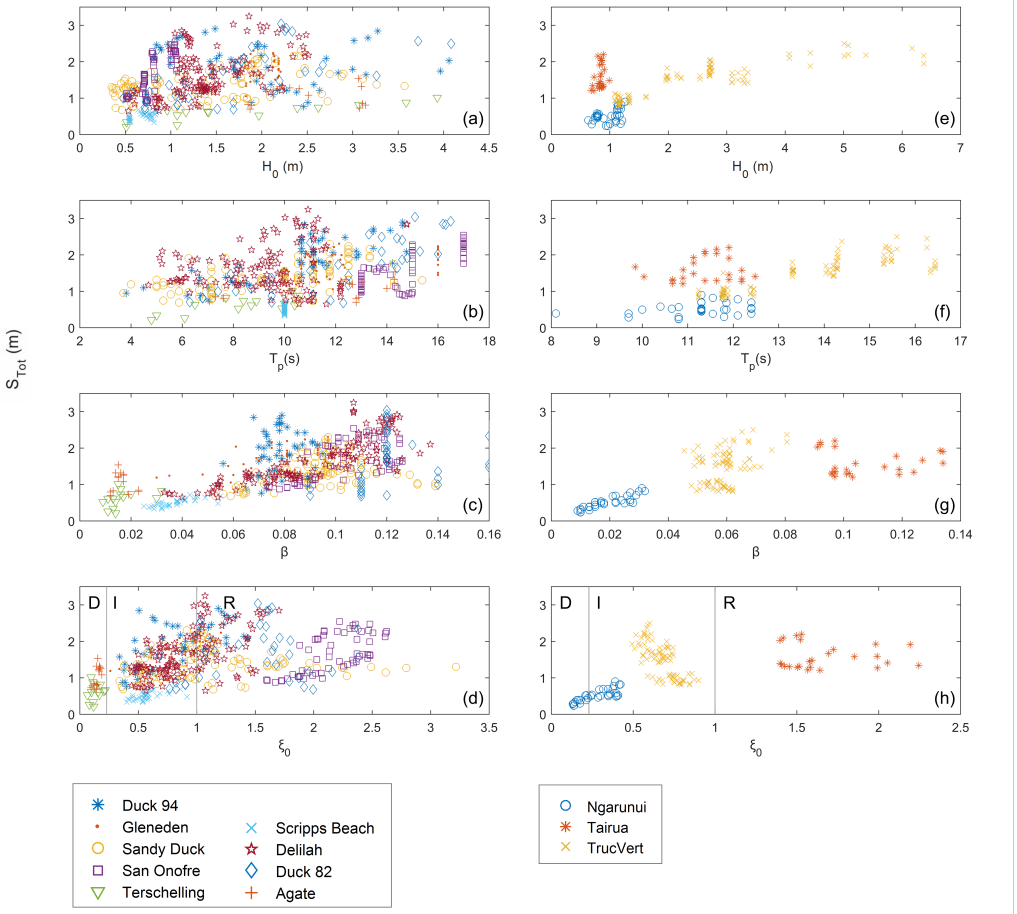

Figure 5.4 Total swash dependence on the environmental variables of the original (a,b,c,d) and new (e,f,g,h) datasets. The variables displayed are: significant wave height (a,e), wave peak period (b,f), beach slope (c,g) and Iribarren number (d,h). Beaches are considered dissipative (D) for values of $\xi_0 < 0.23$, reflective (R) for $\xi_0 < 1$ and intermediate (I) between the two Short (1999a).

(although, during the experiment, the beach also experienced intermediate conditions). The purely intermediate beaches for the original and new dataset are Scripps (USA) and TrucVert (France). Some beaches of the original dataset (USA) represent both intermediate and reflective conditions: Duck 94, Gleneden, Sandy Duck, Delilah and Duck 82. San Onofre for the original and Tairua (New Zealand) for the new dataset are reflective.

5.3 Methodology

The large amount of data available (636 field swash records), including multidimensional variables, supports the feasibility of a ML approach. The data covers a wide range of environmental conditions (including extreme storms) and beach type, ensuring the applicability of our results to sandy beaches spreading from dissipative to reflective.

5.3.1 Genetic Programming

GP is a machine learning approach (defined population-based) which is based on evolutionary computation (Koza, 1994). The four steps which compose the working principle of GP are summarized in Section 5.3.2. In this chapter, the research of the population of solutions is stopped after the GP evaluated 10^{11} formulas because the solutions stabilized and no significant improvement in formula performance was found.

At the end of a routine, when the solutions have stabilized, a final population of solutions exist. A range of final solutions is given by the algorithm — more mathematically complex solutions (with more variables, operators, and coefficients) that minimize error are given alongside more simple, parsimonious solutions with a higher error. These solutions exist along a "Pareto Front" that balances decreases in error with increasing solution complexity. Given a range of solutions with different error and complexity, the author do not know of a perfect method for a user to determine the single best solution from the suite of final solutions — a user must decide on the solution according to different criteria: minimization of the error, computational time, physical meaning. In this work, the criterion of minimization of the error is adopted, with an eye toward the ability to interpret physical meaning from the formulas. A compromise between error reduction (more complex predictors) and the ability of the predictors to generalize (predictive power on new data) should be found during the selection of a predictor.

All genetic programming in this study is performed using the software "Eureqa" developed by Schmidt and Lipson (2009, 2018) which has successfully been used for a range of coastal problems (e.g., Goldstein et al. (2013); Tinoco et al. (2015). Predictors of total and infragravity swash elevation are searched — ultimately researching for the best equation that satisfies $S_{Tot/Ig} = f(H_0, L_0, \beta, T_p)$. Note also that some experiments are performed searching for total and infragravity swash as a function of composite variables like wave steepness, wave power (P_w), and the Iribarren number.

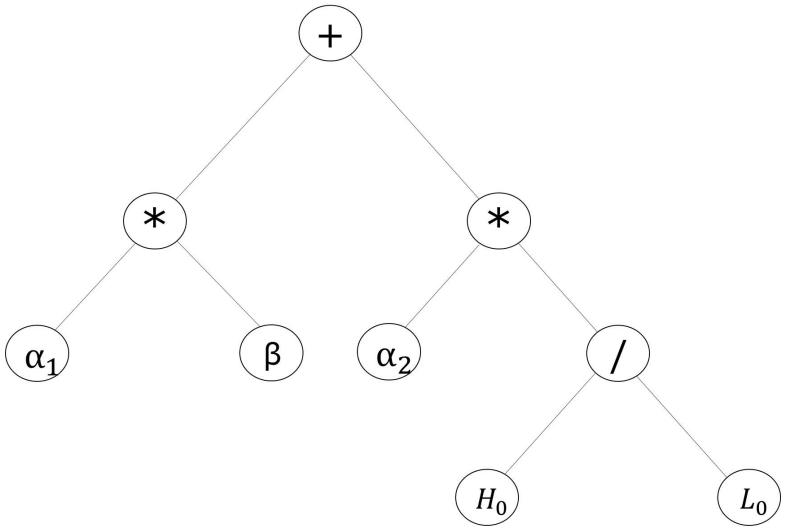

$$S_{Tot} = \alpha_1\beta + \alpha_2 \frac{H_0}{L_0}$$

Figure 5.5 Schematics of the GP structure and principle of operation for an example of simple total swash predictor. α_1 and α_2 are the coefficients, β, H_0 and L_0 the variables and $+$, $*$ and $/$ the mathematical operators.

However, the predictors did not show improvement — also keep in mind that the GP can autonomously find these interrelationships between the basic parameters themselves, leading to the appearance of these composite variables in each optimization experiment. In addition to physical parameters, constants are included in the research and the mathematical operations allowed to the GP are: addition (+), subtraction (-), multiplication (*), division (/), exponential ($\wedge$) and square root ($\sqrt{}$). Predictors developed on the training subset are assessed on the validation subset, using an error metric (also known as fitness function). From the available metrics, selected the mean squared error (MSE, Eq.(4.2)) is selected.

All selected formulas from the genetic programming routine are further optimized. First, the formulas are rearranged algebraically to ease interpretation by the user. Second, two coefficients of each selected formula are further optimized using a gradient descent algorithm in an iterative process.

5.3.2 Training, Validation and Testing

In order to obtain generalizable predictors, it is necessary to train, validate and test any ML routine on distinct and non-overlapping subsets of data (e.g.,Domingos (2012)). There is no universal, optimal method to select enough data to explain variability of the dataset while still retaining the most data to use for testing — recent work by Galelli et al. (2014) highlights that, even with the numerous input variable selection methods

that have been proposed, there is no single best method for all the typologies of environmental datasets, and for all environmental models.

The maximum dissimilarity algorithm (MDA) is adopted as selection routine (e.g., Camus et al. (2011)), already successfully tested in other works of predictors developed by GP for physical problems (e.g., Goldstein and Coco (2014)). The MDA is a routine for the selection of the most dissimilar points in a given dataset. Each data point is a vector composed by all the variables of our dataset (η, S_{Tot}, S_{Ig}, S_{in}, H_0, L_0, β, T_p, ξ_0, P_w, R), where each variable is normalized between 0 and 1. At each iteration (i=1...n), the MDA finds the most different data point from the data selected in all previous iterations. Consequently, the MDA selects a diverse set of data from the original 491 data points used by Stockdon et al. (2006). The operator must set the number of data points selected — the MDA is applied to 150 data points ($\sim$30% of the original dataset). The analysis is also run using a subset of variables (not including the variables representing swash elevations) but no significant loss in prediction power of the algorithms developed by the machine learning algorithm was observed. The data selected by the MDA is used as the training subset and the remaining data ($\sim$70 % of the original dataset, not selected) is used as validation subset.

The predictors developed by the GP using this training data is tested using the new dataset from Guedes et al. (2011, 2013); Senechal et al. (2011). This new dataset is completely independent from the training and unknown at the GP algorithm providing a test in the ability of the GP parameterization to generalise, even beyond the range of the testing and validation data (Fig. 1). The performance of our predictors using the testing data is compared to the Stockdon et al. (2006) predictors using three error metrics.

The testing phase and for comparing our predictor with known predictors in the literature the mean square error, as defined in Eq.(4.2), the root mean square error (RMSE, Eq.(4.3)), and the maximum absolute error (MaxE, Eq.(4.4)) are used, Where N is the number of measurements in the dataset, y_i is observed and x_i the value predicted by GP.

5.4 Results

5.4.1 Results of GP experiments

After $\sim 10^{11}$ formulas were evaluated, the solutions from the GP algorithm for both S_{Tot} and S_{Ig} follow a "Pareto front" where the error decreases (compared with the validation subset) as the size (or complexity) of the formula increases. Generally, extremely complicated predictors fit the training and validation dataset better than simpler predictors but they may lose generalization power when tested on a separate testing dataset (overfitting). In other words, a predictor with overfitting could represent the noise in the training and validation subsets instead of defining a general predictive rule (Dietterich,

1995) and therefore it will result in smaller training errors but in higher testing errors. Several viable techniques exist for selecting the best solution to avoid overfitting, all meant to balance the fact that simpler solutions (the minimum description length) might risk losing more accurate information contained in more complex models (e.g., ONeill et al. (2010)). Picking a solution is a subjective task, and relies on specific domain knowledge on the part of the user — here the focus is on predictors with clear physical plausibility (avoiding predictors with physical nonsense such as increase of S_{Tot} as H_0 decreases) and avoid predictors that are difficult to interpret, (e.g., extremely nonlinear relationships, possibly a result of overfitting the training dataset). The focus is also on two predictors for both the S_{Tot} and S_{Ig}, evaluating a simpler and more complex predictor to determine if the more complex expression warrants use when generalized to the testing dataset.

5.4.2 Total Swash

Following the principle of error reduction and physical interpretability of the results, and finally from the pool of candidate solutions available from the GP experiments, two formulas for S_{Tot}, one simpler (Eq. 5.1) and one more elaborate (Eq. 5.2) are selected.

$$S_{Tot} = 12.314\beta + 0.087T_p - 0.047\frac{T_p}{H_0}, \tag{5.1}$$

$$S_{Tot} = 146.737\beta^2 + \frac{T_p {H_0}^3}{5.800 + 10.595{H_0}^3} - 4397.838\beta^4. \tag{5.2}$$

Note that the coefficients of both Eq. 5.1 and 5.2 are dimensional. Eq. 5.1 represents the best solution in terms of error reduction while maintaining a physical interpretability. It also stands out for its simplicity and only weak nonlinearity — it looks similar to a multiple linear regression.

The first term in Eq. 5.1 indicates the dependence of the S_{Tot} on the beach slope (direct proportionality: S_{Tot} increases as β increases), the second term on the only peak period (direct proportionality: S_{Tot} grows as T_p increases) and the third (note that is subtracted to the sum of the other two) indicates the relationship of S_{Tot} with the ratio T_p/H_0. This ratio increases for long period and small waves. In Eq. 5.2 the first and the third term depend exclusively on β, while the second term includes the contribution of the incident waves.

For understanding the different contribution of the three terms of Eq. 5.1 and 5.2, 5 simple case studies (Table 5.2) are evaluated. The case studies combine minimum and maximum environmental forcing conditions of the new dataset varying β, H_0, T_p (excluding the minimum H_0 because resulting in too small swash for coastal hazard applications), results are displayed in Fig. 5.6.

Table 5.2 Cases used for evaluating the contribution of terms of Eq. 5.1 and 5.2 to S_{Tot} prediction.

Case	H_0 (m)	T_p (s)	L_0 (m)	β	ξ_0	Beach type
1	1.5	8.1	102.44	0.01	0.08	D
2	1.5	16.4	419.93	0.01	0.17	D
3	2.5	8.1	102.44	0.13	0.83	I
4	6.4	16.4	419.93	0.13	1.05	R
5	6.4	16.4	419.93	0.075	0.61	I

The second term of Eq. 5.1 has a higher weight than the third (Fig. 5.6 a). This difference in weight between the second and third term is enhanced as the wave height grows. Therefore from this formula seems that the contribution of T_p is more important than H_0. The First term is smaller than the other two for small β (e.g. 0.01 minimum of new dataset, case 1 and 2 in Fig. 5.6 a) while it overpasses them for higher values of slope (e.g. 0.13 maximum of new dataset case 3 and 4 in Fig. 5.6 a). While Eq. 5.1 describes more linear aspects of the problem, in Eq. 5.2 more non-linear terms appear, adding possibly useful information about the swash process.

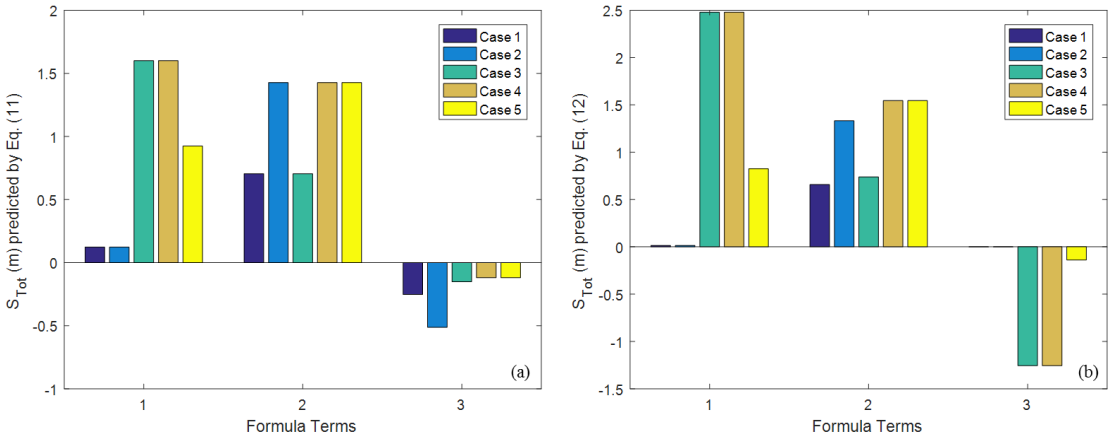

Figure 5.6 Contribution of terms of 5.1 and 5.2 to total swash predicted for 5 case studies.

The weight of the single terms in Eq. 5.1 varies depending strongly on the values assumed by the variables: β, H_0, T_p (Fig. 5.6 b) probably due to the nonlinearity introduced in this more complicated model. For instance:

- typically for small values of β the terms assume an importance with decreasing order: second, first and third. Eq. 5.2 indicates that in this case, the beach slope terms count greatly less than the term of the incoming waves (mostly independently form variation in H_0 and T_p).

- However for greater β the first term has a higher weight than the other two, and in this case variations in wave conditions influence the relative importance of the second term (changes form Case 3 to 4).
- The second term is bigger than the third for large waves ($H_0 = 6.4$ m and $T_p = 16.4$ s, corresponding to the maximum recorded of the new dataset at the beach TrucVert) while the third seems to exceed the second for smaller waves (e.g. case 3: $H_0 = 2.5$ m and $T_p = 8.1$ s) but, a decrease in slope drastically reduces the contribution of the third term

The behaviour described by both Eq. 5.1 and Eq. 5.2 captures the observations of the new dataset (note that predictors are found by algorithm trained on the original and not on the new dataset). Similar total swash is recorded at TrucVert (intermediate) and Tairua (reflective) beaches, even though the wave height and period during the TrucVert experiment are much higher than at Tairua. On steeper beaches for same wave input (case 5 to 4) the total swash grows, demonstrating the ability of GP to produce predictors which correctly describe the behaviour of different beach types. The distinct contributions of H_0 and T_p cannot be easily deduced in Eq. 5.2 because of the non-linear relationships. Generally, S_{Tot} grows as the waves increase in both H_0 and T_p. As for Eq. 5.1, it seems that an increase in T_p (case 1 to 2) corresponds to an increase in S_{Tot}.

The total swash in both GP predictors is related to the wave peak period (instead of wave length) different from previous formulations (e.g. Stockdon et al. (2006); Holman and Sallenger (1985)). Recently also Poate et al. (2016) used the wave peak period in their runup predictor for gravel beaches. The use of the peak period instead of the wave length has no influence on the physics of the predictor but could allow the users a more direct utilization of the formula.

Figure 5.7 displays a comparison of performance of swash predictors obtained through the ML approach (Fig. 5.7a, 5.7b) and Stockdon et al. (2006) (Fig 5.7c), on the training and validation dataset. This does not constitute a test of the predictors, only a consistency check to see that the predictors are modelling the training and validation data appropriately. Overall Eq. 2.25 shows a higher scatter in the whole original dataset (details on the errors can be found in Table 5.3). It is not clear why all formulas do not successfully fit the data Duck 82 and Delilah (especially for $S_{Tot} > 2$ m). The Stockdon et al. (2006) predictor shows scatter at larger total swash, while the GP predictors show slight underfitting of swash elevation during large events. Stockdon et al. (2006), Eq. 2.25, 2.26 and 2.27 in this contribution, mostly underpredicts the data with the exclusion of the Duck 82 dataset, which is largely over predicted for high values of the swash excursion. Both GP predictors more accurately fit data from dissipative beaches (Agate and Terschelling) compared with the Stockdon et al. (2006) formula.

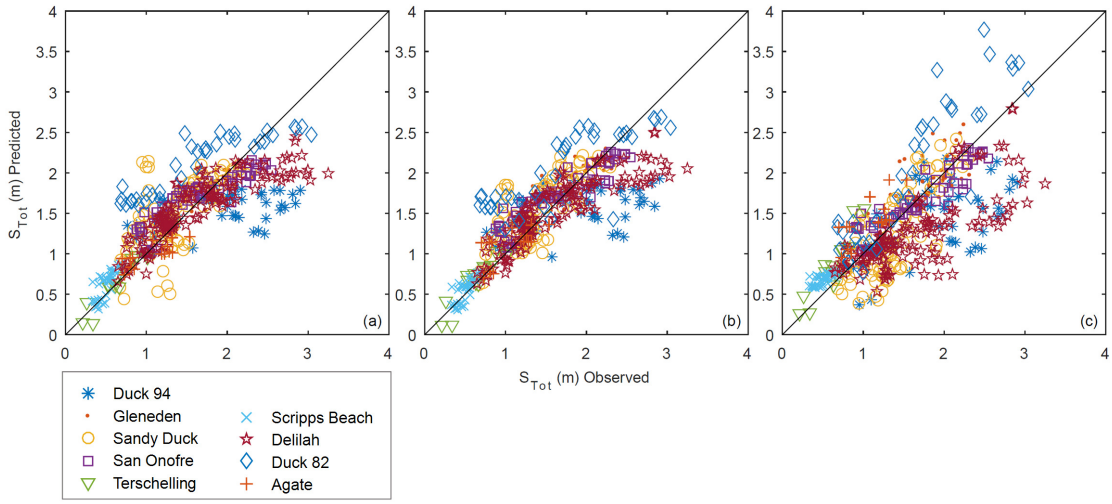

Figure 5.7 Observed versus predicted S_{Tot} using (a) GP Eq. 5.1, (b) GP Eq. 5.2 and (c) Stockdon et al. (2006) Eq. 2.25 for the original dataset (Stockdon et al., 2006). This is not a test of any predictor, only a consistency check — all data was shown to the GP algorithm and used to generate the linear regression in panel c.

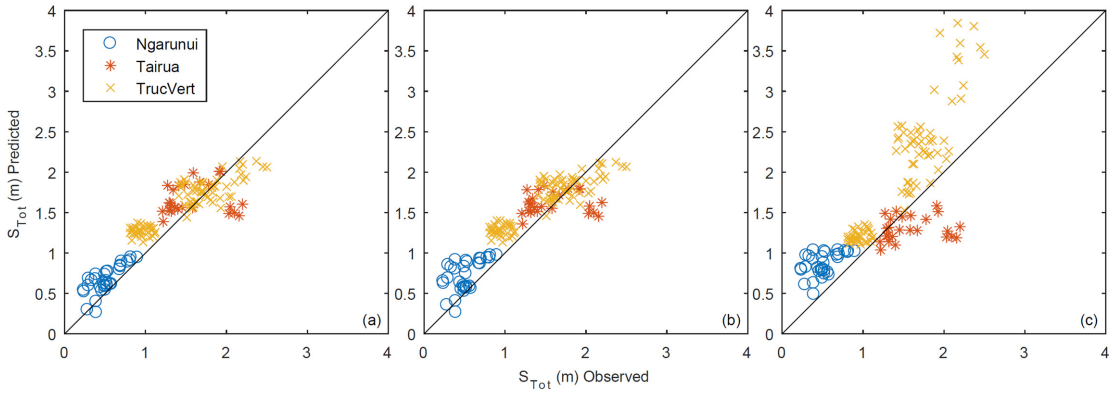

Figure 5.8 Observed versus predicted S_{Tot} with the new independent dataset. (a) GP Eq. 5.1 , (b) GP Eq. 5.2 and (c) Stockdon et al. (2006) — Eq. 2.25.

Table 5.3 Results of error metrics for both total and infragravity swash, calculated for the GP predictors and Stockdon et al. (2006) on both original and new datasets. The results calculated with the original data set (in italics) do not represent a test of any predictor, only a consistency check all original data were shown to the GP algorithm and used by Stockdon et al. (2006).

Target	Formula (methodology)	Error metrics	New data set (Independent)	Original data set, Stockdon et al. (2006)
Total swash	Eq. (11) (GP)	MSE (m^2)	0.074	*0.144*
		RMSE (m)	0.272	*0.380*
		MaxAE (m)	0.695	*1.257*
	Eq. (12) (GP)	MSE (m^2)	0.083	*0.126*
		RMSE (m)	0.288	*0.355*
		MaxAE (m)	0.702	*1.258*
	Eq. (5) Stockdon et al. (2006)	MSE (m^2)	0.325	*0.214*
		RMSE (m)	0.570	*0.462*
		MaxAE (m)	1.771	*1.399*
Infragravity	Eq. (13) (GP)	MSE (m^2)	0.071	*0.047*
		RMSE (m)	0.267	*0.217*
		MaxAE (m)	0.679	*1.019*
	Eq. (14) (GP)	MSE (m^2)	0.047	*0.053*
		RMSE (m)	0.216	*0.231*
		MaxAE (m)	0.587	*1.025*
	Eq. (7) Stockdon et al. (2006)	MSE (m^2)	0.111	*0.068*
		RMSE (m)	0.334	*0.261*
		MaxAE (m)	0.988	*1.056*

Figure 5.8 shows the observed versus the predicted S_{Tot} — both GP models and Stockdon et al. (2006) — for the new, 'testing' dataset. Note that swash values (0- 2.5 m) are lower than the maxima observed in the original data set, but these values represent absolutely new, out of sample prediction for all equations. Overall the Stockdon et al. (2006) formula has higher scatter than both GP predictors (Fig. 5.8), and considerably overestimates swash measurement of Truc Vert (intermediate beach under extreme highly energetic wave storm) and Ngarunui (dissipative beach under mild wave conditions) while underestimates the observations at the reflective beach of Tairua. Equations 5.1 and 5.2, from the GP routine, perform similarly (Fig. 5.8 a, b).

5.4.3 Infragravity swash

The two formulas selected for describing S_{Ig} are Eq. 5.3 and the more complex Eq. 5.4:

$$S_{Ig} = 10\beta + \frac{\beta}{\beta - 0.306} + \frac{H_0 - 0.456}{0.447 + 136.411(\frac{H_0}{L_0})} \tag{5.3}$$

$$S_{Ig} = \frac{\beta}{0.028 + \beta} + \frac{(-1)}{2412.255\beta - 5.521\beta L_0} + \frac{H_0 - 0.711}{0.465 + 173.470(\frac{H_0}{L_0})}, \tag{5.4}$$

As in the case of S_{Tot}, the coefficients of Eq. 5.3 and 5.4 for S_{Ig} are dimensional. The reader should also note that both formulas depend on the beach slope in contrast with Ruessink et al. (1998) and Stockdon et al. (2006), Eq. 2.27, but in agreement with other slope inclusive predictors (Ruggiero et al., 2001, 2004). Eq. 5.4 represents the best solution in terms of error reduction while maintaining physical meaning and Eq. 5.3 is a simpler predictor where the contribution of beach slope and waves to infragravity swash remains separate.

Both Eq. 5.3 and 5.4 have the same nonlinear term $\frac{H_0 - 0.456}{0.447 + 136.411(\frac{H_0}{L_0})}$, with slight difference in the coefficients, that describes the incoming waves. The threshold that flips this term from negative to positive is related to wave height and is probably an indication that for small waves the infragravity component is extremely limited (this term needs to be negative to compensate for other terms that only depend on beach slope and provide a constant contribution). The ML predictor not only suggests that the beach slope is important when predicting infragravity swash but also indicates a nonlinear interaction between waves and beach morphology through the wave length (second term of Eq. 5.4).

To evaluate the role of each term of Eq. 5.3 and 5.4 the same case studies as for S_{Tot} are used (Table 5.2).

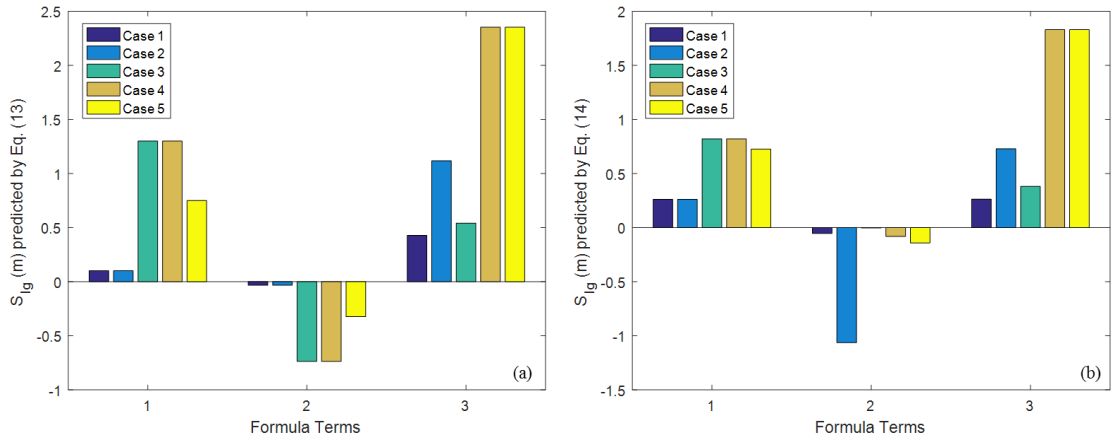

Figure 5.9 Contribution of terms of 5.3 and 5.4 to infragravity swash predicted for 5 selected case studies.

The second term assumes higher values than the other two only in case 2 (Fig. 5.9b) because of the combination of long waves with low sloping beach. In both formulas, contrary to what suggested previously (e.g. Stockdon et al. (2006)) the factors regarding wave characteristics do not always have a higher weight in the formulas. Indeed the terms containing the beach slope can be prevalent (case 3 for both Eq 5.3 and 5.4 and also case 2 for Eq. 5.4, in which case, the interaction between beach slope and wave length is the leading term). These formulas suggest that more studies could be necessary to study the influence of beach morphology on the infragravity motion for shorter waves on steep beaches (case 3), and for longer waves on low sloping beaches (case 2).

Figure 5.10 displays a consistency check, highlighting the performance of swash predictors obtained through a ML approach (Fig 5.10a, b) and Stockdon et al. (2006) (Fig 6c), on the training and validation dataset. It is not clear why all formulas provide a less precise prediction with data from Duck 84 and Duck 82 but it is noted that these two experiments focused on intermediate to reflective conditions with relatively large wave conditions (Table 5.1). Generally, the three formulas seem to perform similarly. Some differences are found in dissipative settings (i.e., Agate and Terschelling) —predictions by Stockdon et al. (2006) tend to overestimate S_{Ig} compared to the GP predictors.

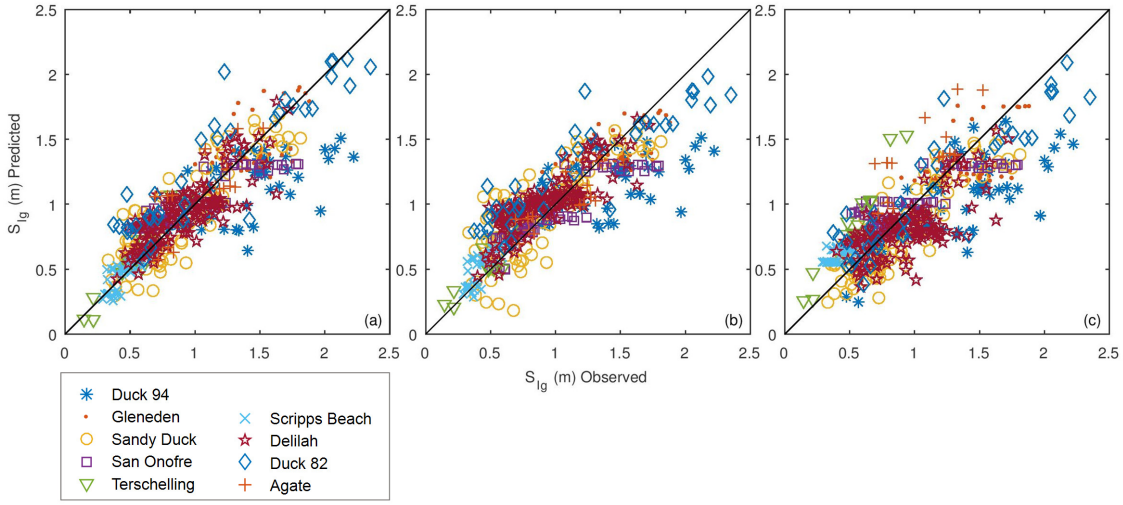

Figure 5.10 Observed versus predicted S_{Ig} using (a) GP Eq. 5.3, (b) GP Eq. 5.4 and (c) Stockdon et al. (2006) Eq. 2.27 for the original dataset (Stockdon et al., 2006). This is not a test of any predictor, only a consistency check — all data was shown to the GP algorithm and used to generate the linear regression in panel c.

The same difficulty in predicting swash excursion on a dissipative beach is observed on Ngarunui (Fig. 5.11). Even though this experiment was performed under mild wave conditions ($H_0 \approx$ 0.6-1.26 (m) and $T_p \approx$8.1-12.4 (s), Table 5.1) compared to the experiments at Agate and Terschelling. Note that dissipative beaches are the one were the infragravity motion has greater importance. Also Truc Vert presents dissipative conditions in the swash zone, while the surf zone is intermediate (ξ_0 up to 0.87 as reported by Senechal et al. (2011)). For this experiment Eq. 5.3 and 2.27 (Fig. 5.11 a, c) overestimate S_{Ig} while Eq. 5.4 has better performance for the dissipative beach Ngarunui, suggesting that it could be the most appropriate for S_{Ig} predictions.

Overall the GP predictors perform better than the Stockdon et al. (2006) formulation for all the error metrics considered and for the new testing datasets (for both S_{Tot} and S_{Ig}). While for S_{Tot} the predictor of smaller size performs better than the more complex predictor, for S_{Ig} the errors decrease with increasing GP predictor size (Eq. 5.3 to 5.4), when tested on the new dataset. Eq. 5.1 has the smallest RMSE (0.272 m), MSE (0.074 m^2) and MaxAE (0.695 m) of the S_{Tot} formulas, evaluated on the new dataset, while the predictor from Stockdon et al. (2006) — Eq. 2.25 — has the highest RMSE (0.570 m), MSE (0.325 m^2) and MaxAE (1.771 m). Eq. 5.4 performs slightly better than Eq. 5.3 in predicting S_{Ig} evaluated on the new dataset, while the difference is larger when compared to the predictor from Stockdon et al. (2006) — Eq. 2.27.

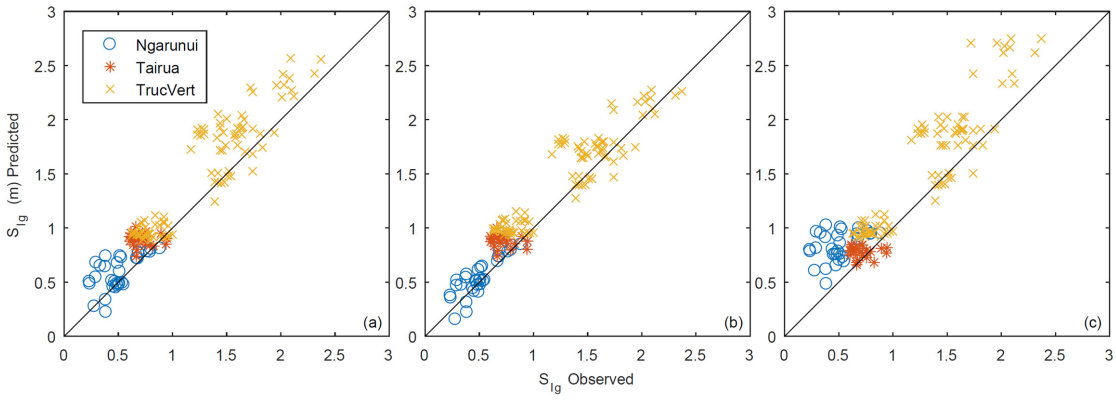

Figure 5.11 Observed versus predicted S_{Ig} with the new independent dataset. (a) GP Eq. 5.3 , (b) GP Eq. 5.4 and (c) Stockdon et al. (2006) — Eq. 2.27.

5.5 Discussion

In this work, the data compiled by Stockdon et al. (2006) are used to build new predictors, by the use of GP, for both total and infragravity swash elevations. The generalizability of these new predictors is then tested using new data (including some extreme conditions). This is different from many previous applications of ML in coastal settings in two ways: First, the ML-derived predictor is tested on data that is collected from a different setting (compared to the training data) — three beaches not included in the training data. Second, the testing data includes events that are outside the data range of the training data — the ML-derived predictor is extrapolated as a test of its generalizability. A single criterion is not assumed for the selection of the best predictors, but a compromise between error reduction (on the testing dataset) and the physical interpretability of the results is found.

Results demonstrate that the GP predictors proposed in this work perform better than existing formulas and that ML can identify nonlinear relationships between the variables of this problem. Specifically, Eq. 5.4 introduces the dependence of S_{Ig} on the beach slope, but also its nonlinear relationship with the wave length. Furthermore, solutions for S_{Ig} found by the GP algorithm with the smaller size (not shown) show a simple linear dependence on H_0 with a constant (identical to early formulation of wave runup e.g. of Guza and Thornton (1982)). More complex predictors add a dependence on L_0, $\sqrt{H_0 L_0}$ (similar to Eq. 2.27 — from Stockdon et al. (2006) and $\frac{H_0}{L_0}$.

The GP algorithm found solutions for S_{Ig} that include the beach slope (β), a variable that is never excluded from predictors of further increasing size. Because the candidate solutions resulted from GP experiments follow a "Pareto front" distribution in which the increase in fitting (smaller MSE) grows as the size of the formula rises, the continuous inclusion of β for more complex predictors implies that including β in S_{Ig}

formulation reduces prediction error. The improvement of classic empirical techniques, by innovation in data-driven methodologies, has already been discussed (e.g. the case of depth-averaged velocities over model vegetation by Tinoco et al. (2015)). Experiments based on GP also highlighted a way to focus on and add dependencies in predictors describing coastal processes (e.g. grain size in the case of prediction of ripple wave length by Goldstein et al. (2013)). The predictors proposed in this work perform well on a wide range of environmental conditions, including, as defined by Nicolae Lerma et al. (2016), the highest stormy condition dataset (Truc Vert beach) recorded in the field and available in the literature. Furthermore, the work here demonstrates that ML derived results, when physically plausible, may be generalizable beyond the limits of the training data, extrapolating to a novel, out of the sample data set.

Looking at the limitation of the proposed models, the variables taken into account (H_0, T_p, L_0, β) are easily accessible but also oversimplify the processes that affect swash. For instance, the influence of the wave directional spread (Guza and Feddersen, 2012)) and of the cross-shore wind component and the tidal range (Vousdoukas et al., 2012) is not included. However, in order to include these and other aspects (e.g., role of underwater vegetation, nearshore bathymetry) it is necessary to perform more field experiments that record swash, runup and other relevant variables. An additional limitation is that the swash formulas obtained in this study approach a nonzero value as wave height approaches zero. While this is physically incorrect, the data used in the analysis does not include the limit condition of 'no waves-no swash'. Consequently, even if the GP formulas obtained do not correctly predict the limit condition corresponding to a no wave scenario, the prediction for both datasets has smaller errors compared to commonly used formulas. Generally, the results from machine learning technique are strictly related to the range of the training and validation datasets (original dataset in Fig.5.1). This work demonstrated that the applicability of the predictors can sometimes be used beyond the range of the testing dataset (new dataset in Fig. 5.11). However it is unknown how predictors will perform in settings beyond those in the present work — future tests on new field data are therefore recommended. Furthermore, parameterizations always work better when free parameters are optimized to a given site by using existing data and it should be considered when proposing universal parameterizations.

The results of this chapter contribute to the discussion on the role of beach slope on the prediction of the infragravity component of the swash. The GP algorithm found a S_{Ig} dependence on beach slope and increasingly more complicated formulas (i.e., more precise predictions) found by the GP all include beach slope as one of the predictive variables. This result is in line with studies such as Ruggiero et al. (2001, 2004) and in contrast with Stockdon et al. (2006), Senechal et al. (2011) and Ruessink et al. (1998). Although difficult to quantify and extremely simplified (this parameter together with sediment diameter should integrate the effect of the entire cross-shore profile), our

results suggest that some parameter involving the beach profile should be considered when predicting runup characteristics.

The results found in this chapter are relevant for a variety of applications where the errors related to empirical formulation obtained by classic regression techniques could be reduced. For instance, in the case of coastal hazards, Stockdon et al. (2006) formulation for wave runup is used by Serafin et al. (2017) for their extreme total water level estimation and by Bosom and Jiménez (2011) in their framework for coastal hazards assessment. Accuracy in runup formulation has consequences for risk and vulnerability assessment as coastal management maps (De Muro et al., 2017a; Perini et al., 2016), and other several studies regarding sediment transport (Puleo et al., 2000), swash zone hydrodynamics and (Puleo and Torres-Freyermuth, 2016).

5.6 Conclusions

Starting from a large dataset covering a wide range of swash, beach and wave field characteristics, two new predictors for total and infragravity swash elevations are developed, using the machine learning technique of Genetic Programming. The new formulas are tested and compared with previously developed and largely accepted parameterizations of swash (e.g., Stockdon et al. (2006)) using independent published datasets. Results of the two GP predictors selected (one for total and one for infragravity swash) show better performance compared with the formulation of Stockdon et al. (2006), evaluated using an independent (unknown to the algorithm) dataset (which included extreme highly energetic wave storm, particularly relevant for coastal hazards). This work contributes to reducing the uncertainty in predicting the swash excursion and consequently in assessing the coastal vulnerability and hazards (e.g. inundation) which depend in part upon wave swash (Bosom and Jiménez, 2011). A better prediction of swash excursion could also influence retreat or accommodation strategies and integrated planning for the mitigation of coastal hazards. Furthermore, GP results indicate that the beach slope influences the infragravity component of the swash — GP predictors improve in performance when the beach slope was included. Therefore is concluded that beach slope is a relevant parameter when predicting the infragravity component of the swash elevation, even though this is contrary to several previous studies (e.g., Stockdon et al. (2006); Ruessink et al. (1998); Senechal et al. (2011)). This have important implications for coastal management highlighting that eventual impacts on beach morphologies (e.g. beach slope modification by beach cleaning and seagrass wrack removal by heavy vehicles) may strongly impacting wave runup. ML and specifically GP can be a useful tool for data-rich problems providing robust predictors and possibly also physical insight. The role and importance of the scientist are not reduced or substituted by the machine but instead improved thanks to a powerful data analysis tool.

Chapter 6

FIELD MEASUREMENTS OF SWASH OSCILLATION WITH PRESENCE/ABSENCE OF SEAGRASS BEACH-CAST LITTER (*Posidonia oceanica* BANQUETTE)

A field experiment was carried out for measuring swash oscillations, coastal waves and environmental conditions with the presence of the seagrass *Posidonia oceanica* in a wave-dominated urban beach in the Western Mediterranean Sea (Cagliari, Sardinia, Italy). The main findings of this chapter will be published in peer-reviewed international journals.

6.1 Introduction

In the last decades, several strategies are proposed to mitigate coastal hazards also induced by climate changes, including managed retreat and accommodation strategies (accommodating natural processes), or protection strategies building of rigid structures or soft intervention, impacting, however, the natural coastal processes and landforms (Masselink et al., 2012a; Nordstrom, 2013). Nowadays, innovative techniques are looking to include vegetation in coastal protection strategies (Demuro and De Falco, 2010; Möller et al., 2014; De Muro et al., 2017b) and proposing ecosystem-based coastal defence (Temmerman et al., 2013). In fact, it was recently shown how the use of ecosystem-based management, in general, could result in an excellent compromise (Barbier et al., 2008).

In this context to preserve, where present, the natural vegetation is becoming even more crucial (Demuro and De Falco, 2010) and understating coastal processes/vegetation interaction seems fundamental. In fact, the role of vegetation in protecting the coast from erosive processes or flooding events is acquiring increasing scientific interest (Loder et al., 2009; Borsje et al., 2011; Guannel et al., 2015; Vacchi et al., 2017). Even during storm events with high storm surge levels salt marshes demonstrated to dissipate waves efficiently and coastal protection scheme was suggested to account for vegetation ecosystems (Möller et al., 2014). The role of several kinds of vegetation in coastal protection was largely studied (e.g. seagrass, mangroves, salt marshes) however, still gaps

exist. In this framework, most of the studies regarding seagrass looked at the influence which seagrass has on waves and currents (e.g. wave dumping) in both laboratories (Luhar et al., 2010; Maza et al., 2015) and field (Luhar et al., 2013; Infantes et al., 2012).

An aspect which received relatively less interest, lacking quantitative assessment, is the effect of seagrass beach-cast litter on waves and coastal protection, which is clearly declared in the literature (e.g. Boudouresque et al. (2015)) even though the discussion is still open (Gómez-Pujol et al., 2013). Vacchi et al. (2017) in a recent review highlight an open issue regarding particularly the role in beach protection by seagrass depositions on the beach face and the interaction of banquettes with approaching waves. It was largely observed that in some cases the amount of seagrass litter which can deposit on the beach face and back beach, can be enormous with $9000\ m^3$ of accumulation peaks recorded in the Western Mediterranean (Simeone and De Falco, 2012). These deposits can reach and influence the dune development and within the banquettes over $60\ kg/m^3$ of sediments can remain trapped (De Falco et al., 2003; Vacchi et al., 2017). Recalling that it is clear how beach-cast litter modifies the cross-shore beach profile, it seems logical that it leads to important modifications to swash motion and erosional/ depositional processes on the beach face. From the author knowledge, the influence of seagrass beach-cast litter on wave swash was never studied, quantified or recorded on the field.

Although the seagrass influence on hydrodynamics was largely discussed in the literature (Luhar et al., 2010; Infantes et al., 2012; Maza et al., 2015; Luhar et al., 2013) and the role of seagrass in protecting the beach from wave action and erosion is largely stated (Boudouresque et al., 2015) the quantification of seagrass berm effect on wave runup seems not to be assessed and measured yet. The limited studies about seagrass depositions morphodynamics and its role in beach protection (Jeudy de Grissac, 1984; Jeudy de Grissac and Audoly, 1985; Mateo et al., 2003) in Gómez-Pujol et al. (2013) are mainly of qualitative nature. This gap in the literature could be linked to the lack of studies relating the seagrass beach-cast litter and the swash hydrodynamics. Only few examples of studies regarding seagrass deposits morphodynamics in relation with storm events exist, (Gómez-Pujol et al., 2013; Simeone et al., 2013) This lack of investigation suggests: how in turn seagrass beach-cast litter on the beach face and berm influences the wave runup and swash process?

The wave swash represents the moving water surface at the beach face (uprush and backwash between the upper and lower limit of runup). During extreme conditions wave runup can account for about 60% of the total water level (Serafin and Ruggiero, 2014), reach the dune, contribute to important (although natural) erosive processes, or flooding within inhabited areas (Komar, 1998; Ruggiero et al., 2001). Wave runup is

included in frameworks for assessing coastal hazards and vulnerability and represents a key parameter largely adopted by coastal managers, engineers, scientists and practitioners when dealing with coastal hazards, climate change management and mitigation (Perini et al., 2016; Bosom and Jiménez, 2011; Vousdoukas et al., 2012). However, the influence of vegetation on this process presents still limited investigation. Some attempts were made both from laboratory (John et al., 2016) and numerical studies (Guannel et al., 2015) however, still gaps exists. No field campaigns are known to the author which investigate wave swash and runup in the case of the presence of vegetation. Furthermore, a quantification of the influence of seagrass deposits on the above-mentioned processes seems also lacking in the literature. A better understanding and quantification of vegetation influence on wave runup and swash process could be critical for $1)$ coastal hazards and climate changes management, prediction and mitigation, as well as for $2)$ enhancing swash zone hydrodynamics and sediment transport knowledge and modelling during these conditions.

This chapter describes a new high-resolution coastal video monitoring system installed in an urban wave-dominated beach in the Mediterranean Sea (Italy) and provide measurements of wave swash, never previously coupled with the presence-absence of seagrass litter (banquette) on the swash and back-beach zones. This chapter aims to enhance the knowledge of the influence of beach-cast litter (deposited on the beach face and berm) on the swash process, and consequent implications for beach protection and management. Section 6.2 describe the field study site. The experimental design, the setting and calibration of the new coastal video-monitoring system, the methodology adopted for image processing and swash extraction is reported in Section 6.3. Section 6.4 shows the findings of the present study. Wave runup and vegetation results are discussed in Section 6.5.1 while seagrass beach-cast litter morphodynamics in Section 6.5.2. Conclusions are drawn in Section 6.6.

6.2 Field Site

The study area (Fig. 6.1 b) "Poetto Beach" is located in the western Mediterranean, in the Gulf of Cagliari, Italy. It is an 8 km long and about 100 m width sandy beach, the shoreface is characterized by a wide *Posidonia oceanica* meadow and it is confined to the west by Sella del Diavolo Promontory (Brambilla, 2014; Brambilla et al., 2016). The beach is characterized by sediments classified as fine and very fine sand for the submerged beach and medium and coarse for the emerged beach (Brambilla, 2014). Poetto beach is classified as dissipative or intermediate depending from the beach sector considered, with morphodynamic states (Wright and Short, 1984; Short, 1999b, 2006) which can vary between longshore bar-trough (LBT), rhythmic bar and beach (RBB), transverse bar and rip (TBR) and low tide terrace (LTB) (Brambilla, 2014; Brambilla

et al., 2016). However, the section of the beach analysed in this chapter is mainly intermediate characterized by LBT morphodynamic state (Brambilla, 2014; Brambilla et al., 2016).

Dominant winds in the study area come from north-west but the winds which give rise to principal wave events come from southern directions (De Muro et al., 2018). The beach is in fact exposed mainly to storms from south-east (41 % of the total energy) south-west (20%) and south-south-east (10%) directions, with a fetch which can overpass 500 km. However, the average wave climate is mild ($Hs \approx 1m$) and the tidal excursion generally does not exceed 0.4 m (De Muro et al., 2018; Brambilla et al., 2016).

This beach can be defined an urbanized beach as it is subject to severe human pressure due to tourism (100000 visitor estimated per day) and nourishment works (Brambilla et al., 2016; De Muro et al., 2017a, 2018).

6.3 Methodology

6.3.1 Experimental Design

The experiment was performed within the wider framework of the project NEPTUNE, acting in the Gulf of Cagliari, studying the coastal geomorphology and hydrodynamics of the area. The experiment was explicitly planned for this PhD thesis research, for recording contextual swash excursion with the contrasting presence-absence of seagrass litter deposition on the beachface. Environmental conditions were monitored during the experiment including hydrodynamical, topo-bathymetric, morphological and meteorological conditions (a weather station was installed in the study site). Acoustic wave and current meters were also set to acquire data contemporaneous to the acquisition interval of the newly installed low-cost video-monitoring system. Contextual cross-shore beach profiles were also acquired by the means of RTK D-GPS surveys. All field data of the experiment are geo-referenced based on the UTM-WGS84 datum coordinate system (UTM zone 32N) and then corrected by local benchmarks.

6.3.1.1 Setting a New Coastal Video-monitoring System

The installation of a new coastal video-monitoring system for hydro- and morphodynamic research purposes is considered a challenging process (Vousdoukas et al., 2011). In fact, it requires to overcome difficulties, as in this case, related to data storage, planning, installation, management, calibration, rectification and geo-referencing of a high-resolution video-monitoring system. In order to overcome those hardships, the procedure applied to the current system follows workflows of previously installed coastal video-monitoring frameworks (Holland et al., 1997; Archetti and Zanuttigh,

2010; Vousdoukas et al., 2011; Taborda and Silva, 2012). The procedure followed here for the setting of a new video-monitoring system consists firstly, in selecting adequate video-cameras and lens according to the purpose of the study. Secondly, the selected instrument was installed at the highest location available in the study area. Thirdly, the system acquisition was set for ensuring that the observation of the temporal and spatial scale of the phenomena studied is guaranteed. As a fourth step, the system needs to be corrected for lens distortions (camera calibration and image correction). Then calibrated images are rectified and image coordinates transformed into real-world coordinates (transformation of oblique images into corresponding plan view images). At this point, images are ready for further processing aimed to features extraction for quantifying the investigated coastal process (in this case time stacks images are created for wave swash digitalization).

Two cameras were installed for this research, monitoring coastal processes at the urban beach "Poetto". The main purpose is to increase the understanding of seagrass influence on near-shore and swash processes, starting from field observations. The system is operating from October 2016 onwards and the data used for this work are spanning the same operational period of an Acoustic Wave and Current Profiler (AWAC) and an Acoustic Doppler Profiler (ADP) from 30/03/2017 until 17 /05/2017. Only data from Camera 1 and AWAC are used for the purpose of this chapter, which was set for wave runup measurements with presence-absence of seagrass litter on the beachface.

The digital IP video-cameras selected are two 12 Megapixel Ultra HD Network Cameras (Ajhua Technology, model DH-IPC-HF81200E, Fig. 6.1 a) which ensure a high-resolution dataset. Camera 1 was installed on the Sella del Diavolo Promontory (UTM coordinates: 4337871.75179 m North, 513664.756181 m East) at a high of 125 m above SWL, using an existing steel structure of a previous video-monitoring system and powered by solar panels (Brambilla, 2014; Brambilla et al., 2016). Camera 2 is installed on the roof of the Marino Hospital building (UTM coordinates: 4340526.002 m North, 515027.048 m East) at 34 m height (Fig. 6.1), where the data from both camera 1 and 2 are received. The system is set to record snapshots for 6 times per day (starting at 07:30 a.m. local time) every 2 hours, for 30 minutes long intervals at a frequency of acquisition of 4Hz. The high amount of data collected, due to the high spatial and temporal resolution required by the experiment, are stored in a local server before analysis.

In order to correct the images from the distortions induced by the camera lens the internal camera parameters were computed (e.g. focal length, principal point position, radial and tangential distortion coefficients). The calibration of the coastal video monitoring system was performed using 14 selected snapshots of a regular pattern, positioned at numerous different angles from the camera (Fig. 6.2). The images were ac-

Figure 6.1 (a) Video-camera adopted for coastal video-monitoring station at Poetto beach. (b) Location of the study area in Western Mediterranean Sea, Cagliari Gulf, Sardinia, Italy. (c) 3D view of cameras, weather station, AWAC and ADP location during "Poetto" experiment, courtesy of Google Earth.

quired at the installation location of the cameras (including camera cover lens effects) with the selected working focal length of the experiment. Thanks to the calibration images, a relation between the geometry of calibration objects (chessboard) and their re-projection by the camera is created. The calibration process was implemented using the open source toolbox "Camera Calibration Toolbox for MATLAB" (Jean-Yves Bouguet, 2018), largely adopted in the literature for coastal studies (e.g. Vousdoukas et al. (2011); Taborda and Silva (2012)). The size of the acquired images is nx = 4096, ny = 2160 pixels.

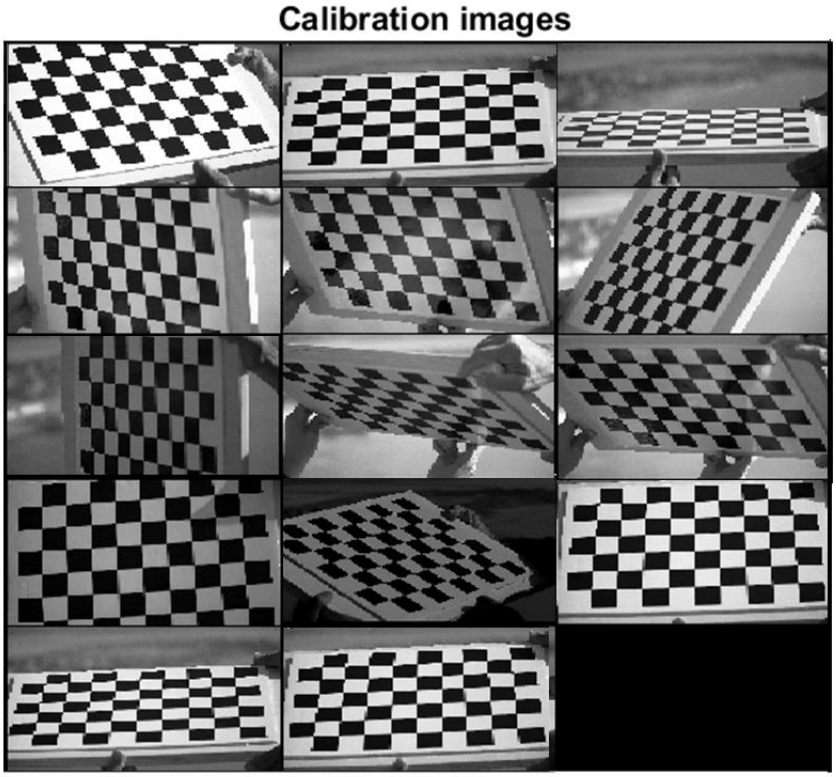

Figure 6.2 Calibration images mosaic used for Camera 1 Calibration.

The results of Camera 1 calibration are reported in Fig. 6.3 and 6.4,

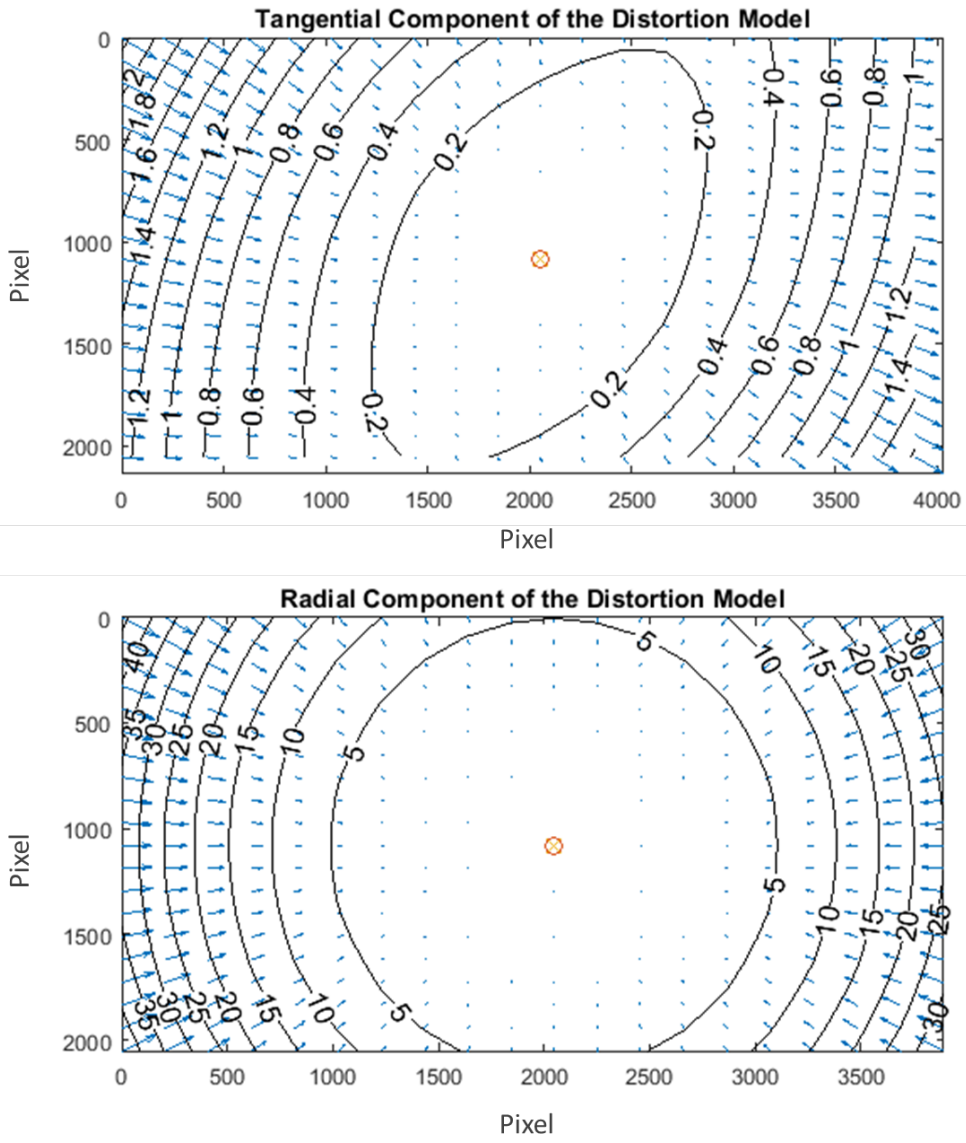

Figure 6.3 Tangential (upper panel) and radial (lower panel) components of camera 1 distortion model.The effects of the distortion introduced by the lens is shown for pixels image, blue arrows indicate the displacement of pixels due to lens distortion. Contour line indicates pixel displacement. The center of the image (cross) and the principal point (circle) are also reported in red.

The complete distortion model (including radial and tangential components Fig. 6.3) resulted by Camera 1 calibration process is reported in Fig.6.4. The distortion resulted dominated by the radial component as already found in previous coastal studies adopting non-metric cameras (Taborda and Silva, 2012). From these results, undistorted images were created and stored automatically for selected time intervals of interest, by a MATLAB routine. The undistorted images resulted in errors of the order of 0.15 pixels.

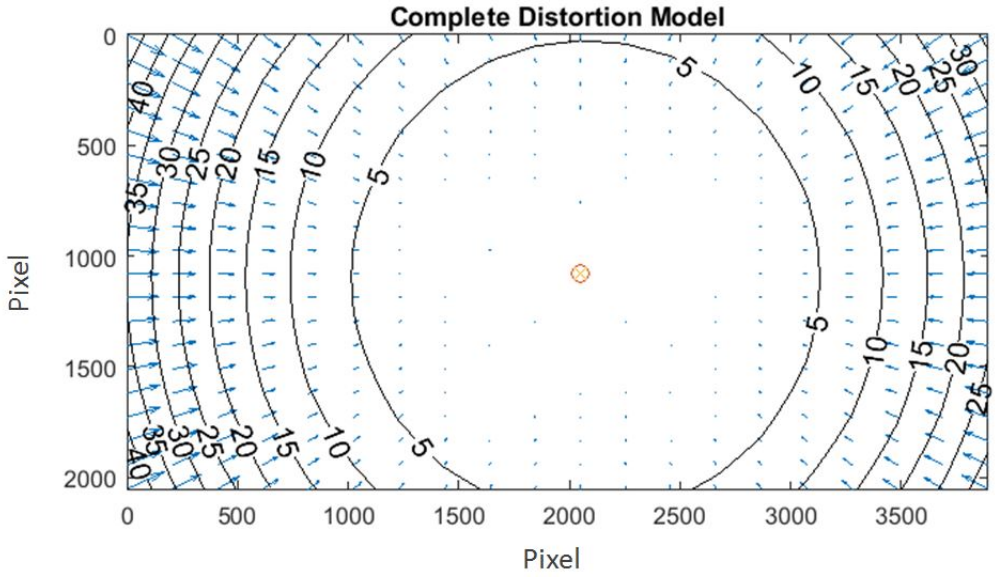

Pixel error	= [0.1567, 0.1413]	
Focal Length	= (19857.9, 20234.5)	+/- [13.51, 17.2]
Principal Point	= (2047.5, 1079.5)	+/- [0, 0]
Skew	= 0	+/- 0
Radial coefficients	= (-1.689, 14.61, 0)	+/- [0.02949, 3.101, 0]
Tangential coefficients	= (0.001619, 0.002315)	+/- [0.0003088, 0.0001682]

Figure 6.4 Results of camera 1 lens calibration, complete distortion model. The effects of the distortion introduced by the lens is shown for pixels image, blue arrows indicate the displacement of pixels due to lens distortion. Contour line indicates pixel displacement. The center of the image (cross) and the principal point (circle) are also reported in red.

The acquired images once corrected by lens distortion are rectified and geo-referenced by the means of 14 ground control points (GCPs) collected by RTK DGPS surveys and contemporaneously recorded by camera 1 within the study area. For each GCP the image coordinates in pixel (2D) are associated with real-world ground coordinates (3D). The correlation between GCPs image and ground coordinates was found manually by the operator. The above information is necessary for accomplishing the procedure of image orto-rectification shown in Holland et al. (1997) and solving, therefore, the collinearity equations. This technique defines the correlation between the ground coordinates, the image coordinates and the projection centre. Thanks to the knowledge of the internal (results of camera calibration) and external (real-world camera position and orientation) camera parameters, the image orto-geo-referencing problem is solved. In other words, the deformation due to the obliquity of the camera is corrected with this procedure (the reason why it is necessary to install the camera at the highest location available in the study area - for camera 1 installation heigh is 125 m above SWL). The resulting plan view images are created on a grid of 0.15 x 0.15 m. The root

mean squared error for the GCPs resulted for the longitude and latitude respectively $RMSE_E$= 0.13 m and $RMSE_N$= 0.38 m. An example of a rectified geo-referenced image is given by Fig. 6.5.

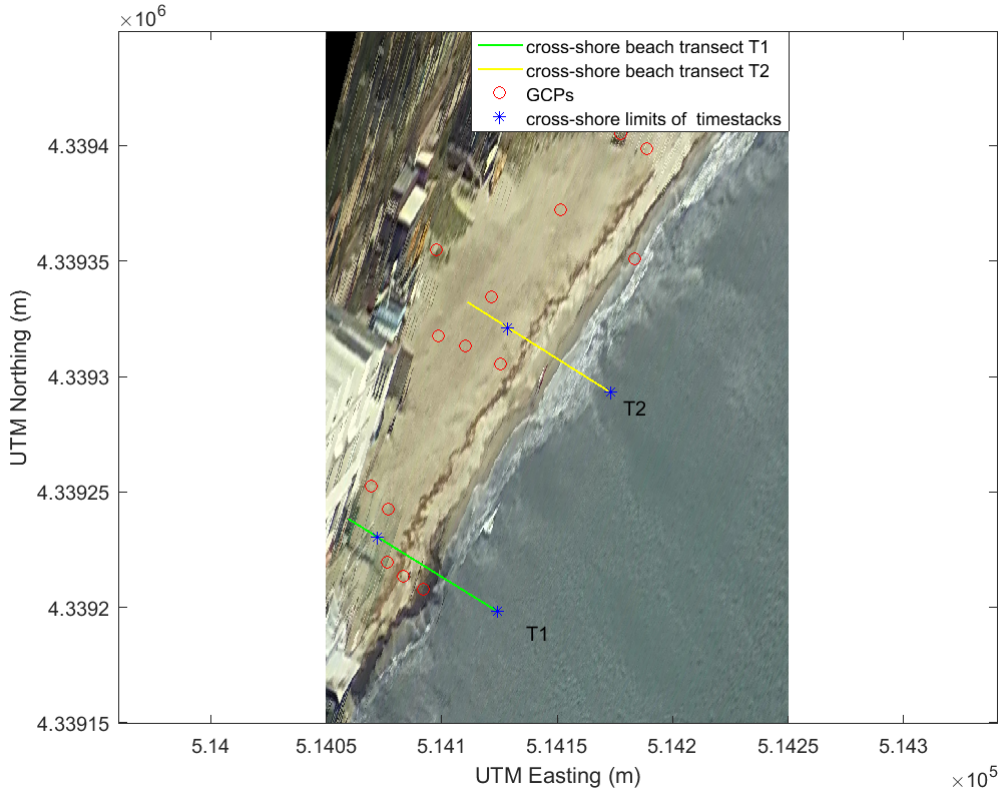

Figure 6.5 Geo-referenced rectified snapshot, UTM zone 32N, during $28/04/2017$ wave event with banquette deposited on T1. Circles indicates locations of GCPs used for image rectification for Camera 1 and asterisk the cross-shore begging and ending of time stacks on T1 (green) and T2 (yellow).

6.3.1.2 Monitoring Environmental Conditions

Contextual and contemporaneous measurements of environmental conditions at the study site were performed during the experiment. An AWAC by Nortek and an ADP by Sontek were installed at 18.5 and 8 m depth respectively (Fig. 6.1 c and Fig. 6.6). The AWAC was installed within an intermatte (an opening in the *Posidonia oceanica* meadow) on sandy substratum and it was operating at 1MHz, from 30/04/2017 at 7.32 a.m. to 17/05/2017 at 03.32 p.m. (local time). The instrument worked for about 20 minutes at the beginning of the hour with a burst every 2 hours in order to be synchronized with camera acquisition intervals. Waves samples were set as 2048 at a sampling rate of 2 Hz. Once the instrument switched from wave to current measurements the following settings were used: averaging interval of 120 s, profiling interval 7200 s. Internal

AWAC processing provided statistical wave parameters (e.g. significant wave height, mean and peak period). Wave measured were back-shoaled by means of linear wave theory in order to obtain deep water wave data. The head of the instrument was installed at 0.5 m from the seabed. The current data consists of one measurement every vertical cell of 0.5 m height, starting from a blank distant of 0.4 m due to instrumental working principle constraints. Additional current measurements were collected in the surf zone by an Acoustic Doppler Profiler (ADP 500kHz by Sontek), located in correspondence of an opening of the *Posidonia oceanica* meadow on a sandy bottom. Current data are not presented here, being out of the purpose of this chapter.

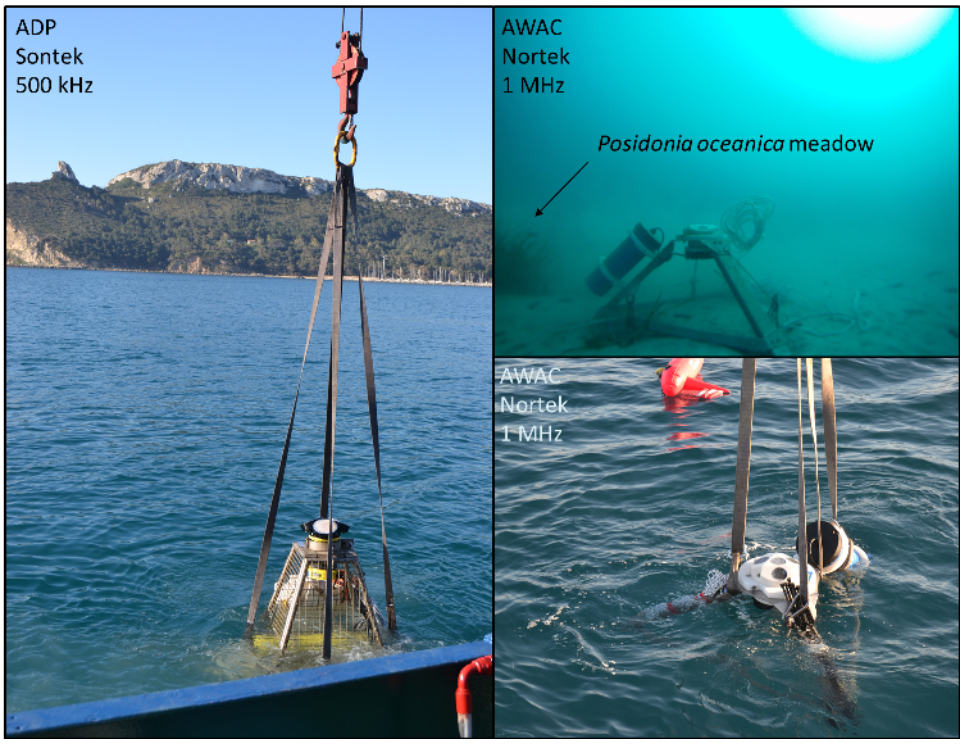

Figure 6.6 Acoustic wave and current meters deployment AWAC underwater at 18.5 m depth APD at 8 m depth.

The cross-shore RTK beach profiles were planned to be repeated on two profiles in correspondence of camera 1 and camera 2 study areas (profiles out of the purpose of the present chapter will not be presented here). The acquisition of topo-bathymetric profiles (until about -1 m) were performed before and after (or ending of) wave events: 06/04/2017, 22/04/2017, 28/04/2017 and 11/05/2017. Observational field campaigns were also performed in order to monitor the presence/absence of seagrass beach-cast litter in relation with wave events and to accordingly plan the RTK cross-shore surveys. The location of transects was therefore selected according to the presence of banquette deposition on the beachface and berm. This chapter focusses on two cross-shore beach profiles recorded with RTK DGPS NavCom SF3040 (Fig. 6.7), within the camera 1

framing, named hereafter T1 and T2 (Fig. 6.5).

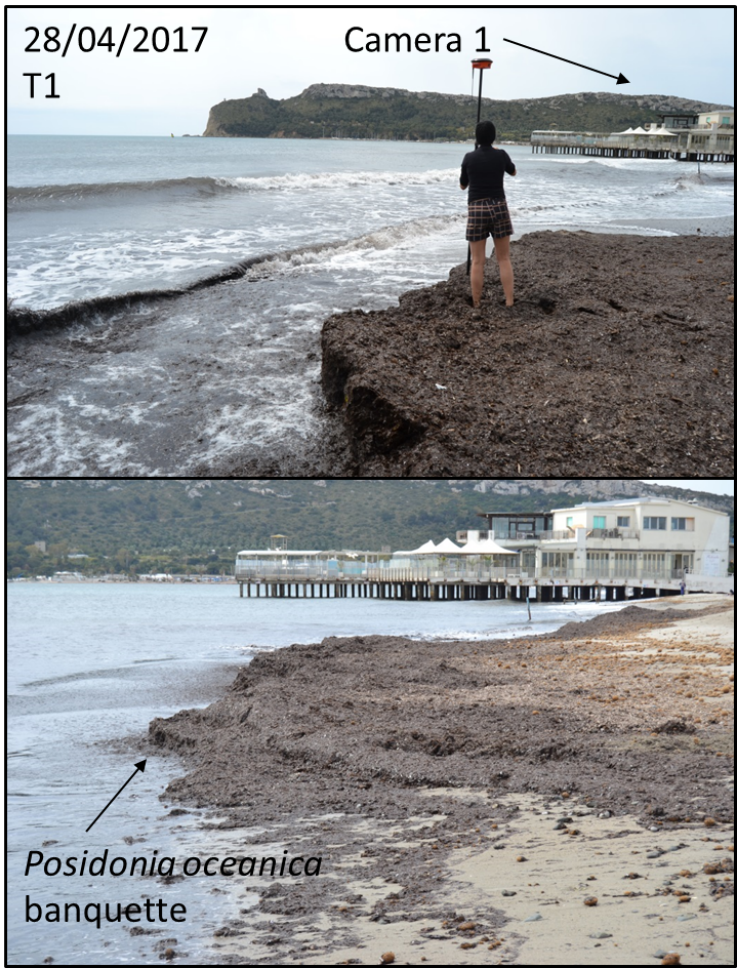

Figure 6.7 *Posidonia ocenaica* banquette accumulation at T1 during the end of E2 (28/04/2017), pictures taken simultaneously to TMSK2 interval.

Meteorological parameters (e.g. atmospheric pressure, wind direction and intensity etc.) were also monitored during the experiment by an ad hoc installed weather station, at the same location of camera 2.

6.3.2 Wave Swash

In order to select within the experimental period the more appropriate intervals of time for studying wave swash, a preliminary analysis of the environmental conditions was performed. The aspects taken into account are the appropriate environmental conditions which would ensure wave swash to be appreciable from the video-monitoring system, contextual with the presence/absence of seagrass beach-cast litter on the beachface, in correspondence of the two beach profiles (T1 and T2). Eq. 5.2 found in Chapter 5 was used to predict the total wave swash (Fig. 6.8c) which could occur during the ”Poetto experiment”. Figure 6.8 show wave parameters (deep water significant wave

height (a), peak period-panel (b) and predicted total swash by Eq. 5.2 (c). Swash events predicted > 0.7m are identified from which four wave events are found (E1-4). The most energetic wave event (E2) is selected for producing four time stacks.

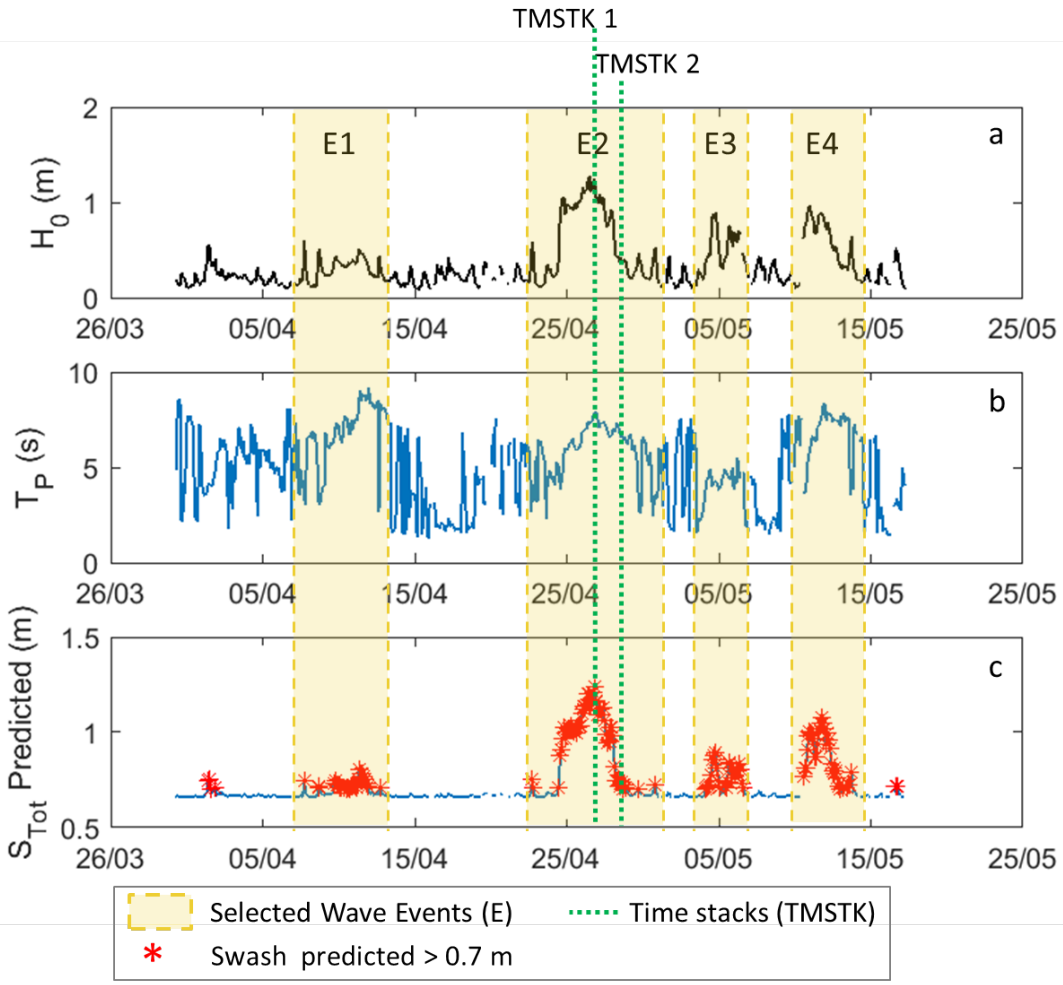

Figure 6.8 Wave events and time stacks identification. Significant wave height (H_0), peak period (T_p) and total swash (S_{Tot}) predicted by Eq. 5.2 are plotted for the entire experiment duration. Four selected wave events (E) are highlighted by yellow bands. Two time stacks are defined (green dotted lines) during the most energetic wave event ($E2$).

The wave swash is measured by the means of time stacks images (Aagaard and Holm, 1989), obtained as pixel intensity "stacked" over time, along defined cross-shore transects. The time stacks images were produced on two cross-shore beach transects T1 and T2 located at 100 m apart Fig. 6.5 (landward and seaward edges of time stack are identified by asterisks). The profile T1 is in some cases characterized by the presence of abundant seagrass beach-cast litter (Fig. 6.7) and the other without (T2). The time stacks span a time interval of 30 minutes with a resolution of 4 Hz. The time stacks

at T1 and T2 are both referred to the same cross-shore reference system so that swash results of the two profiles are comparable cross-shore. The time stacks cover a cross-shore extension of roughly 61 m for T1 and 53 m for T2.

TMSTK 1 is defined for the wave event, recorded by the video-monitoring system (26/04/2017), which is predicted to produce the highest swash (Fig. 6.8). TMSTK 1 it is created both on T1 and T2 in this case, however, both T1 and T2 are free of beach-cast-litter. TMSTK 2 is defined during the highest and more abundant accumulation of seagrass in the experiment (mainly *Posidonia oceanica* banquette Fig. 6.7). Accumulation happened on T1 and the time stacks are created on both T1 and T2. TMSTK 2 is digitalized by two operators for checking the subjectivity in swash extraction from time stacks due to the operator perception, also in the case of beach-wrack accumulation.

The horizontal wave swash was extracted from time stacks manually by digitalization of the shoreline oscillations by an ad hoc programmed Matlab routine. The routine thanks to the field measurements of elevation along the transect, associates to the time stack images the 3D real-world coordinates. Two vectors of time and cross-shore position are created for the shoreline. The horizontal swash time series obtained was then converted into vertical swash by the measured foreshore slope. The foreshore beach slope is calculated for the region defined between +- 2 standard deviation of mean runup elevation, obtained by video-imagery, following the largely adopted method in the literature (Stockdon et al., 2006; Senechal et al., 2011).

The wave swash is calculated from spectral analysis of detrended vertical swash time series data obtained from the 30 min-long time stacks elaboration. The vertical swash signal is transformed from the time domain to the frequency domain through the use of the Fast Fourier Transform (FFT), by a Matlab routine. The FFT is applied to 6 overlapped segments of the series, 512 s long (the routine automatically finds the optimal number of segments for an overlap of about 50%). Both the amplitude and the energy spectra are calculated. The energy spectrum obtained is used for calculating the vertical wave swash from the following accepted formula (Stockdon et al., 2006; Senechal et al., 2011):

$$S_{Tot} = 4 * \sqrt{\sum PSD(f) df} \tag{6.1}$$

where $PSD(f)$ is the energy spectrum and f the frequencies. In this study the analysis was performed for $0 < f < 2\ Hz$ and $df = 0.002\ Hz$. A frequency partition (threshold $f = 0.05\ Hz$) was also applied to runup spectra for obtaining incident and infragravity swash contributions to the total swash.

6.4 Results

6.4.1 Environmental Parameters

Figures 6.9 (T1) and 6.10 (T2) show the topo-bathymetric beach profiles recorded before (22/04/2017) and at the ending (28/04/2017) of the most energetic wave event (E2).

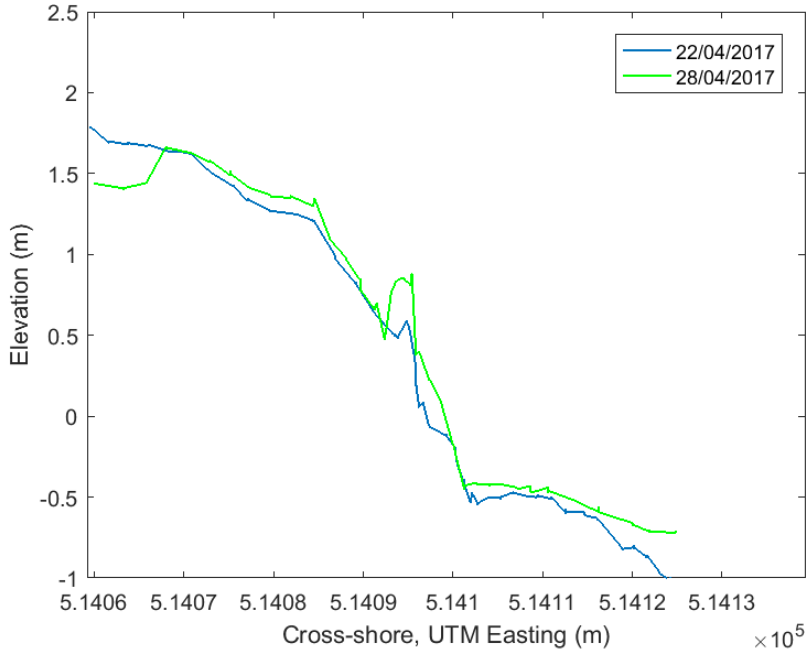

Figure 6.9 T1 cross-shore topo-bathymetric beach profiles recorded on $22/04/2017$ (blue) and $28/04/2017$ (green). Beach profile recorded on $28/04/2017$ includes the accumulation of banquette on the beach face and berm.

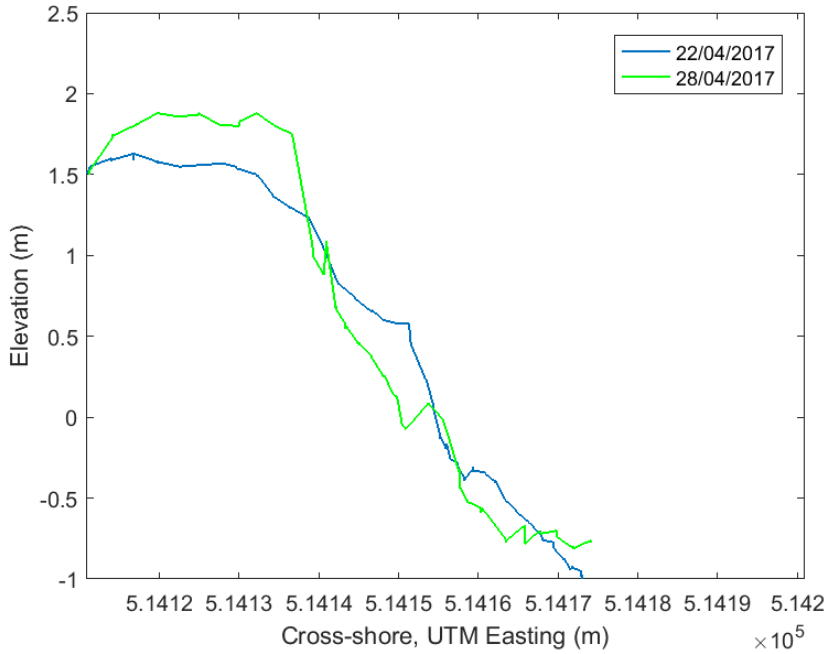

Figure 6.10 T2 cross-shore topo-bathymetric beach profiles recorded on $22/04/2017$ and $28/04/2017$.

The recorded waves during the "Poetto experiment" are prevailing from ESE direction (Fig. 6.11). The maximum significant wave height and period recorded are 1.27 m and 9.17 s. Mean wave height and period resulted respectively 0.35 m and 5.08 s. The mild wave conditions are linked to the spring season in which the experiment took place. The more intense wave events are connected to ESE direction even though oscillations in wave direction are found due mostly to daily breeze effect.

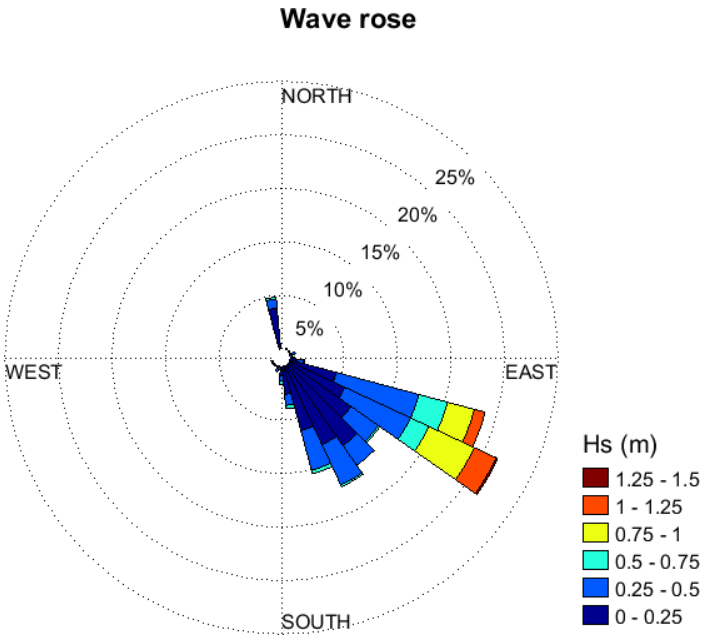

Figure 6.11 Significant wave height and direction recorded by the installed AWAC during the "Poetto experiment" (30/04/2017 - 17/05/2017).

6.4.2 Beach Morphology

One of the two transects analysed in this work, T1, resulted characterized by the presence of beach-cast litter deposition (mainly *Posidonia oceanica* banquette). The elevation of the banquette accumulation is recorded by cross-shore RTK measurements resulting in a maximum height of 0.5 m. Beach-cast litter is found along T1 (Fig. 6.7), during the descending phase of the stormy event E2, from 28/04/2017 until 29/04/2017 (temporal interval during which TMSTK 1 is created 28/04/2017 from 11:30 a.m. to 11:59 a.m., local time, in Fig. 6.13 a and c). Banquette accumulation persisted, with slight variation in shape, until the next wave event of the interval 04/05-06/05, during which erosion of the banquette happened. The dismantling of beach wrack depositions started in the morning of 04/05/2017 ($\approx$ at 07:30 a.m.) and ended the night of 05/05/2017. At the first daily recording of the camera system (06/05/2017 at 07:30 a.m.) the dismantling was completed and only few seagrass deposits were found at higher sea water levels on the beach face, probably due to lowering of the tide.

From time stack analysis at the same time of cross-shore RTK survey, the total cross-shore length covered by beach-cast litter (identified by brown colour versus typical sandy colour) results in 7.2 m (dry plus wet in Fig. 6.13 a). However, the cross-shore extension of banquette associated to a notable change in elevation in beach profile (by field cross-shore RTK measurements), is recorded as 3.4 m (Fig. 6.9, green line). This value is in general agreement with a net difference in colour (darker brown, associated to wet seagrass in Fig. 6.13 a) in time stack, suggesting that a colour-classes based

analysis of time stacks could be used for classifying the different morphologies and morphodynamics in case of seagrass beach-cast litter presence.

6.4.3 Wave Swash

Segments of TMSTK 1 including the maximum swash event on both T1 (a and c) and T2 (b and d) are reported in Fig. 6.12. During TMSTK 1 both profiles are free from seagrass beach wrack. Note that the cross-shore scale is the same for both T1 and T2 and the temporal scale is consistent between panel a and b. Swash events recorded on TMSTK 1 are higher than those during TMSTK 2 (Table 6.1) because of the higher forcing conditions taking place during the peak of wave event E2, while TMSTK 2 is created on the descending phase of E2 (Fig. 6.13 and Table 6.2 including environmental conditions associated to the time stacks). Table 6.1 reports the maximum (and mean) horizontal and vertical swash recorded, during TMSTK 1, which are respectively on T1 19.5 m (10.5 m) and 2.0 m (1.09 m), on T2 are 24.7 m (13.6) and 2.2 m (1.21 m). The standard deviation is around 3 m for the horizontal swash and 0.3 m for the vertical one, for both profiles. In TMSTK 1 longer horizontal swash (both maximum and mean) for T2 corresponds to higher vertical swash when compared with T1 (Table 6.1).

Table 6.1 Results of time stacks analysis, maximum (max), mean and standard deviation (stdv) vertical and horizontal swash, for the two time stacks and the two beach profiles analysed.

	Horizontal Swash (m)	Vertical Swash (m)	Horizontal Swash (m)	Vertical Swash (m)	Horizontal Swash (m)	Vertical Swash (m)	Horizontal Swash (m)	Vertical Swash (m)
Time-Stacks	TMSTK 1				TMSTK 2			
Beach Profile	T1	T1	T2	T2	T1	T1	T2	T2
max	19.5	2.0	24.7	2.20	5.37	1.02	11.42	0.65
mean	10.5	1.09	13.6	1.21	1.91	0.36	5.67	0.32
stdv	3.08	0.32	3.95	0.35	1.23	0.23	1.76	0.1

Segments of TMSTK 2 are reported in Fig. 6.13, during which T1 is characterized by an abundant deposition of seagrass beach-cast litter. The swash digitalized by the two operators is also plotted on the time stacks and the derived swash height difference due to subjectivity of the operators resulted always less than 6.7 %.

Note that the cross-shore scale is the same for both T1 and T2 and the temporal scale is consistent between panels a-b and c-d. The horizontal swash on T1 does not exceed the cross-shore limit (located at about 30 m) given by the seagrass deposition (banquette, Fig.6.13 a and c). In contrast, on T2 both on normal conditions (b) and during the maximum swash event (c) the swash oscillations result shifted onshore, easily

exceeding the above-mentioned limit. In fact, the uprush seems to be limited by the presence of seagrass accumulation and it does not exceed the banquette cross-shore position. This behaviour is also appreciable in detrended vertical swash, which presents a net up-rush limit (Fig. 6.14 c). Only rarely, however, overtopping of the banquette by waves was observed. From Table 6.1 the maximum (and mean) horizontal and vertical swash for TMSTK 2 are on T1 5.37 m (1.91 m) and 1.02 m (0.36 m), on T2 they result in 11.42 m (5.67) and 0.65 m (0.32 m). The standard deviation is respectively for T1 and T2, 1.23 m and 1.76 m for the horizontal swash, 0.23 m and 0.1 m for the vertical one. In contrast, with TMSTK 1 longer horizontal swash (both maximum and mean) for T2 correspond to lower vertical swash than T1 (Table 6.1). In other words, in case of seagrass wrack, even though Table 6.1 shows smaller horizontal runup oscillations, these oscillations results in greater vertical swash (as appreciable also in Fig. 6.14 c-d).

In regards of the seagrass beach-cast morphodynamics, observations of TMSTK 2 on T1 indicates that no change in cross-shore position of the seaward limit of the banquette was observed between begging and ending of the 30 min time stacks.

Table 6.2 Results of environmental parameters and swash analysis.

Time-Stacks	Beach Profile	H_0 (m)	Tp (s)	L_0 (m)	H_0/L_0	β	ξ_0	Beach Type	S_{Tot} (m)	S_{Ig} (m)	S_{inc} (m)
TMSTK 1	T1	1.22	7.64	91.13	0.013	0.103	0.890	I	1.20	0.75	0.94
TMSTK 1	T2	1.22	7.64	91.13	0.013	0.089	0.769	I	1.32	0.89	0.98
TMSTK 2	T1	0.37	6.87	73.69	0.005	0.187	2.645	R	0.86	0.32	0.80
TMSTK 2	T2	0.37	6.87	73.69	0.005	0.056	0.797	I	0.35	0.21	0.28

Wave forcing conditions for TMSTK 1 (Table 6.2) are H_0 =1.22 m and Tp = 7.64 s with a consequent wave length (L_0) of 91.13 m and a wave steepness of 0.013. The beach slope for T1 resulted in 0.103 and for T2 0.089, and the profiles are classified both as intermediate according to Short (1999b) due to their resulting Iribarren numberd. The emerging total swash for TMSTK 1 is 1.20 m on T1 and 1.32 m on T2, with the incident component slightly prevailing on the infragravity one, (for T1 S_{inc}=0.94 m and S_{Ig}=0.75 m and for T2 S_{inc}=0.98 m and S_{Ig}=0.89 m). Wave forcing conditions for TMSTK 2 (Table 6.2) are H_0=0.37 m and Tp = 6.87 s with a consequent wave length (L_0) of 73.69 m and a wave steepness of 0.005. The beach slope for T1 resulted 0.187 and for T2 0.056, consequently T1 is classified as reflective and T1 as intermediate (Short, 1999b), because of ξ_0 for T1 $>>$ ξ_0 for T2. The resulting total swash for TMSTK 2 is 0.86 m on T1 and 0.35 m on T2, with S_{inc}=0.80 m $>>$ S_{Ig}=0.32 m for T1, while for T2 S_{inc}=0.28 m $\approx$ S_{Ig}=0.21 m).

The runup energy spectra from TMSTK 1 (Fig. 6.15) resulted in similar results for

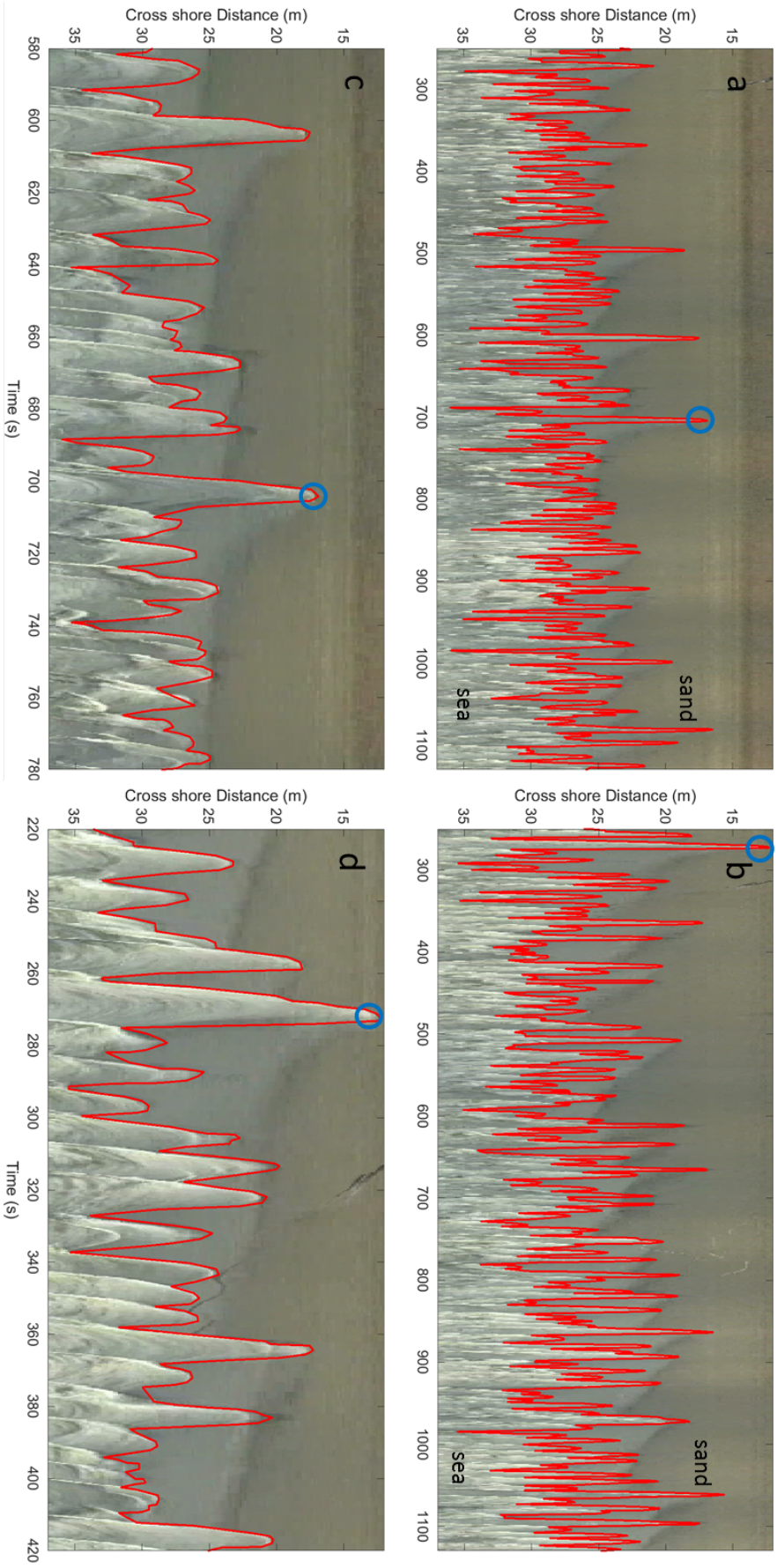

Figure 6.12 TMSTK 1 a and c on T1, b and d on T2; a and b portion of time stacks which includes maxima swash event (blue circles), c and d temporal zoom 200 s long of swash maxima, red line indicates digitalizations of horizontal swash.

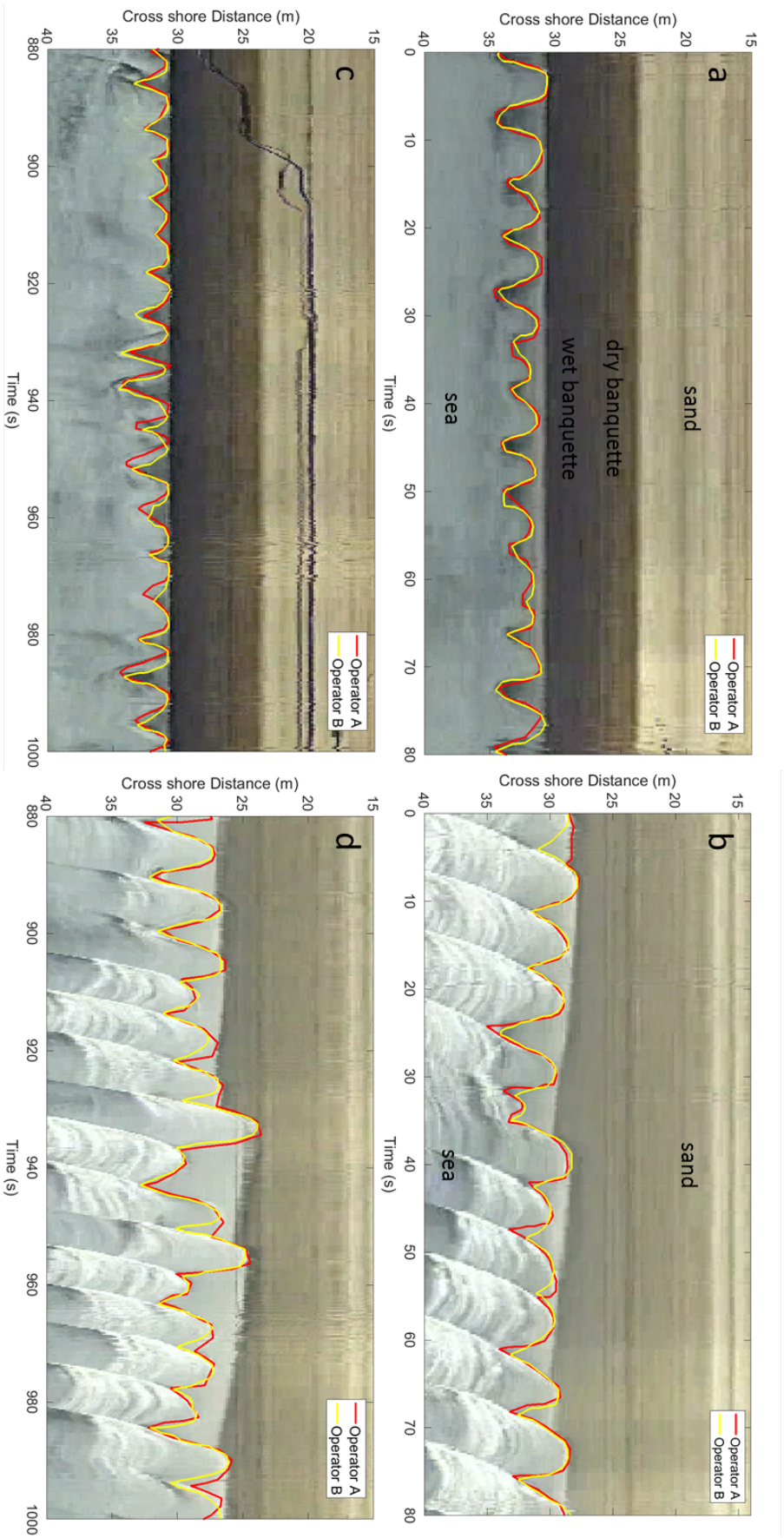

Figure 6.13 TMSTK 2 a and c on T1, b and d on T2; a and b at the beginning of the time stack, c and d temporal zoom during maximum swash event on T2. Red and yellow line indicates two different operator digitalizations.

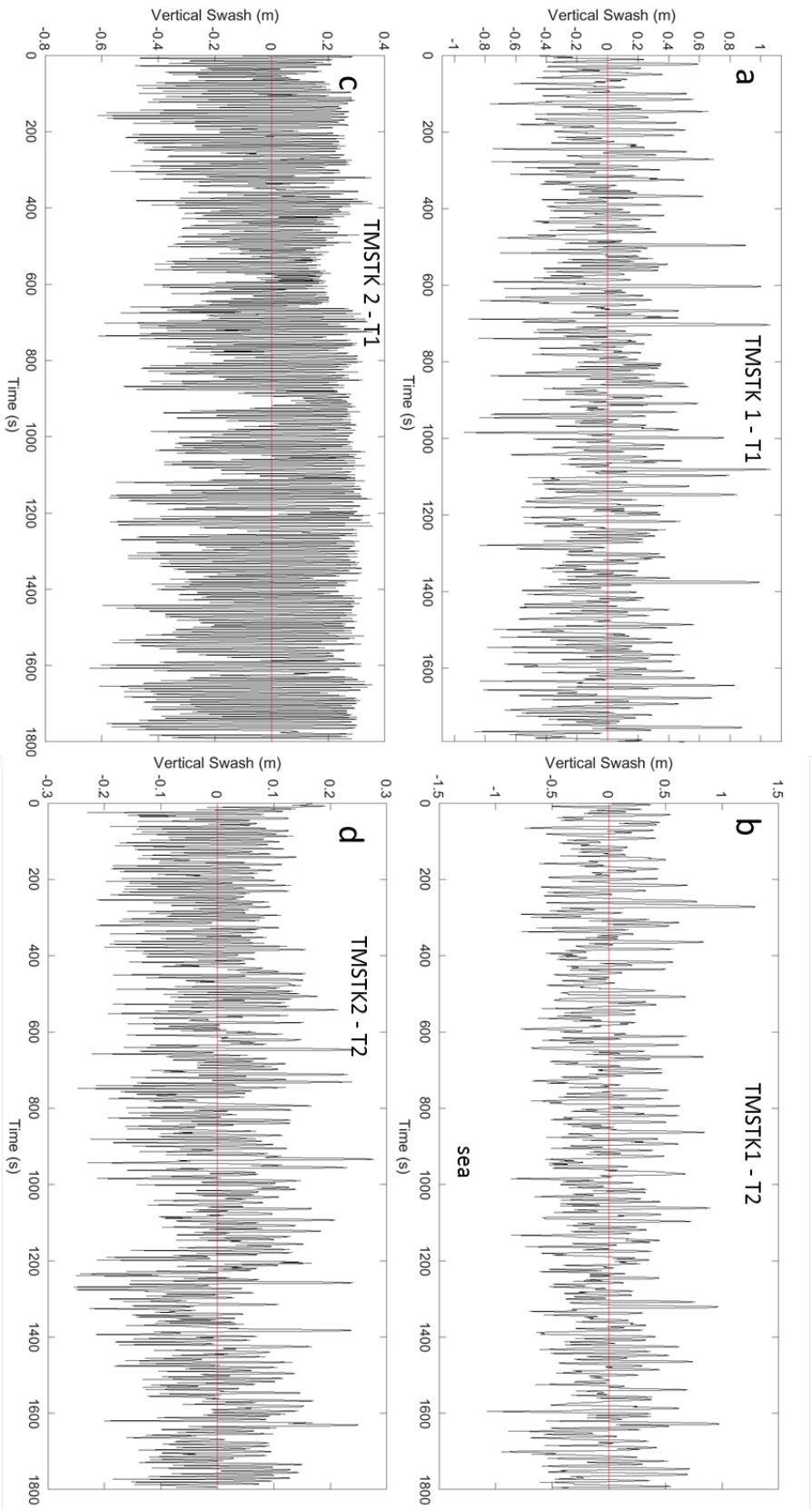

Figure 6.14 Detrended vertical swash. Panels a and c on T1, b and d on T2, panels a and b TMSTK 1, and c (case with beach-cast litter) and d on TMSTK 2.

the cross-shore beach profiles analysed, which are both characterized by the absence of seagrass litter. Both profiles peak frequencies resulted within the infragravity band of the spectrum, nevertheless resulted that $S_{inc} > S_{Ig}$, even if only slightly (Table 6.2).

In contrast, for the case of TMSTK 2 (Fig. 6.16) the spectral results seem different between T1 (characterized by the presence of beach-cast litter on the beach face and berm) and T2 seagrass depositions free. The energy content seems higher in case of banquette deposition. The wave swash peak frequency for T1 is in the incident band of the spectrum (blue vertical dashed line in Fig. 6.16) accordingly with the incident swash being higher than the infragravity one (table 6.2). It appears that a great amount of energy is concentrated within this band. In contrast, the swash peak frequency for T2 is located in the infragravity band. Moreover, a secondary peak is identified for both profiles, which resulted reversed with respect to the primary peak: for T1 in the infragravity band and for T2 in the incident one.

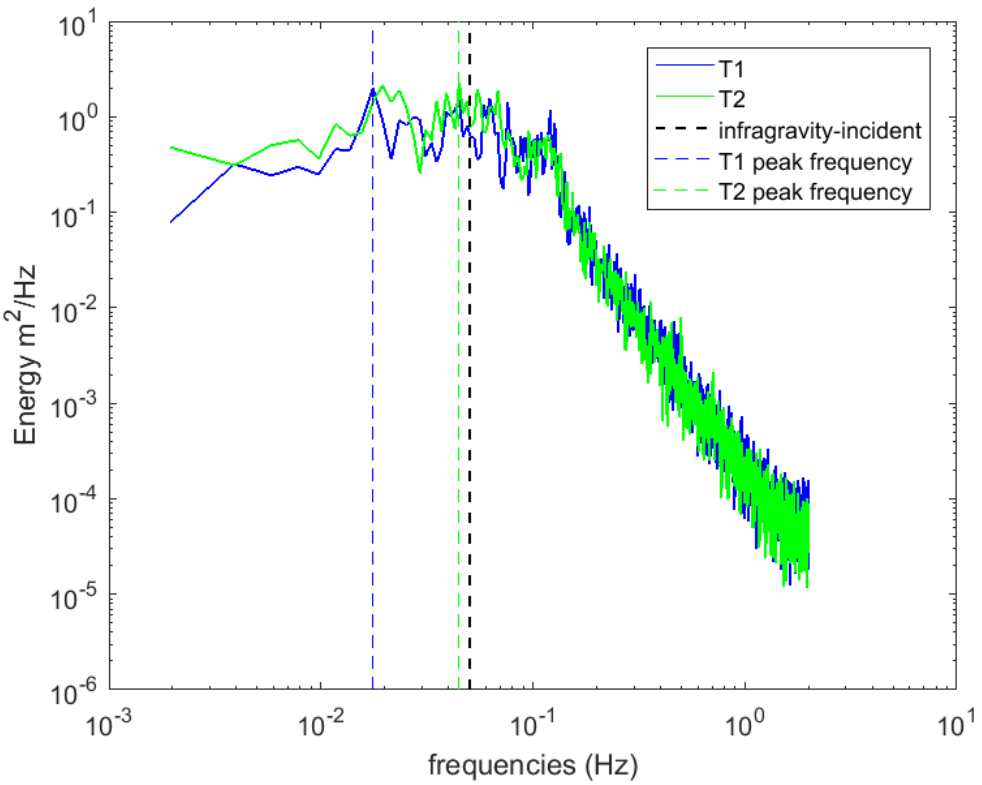

Figure 6.15 Wave runup energy spectra for TMSTK 1, thick blue line for T1, green thick line for T2. Vertical black dashed line indicates separation between incident ($>$ $0.05\ Hz$) and infragravity ($<$ $0.05\ Hz$) frequency band. Vertical blue (T1) and green (T2) dashed lines indicates swash peak frequency.

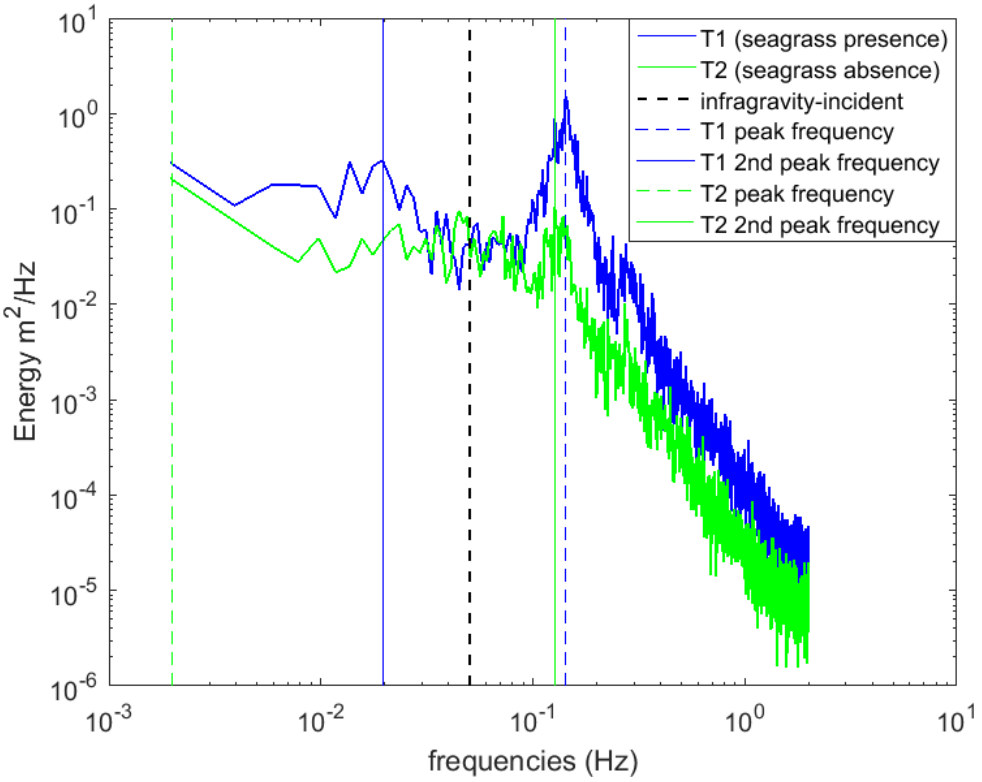

Figure 6.16 Wave runup energy spectra for TMSTK 2, thick blue line for T1 (seagrass presence), green thick line for T2. Vertical black dashed line indicates separation between incident ($> 0.05\,Hz$) and infragravity ($< 0.05\,Hz$) frequency band. Vertical blue (T1) and green (T2) dashed lines indicates swash peak frequencies.

Table 6.3 Dimensionless swash results, adimensionalized by total swash (S_{Tot}) and offshore incident significant wave heigh (H_0).

Time- Stacks	TMSTK 1	TMSTK 1	TMSTK 2	TMSTK 2
Beach Profile	T1	T2	T1	T2
S_{inc}/ S_{Tot}	0.78	0.74	0.93	0.80
S_{Ig}/ S_{Tot}	0.62	0.67	0.37	0.60
S_{Tot}/H_0	0.98	1.09	2.32	0.94
S_{inc}/ H_0	0.77	0.80	2.16	0.75
S_{Ig}/ H_0	0.61	0.73	0.86	0.56

6.5 Discussion

6.5.1 Wave Runup and Vegetation

The results presented here indicate that the presence of seagrass deposition on the beach face influence the wave runup process. In fact, the whole runup process is shifted seawards by the accumulation of seagrass, the horizontal swash associated with runup is

reduced while the vertical swash increased, furthermore an increased swash energy content is also recorded. This could have clearly important implications for beach and hazards management (considering that bad practices exist regarding artificial mechanical removal of such deposition (Duarte, 2004; Simeone, 2008; Nordstrom, 2013; Demuro and De Falco, 2015)) as well as for beach morphodynamics and sediment transport.

The swash analysed on a profile characterized by seagrass presence (when compared with one by seagrass absence) indicates that the frequency distribution is shifted towards higher frequencies, with the peak frequency being located within the incident band, in contrast with a nearby (100 m apart) seagrass-free profile under the same wave forcing condition (TMSTK 2). On the seagrass-free profile, the peak frequency is indeed located in the infragravity band. This seems to be additionally confirmed by the nondimensional swash parameter results, for which the deviation between S_{inc}/S_{Tot} and S_{Ig}/S_{Tot} is higher for T1 (seagrass presence) than for T2 (seagrass absence). In other words, for TMSTK 2, even though the incident swash is bigger than the infragravity swash for both profiles, in the case of seagrass presence this disparity is enhanced (the difference between S_{inc}/S_{Tot} and S_{Ig}/S_{Tot} for T1 is bigger than that one for T2, Table 6.3).

These results could be re-conducted to the change in foreshore beach slope which is induced by the accumulation of seagrass beach-cast, making the profile steeper (for T1 $\beta = 0.187$, versus $\beta = 0.056$ for T2, case of seagrass absence). As a consequence, the two profiles exposed to the same wave input, result in a different behaviour: the first (seagrass presence) presenting a higher Iribarren number (2.645) which falls in a classification of reflective condition, and the second (seagrass absence) in smaller Iribarren number (0.797) which can be re-conducted to intermediate conditions. These disparities produce consequences in wave swash oscillation on the beach face. In fact, from time stacks analysis (on TMSTK 2) longer horizontal swash (both maximum and mean) for T2 (seagrass absence) correspond to lower vertical swash than T1 (seagrass presence) see Table 6.1. This is in contrast with what happens for TMSTK 1 when slopes for T1 and T2 are instead similar.

The present study is limited to mild wave conditions, recorded during the "Poetto experiment" and relay on two time stacks for each of two cross-shore profiles, which were located on a single beach. Extension of the present work could include the digitalization of more swash events, on more transects, associated to a more spread out wave and environmental conditions, including extreme events and other study sites. In order to better relate wave swash to seagrass deposition, other seagrass-beach-cast parameters should be collected during field campaigns (e.g. width, stage of biodegradation, elasticity of the deposited leaves, brittle leaves, etc). From a wider dataset, a predictor of wave runup in the case of presence of seagrass deposits could be developed, derived potentially by data-driven techniques as Machine Learning (following the work of Chapter

5).

Indeed, both field measurements and formulation of wave runup which account for vegetation effects are highly demanded in the literature (Guannel et al., 2015; Van Rooijen et al., 2016). Although, Guannel et al. (2015) proposed a modelling framework accounting for underwater vegetation effects on wave set up and incident swash (adding specific terms in Stockdon et al. (2006) formulation), neither the effect of vegetation on infragravity swash component nor the cases of seagrass beach-cast litter were considered. Moreover, Van Rooijen et al. (2016) included in Xbeach model new formulations for accounting for vegetation effects on the incident and infragravity waves as well as on wave setup. Even though Van Rooijen et al. (2016) study is directly related to wave runup, neither a direct consideration of swash and runup process nor the eventual presence of seagrass berm was included. Both studies explicitly highlight the importance of field measurement of runup process with presence of vegetation, no field datasets for validating their formulas were in fact available.

6.5.2 Seagrass Beach-cast Litter Morphodynamics

This study may be useful for improving our understanding of seagrass wrack depositional and erosional processes, and therefore of banquette morphodynamics. In fact, recent studies (Oldham et al., 2014) clearly stated that the wrack discharge from the beach is related to swash hydrodynamics. According to Oldham et al. (2014), the depositional process of wrack on the beach is likely to be due to a complex process, involving changes in bulk density of both accumulations and particles (increase in density through compaction and decrease due to drying). In Oldham et al. (2014) is suggested that erosion of beach wrack is likely to be due, apart from wave action at the base of the banquette producing collapse proposed by Mateo et al. (2003), to floating particles. After a period in which the particles dried, the percentage of particle floating in their experiment increases. They also pointed out that the deposition might be produced by high-water events. The innovative coupled seagrass/swash field observations of this chapter represent a solid basis for further investigations of the vegetation wrack morphodynamics on beaches. In fact, is observed that both dry and wet material compose beach-cast litter accumulations and that they are differentiable by an easily reproducible low-cost video-monitoring system, which could also trace their dynamics both in space and time at different scales at high resolution.

Although its potential, still a limited image analysis and quantification of banquette morphodynamics were performed in this chapter, providing mainly general descriptive and conceptual results which, however, open the investigation to a successive more detailed analysis of seagrass beach-cast morphodynamics, on several coastal settings. This work also presents a first contribution for measuring on the field, wave swash with

the contrasting presence/absence of seagrass deposition on the beach face and berm. However, more field experiments are needed, which could monitor other swash zone processes (e.g. littoral drift, sediment transport) in presence/absence of seagrass litter. Furthermore, they could be performed on varying and spread out environmental conditions (wave severity, direction, duration, spectral characteristics, tidal regime, water level, storm surge, beach type, slope and alongshore variability, seagrass deposition type and characteristics, storm/seagrass deposition timing). This work represents a first attempt in clarifying the consequences of such depositions on wave runup, a process recognized fundamental for beach management and coastal hazard applications. However, this attempt remains limited to the experimental setting here investigated, therefore the author is not responsible for any practical application of these preliminary sites- and time- specific results here obtained, which are not meant to be general or directly functional.

The debate on the role of the vegetation in beach protection has historically been open and still seems to attract interest in the literature. Probably, because our understanding is nonetheless limited especially of seagrass beach-cast deposition on the beach face and its interaction with the complex beach morphodynamics, as well as because the banquette morphodynamics itself is defined as a complex phenomenon (Gómez-Pujol et al., 2013; Oldham et al., 2014). According to Gómez-Pujol et al. (2013) *Posidonia oceanica* banquettes uses to be removed in low wave energy conditions, and seagrass wrack, in general, tends to be accumulated by high energy events (Oldham et al., 2014), results indicate that hardly they persist until a next wave stormy event. However, in this work is found that accumulation can occur between two successive stormy events (from 28-04-2018 to 04-05-2018), and dismantling of banquette starts indeed during the next storm. This possibly influences wave-foreshore interaction and therefore morphology and morphodynamics having a direct effect on wave swash and runup processes. These aspects can conduce to important implications in beach protection services furnished by the banquette, likely slowing down the beach erosional process, and therefore to beach and hazards management. However, the results of this chapter are not completely in contrast with those of Gómez-Pujol et al. (2013) since the deposition of the banquette started during the end of the second storm (E2) when the wave conditions already were decreased. This seems in agreement with Gómez-Pujol et al. (2013) which observed deposition during mild wave conditions.

Finally, in this study simultaneously with the dismantling of the banquette on T1, another accumulation of seagrass, further at east on the bachface and berm, was recorded to grow, increasing its extension seaward. This second previously existing seagrass-accumulation (it was recorded to be completely formed during the day 29/04/2018), was located $\approx$ 300 m apart from the T1 deposit, and extended towards the sea during the dismantling of T1 banquette. The observations including this second seagrass accumu-

lation indicate 1) that very probably the material eroded from T1 deposit was moved to another nearby location on the beach, 2) that possibly interaction between waves, swash motion, near-shore currents, littoral drift within the swash zone resulted in this translation of material, 3) potentially making of seagrass deposits a natural lagrangian tracers of nearshore, swash hydrodynamics and sediment transport 4) additionally it suggests that possibly banquette morphodynamics could be studied as a self-organization process, because the second accumulation increases and grows, starting from an initial discontinuity within the foreshore, where released free material of seagrass deposits, tended to accumulate interacting with waves and currents.

6.6 Conclusions

A new low-cost easily reproducible high-resolution video-monitoring system is installed to observe the interaction between seagrass beach-cast deposition on the beach face and swash flow. Results show the influence that seagrass deposits on the beach have on wave runup on a wave-dominated sandy beach in the Mediterranean Sea. This work furnishes innovative never previously recorded field observations of shoreline time series with the contrasting presence/absence of seagrass beach wrack during mild offshore wave conditions (max H_0 =1.22 m and max Tp = 7.64 s).

In case of seagrass presence, the swash process results shifted offshore with a reduced horizonatal swash and an increased vertical swash, compared with a 100 m apart seagrass-free profile. This change seems to be ascribable to the foreshore slope becoming steeper, from β = 0.056 (seagrass absence) to β = 0.187 (seagrass presence) which induced the beach profile to become reflective (ξ_0 = 2.645) in contrast with the seagrass-free intermediate profile (ξ_0 = 0.797). From runup energy spectrum analysis the energy content seems generally to rise, with the incident swash becoming mainly dominant on the infragravity component. The swash peak frequency is recorded on the incident band for seagrass presence and on the infragravity band for seagrass absence. It seems that the banquette deposition acts as a barrier to swash process, inhibiting the horizontal swash to extend onshore, in fact, the uprush seems to be limited by the presence of seagrass accumulation and it does not exceed the banquette cross-shore position.

This behaviour could have important implications in coastal hazards, management, swash zone morphodynamics and sediment transport. This work partially confirms the role of seagrass beach-cast litter in beach protection, creating shoreline accretion and therefore shifting the wave runup process offshore. From the findings in this contribution, artificial removal of seagrass wrack from the beach face, berm and back-beach, would possibly have a new negative impact to be added to the existing list of seagrass eco-system services impacted by this bad practice (Duarte, 2004; Simeone, 2008; Demuro and De Falco, 2010; Nordstrom, 2013; Boudouresque et al., 2015). The wave

swash process would be shifted towards the coast and the wave runup process would act at the beach without the natural barrier constituted by the seagrass berm. Still, uncertainty remains on the long-term effect of such deposition during storm events, seasonality, the severity of storms and beach type. However in this work, differently from what found in Gómez-Pujol et al. (2013), banquette deposition was observed to occur also between two successive wave events and persist until the beginning of the next storm possibly providing an initial beach-protection service. Open questions remain regarding the beach management and coastal hazard implications. For instance, which may be the effects of mechanically removing seagrass deposits by humans, in terms of wave runup?

In the future, from the field data available a predictor for wave swash in presence of seagrass wrack should be obtained, contributing to the increasing demand of both field measurements and models of runup in case of vegetation (Guannel et al., 2015; Van Rooijen et al., 2016) adding at the same time a new factor to be taken into account: the seagrass beach-cast litter. New different experimental settings could be further investigated additionally by the means of both numerical and physical modelling, also in relation with protection strategies for coastal hazards and management applications. Low-cost video-monitoring systems are confirmed useful tools when studying beach swash hydro- and morpho-dynamics. This work suggests that dry and wet material are differentiable by these techniques potentially giving insight on seagrass deposition morphodynamics at different spatial and temporal scales. As already proposed for several swash-zone and shoreface morphodynamic phenomena (e.g. beach cusps, sand bars), future research could investigate if seagrass wrack morphodynamics responds to self-organization process being governed by a mutual adjustment of swash flow, beach-cast litter and sand particles.

Finally, this work demonstrated to contribute to enhancing the knowledge of swash zone hydro- and morphodynamics. Results and feature developments of this work can be of interest for scientists, managers engineers, practitioners, studying and dealing with sediment transport, hydro- and morpho-dynamics modelling, coastal hazards and vulnerability prediction and management, aspects which nowadays acquired critical importance and urgency by ongoing climate change.

Chapter 7

CONCLUSIONS

This work contributed to improving the knowledge and the predictability of swash processes useful to the purpose of coastal protection, management, hazards mitigation and prediction. The original contributions to the research of this PhD consist of the following points:

- While previous works mainly assessed wave runup parametrization performances, in this contribution the prediction and universality of existing vertical swash formulas were evaluated on a wide field dataset, including extreme conditions, on worldwide beaches.
- Widely adopted runup and swash predictors, in the fields of coastal management, hazards assessment, prediction and mitigations, still showed high errors. In this dissertation, two new predictors for vertical total and infragravity swash are proposed showing to improve predictability compared with previously largely adopted predictors in the literature.
- While existing formulas for wave swash were mainly obtained by classical regression techniques, in this contribution the 4 swash formulas proposed are found by the means of innovative machine learning technique.
- Despite machine learning generally and genetic programming, in particular, demonstrated a high potential for coastal data-rich problems, they were never applied to vertical swash formulation of natural sandy beaches. This work demonstrates the utility of the genetic programming technique for obtaining reliable predictors which maintain a physical insight into the swash process.
- Although previous research largely investigated the infragravity swash phenomenon is not clear which are the environmental parameters on which the infragravity swash excursion depends on and still contrasting opinions exist on the contribution of the beach slope on the infragravity swash. In this work, the powerful data-mining technique of machine learning shows that introducing the beach slope into vertical infragravity swash formulas improves predictability reducing errors when tested on independent (unknown to the algorithm) field dataset.

- Even though the role of vegetation in protecting the coast was largely stated in the literature, nowadays still gaps and contrasting opinions exist on the role of seagrass beach-cast litter in beach protection and its influence on wave runup. This work contributes to enhancing the knowledge of seagrass beach-cast litter/ swash interaction which shows potential implications for beach protection from hazards.

- Seagrass wrack influence on wave swash was never recorded in the field or quantitatively assessed. In this PhD thesis field measurements of never previously recorded swash oscillations with the condition of presence/absence of seagrass deposition on the beach face and berm are presented. Comparisons between the presence and absence condition reveal the influence on swash excursions exercised by the seagrass wrack. These findings constitute the first step in the knowledge enhancement of the interaction between wave runup and seagrass beach-cast litter.

The key findings of this research are summarized below for Chapters 4, 5 and 6.

1. Even though numerous vertical swash predictors were developed in the literature, it is not clear whether the existing formulations are applicable to a wide range of beaches and wave conditions.

   The test, in Chapter 4, of 13 existing swash formulas (total, incident and infragravity) on 636 published field swash measurements (collected on beaches worldwide) was performed for improving understanding about the universality of existing swash formulas. Results show that the formulas both over and under-predict the field observations. Stockdon et al. (2006) predictor for total swash resulted in smaller errors than Guza and Thornton (1982), both formulas both over and underestimating the field data. Ruggiero et al. (2004) S_{in_Rg01} formula (including beach slope) showed smaller errors, both incident swash formulas mainly under predict observations. Between the infragravity swash formulas analysed Stockdon et al. (2006), Holman and Sallenger (1985), Ruggiero et al. (2004) and Senechal et al. (2011) better reproduced the observed infragravity swash.

2. From a review of the literature in Section 2.1.4.1 stands out that the most largely adopted empirical parametrizations of wave runup (e.g Stockdon et al. (2006)) show large errors and strongly underestimate observations. The discrepancy of observed and predicted runup is large especially during extreme storms, particularly relevant to coastal hazards, which suggests that new formulations of wave swash could be proposed trying to reduce the prediction errors. Furthermore, the influence of the beach slope on the infragravity component of the swash is

discussed controversially by several authors. Although machine learning (ML) techniques have demonstrated to have a high potential in modelling nearshore processes, they are not yet being used for finding predictors of wave swash on sandy beaches.

In Chapter 5, genetic programming (GP), a type of machine learning approach is adopted to predict the total and infragravity swash excursion using previously published data sets that have been used extensively in swash prediction studies. Three previously published works with a range of new conditions are added to this data set to extend the range of measured swash conditions.

Using this newly compiled data set is demonstrated that a ML approach can reduce the prediction errors compared to well-established parametrizations and therefore, it may improve coastal hazards assessment (e.g. coastal inundation). Predictors obtained using GP can also be physically sound and replicate the functionality and dependencies of previous published formulas. Overall, it is shown that ML techniques are capable of both improving predictability (compared to classical regression approaches) and providing physical insight into coastal processes. Furthermore, GP results indicate that the beach slope influences the infragravity component of the swash (the predictors obtained by GP showed smaller errors as the beach slope was included).

3. Reviewing the literature in Section 2.2.3, the debate on the role of seagrass beach-cast litter in protecting the coast from hazards as erosion or flooding resulted still open. The influence that seagrass depositions on the beach face and berm has on the swash process and wave runup has not being assessed, measured or quantified yet. Therefore, also the implications which this lack of knowledge could have on coastal management, and hazards are still open questions.

   In Chapter 6, a field experiment was carried out for measuring swash oscillations, coastal waves and environmental conditions during presence/absence of seagrass depositions on the beach face of a wave-dominated urban beach in the Western Mediterranean Sea (Cagliari, Sardinia, Italy). The never previously recorded field observations of wave swash with the presence of seagrass beach wrack were obtained through times stack images recorded by the means of an ad hoc newly installed coastal video-monitoring system. In the present work, due to the presence of the seagrass berm, the whole swash process resulted moved offshore compared with a nearby seagrass-free beach profile. Furthermore, the cross-shore beach profile characterized by the presence of seagrass beach-cast litter becomes steeper. The beach slope measured is greater (while wave conditions are constant) resulting in the profile with the presence of seagrass falling in the reflective beach

classification. Furthermore, in that case, the incident swash resulted mainly dominant on the infragravity component. The influence which seagrass deposition on the beach face has on wave swash could have implications for beach management. Bad practices as the removal of such depositions could affect the swash process and move the runup process back towards the coast. The related coastal hazards and human impact implications of the findings of this research should be better investigated and taken into account in future coastal management plan and strategies.

When testing swash predictors in Chapter 4, for evaluating existing swash formulas on wide and comprehensive field datasets, two aspects stand out: a) the importance of considering the kind of data used for developing the formula (and how it might limit) their universality and b) that the scatter between observations and predictions for large swash excursion increases for all formulas. Caution is needed when applying parametric swash formulas mostly during extreme events. The large scatter between observed and predicted swash of existing formulas encouraged the development of new swash predictors in Chapter 5.

New formulations of swash elevation on sandy beaches were proposed in Chapter 5 for improving runup predictability. From the research performed in Chapter 5 is concluded that even though some previous studies disagree (e.g. Stockdon et al. (2006); Ruessink et al. (1998); Senechal et al. (2011)) the beach slope is a relevant parameter when predicting the infragravity component of the swash elevation. This could have important implications in coastal hazard and beach management, for instance in relation with bad practices as beach cleaning and seagrass wrack removal by heavy vehicles, which can modify beach morphologies (and slope), potentially strongly impacting wave runup. Furthermore, ML techniques (specifically GP) is confirmed as a powerful tool for data-driven analysis in coastal setting, also in the case of wave swash on sandy beaches. GP analysis results in robust predictors while maintaining a physical insight into the results. The role and importance of the scientist in this process are not reduced or substituted by the machine but instead improved thanks to a powerful data analysis tool.

Never previously measured swash oscillations on sandy beaches with the presence of underwater vegetation and its litter were performed on the field experiment reported in Chapter 6. From this chapter is concluded that seagrass beach cast-litter can influence wave runup process and beach morphology, shifting the swash process seawards, acting as a barrier to uprush, making the beach profile steeper, classified as reflective. Furthermore in case of seagrass accumulations the swash energy is shifted towards higher frequencies, with the swash peak frequency being located within the incident band, in contrast with a nearby seagrass-free profile under the same wave forcing condition, ris-

ing the dominance of incident swash on the infragravity component. These findings could have implications in coastal and hazards management and mitigation. The influence that bad practices could have on wave runup and coastal hazard, as the removal of seagrass depositions from the beach, should be better assessed under the light of the new findings.

This research can be useful to researchers and practitioners finding applicability to coastal management, hazards, risk and vulnerability assessment, a better prediction of swash excursion could also influence retreat or accommodation strategies and integrated planning for the mitigation of coastal hazards (Demuro and De Falco, 2015; Simeone, 2008; Stockdon et al., 2007; Serafin et al., 2017; Bosom and Jiménez, 2011; Perini et al., 2016). Furthermore it is relevant to several studies regarding sediment transport (Puleo et al., 2000), swash zone hydrodynamics and processes (Puleo and Torres-Freyermuth, 2016). The applicability of the findings of this research to the above-mentioned fields is connected to the assessment of performance and universality of existing swash predictors (component of wave runup) largely adopted in these settings; to the proposal of new total and infragravity swash formulas which demonstrated to reduce the uncertainty in runup prediction, consequently decreasing the uncertainty in their possible coastal hazards and management applications; to the enhancement of the knowledge of previously neglected interaction of swash process with seagrass beach-cast litter on the beach face.

Further investigation on the applicability of parametric swash formulas for extreme conditions is recommended. ML learning techniques are recommended for data-rich problems in coastal settings and their application is encouraged as in this work showed high potential in both improving predictability and giving insight into the physical process (importance of beach slope in infragravity swash).

This work presents a first attempt of field measurement of swash zone processes with the contrasting presence/absence of seagrass deposition on the beach face and berm. However, more field experiments are needed on a wide range of environmental forcing conditions (wave severity direction, duration, spectral characteristics, tidal regime, water level) beach type, seagrass deposition type and characteristics, storm/ seagrass deposition-erosion timing. In the future, from the field data available a predictor for wave swash in presence of seagrass beach-cast litter depositions should be obtained for enhancing the predictability of wave runup in the case of seagrass deposition.

Further research is needed to clarify and enhance our knowledge of beach morphodynamics in case of seagrass beach-cast litter. The findings of this work motivate further research in the dynamics of deposition and erosion of banquettes (beach wrack morphodynamics) in relation with swash process, beach type, storm intensity and tim-

ing remains not clear and further research in this field is suggested. For this purpose video-monitoring systems seems to have high potential recording beach wrack morphodynamics at a different time and spatial scales, with different colours being associable to different seagrass deposition characteristics (e.g. dry/wet). It is likely that banquette behaviour would be governed by a mutual adjustment of swash flow and beach-cast litter, as already studied and proposed for several swash and shoreface morphodynamic phenomena (e.g. beach cusp, sand bars). Further investigations are therefore needed in order to assess whether the banquette morphodynamics responds to self-organization process.

Coastal protection and management in relation with human impact and hazards represent challenges which coastal practitioners and researchers should face together, especially nowadays in a changing climate. This work contributes to reducing uncertainties and enhancing the knowledge and predictability of wave runup, strictly connected to coastal protection and management as well as to coastal hazard mitigation and prediction.

Bibliography

Aagaard, T. and Holm, J. (1989). Digitization of wave run-up using video records. *Journal of Coastal Research*, 5(3):547–551.

Aagaard, T. and Masselink, G. (1999). *Handbook of beach and shoreface morphodynamics*, chapter The surf zone. John Wiley and Sons, New York, NY, USA.

Abolfathi, S., Yeganeh-Bakhtiary, A., Hamze-Ziabari, S. M., and Borzooei, S. (2016). Wave runup prediction using m5 model tree algorithm. *Ocean Engineering*, 112:76–81.

Airy, G. (1845). On tides and waves. Encyclopaedia Metropolitana. Mixed Sciences, volume 5, London.

Anders, F. J. and Leatherman, S. P. (1987). Effects of off-road vehicles on coastal foredunes at fire island, new york, usa. *Environmental Management*, 11(1):45–52.

Archetti, R. and Zanuttigh, B. (2010). Integrated monitoring of the hydro-morphodynamics of a beach protected by low crested detached breakwaters. *Coastal Engineering*, 57(10):879–891.

Atkinson, A. L., Power, H. E., Moura, T., Hammond, T., Callaghan, D. P., and Baldock, T. E. (2017). Assessment of runup predictions by empirical models on non-truncated beaches on the south-east Australian coast. *Coastal Engineering*, 119:15–31.

Austin, M., Scott, T., Brown, J., Brown, J., MacMahan, J., Masselink, G., and Russell, P. (2010). Temporal observations of rip current circulation on a macro-tidal beach. *Continental Shelf Research*, 30(9):1149–1165.

Bagnold, R. (1940). Beach formation by waves: Some model experiments in a wave tank.(includes photographs). *Journal of the Institution of Civil Engineers*, 15(1):27–52.

Bakhtyar, R., Yeganeh Bakhtiary, A., and Ghaheri, A. (2008). Application of neuro-fuzzy approach in prediction of runup in swash zone. *Applied Ocean Research*, 30(1):17–27.

Barber, N. F. and Ursell, F. (1948). The generation and propagation of ocean waves and swell. i. wave periods and velocities. *Phil. Trans. R. Soc. Lond. A*, 240(824):527–560.

Barbier, E. B., Koch, E. W., Silliman, B. R., Hacker, S. D., Wolanski, E., Primavera, J., Granek, E. F., Polasky, S., Aswani, S., Cramer, L. A., et al. (2008). Coastal ecosystem-based management with nonlinear ecological functions and values. *Science*, 319(5861):321–323.

Battjes, J. A. (1975). Surf similarity. In *Proceedings of the 14th International Conference on Coastal Engineering, American Society of Civil Engineers, New York, 1974, 466-480*.

Bodge, K. R. and Dean, R. G. (1987). Short-term impoundment of longshore sediment transport. Technical report, Florida Univ Gainesville Dept of Coastal and Oceanographic Engineering.

Bonakdar, L. and Etemad-Shahidi, A. (2011). Predicting wave run-up on rubble-mound structures using m5 model tree. *Ocean Engineering*, 38(1):111–118.

Borsje, B. W., van Wesenbeeck, B. K., Dekker, F., Paalvast, P., Bouma, T. J., van Katwijk, M. M., and de Vries, M. B. (2011). How ecological engineering can serve in coastal protection. *Ecological Engineering*, 37(2):113–122.

Bosom, E. and Jiménez, J. (2011). Probabilistic coastal vulnerability assessment to storms at regional scale-application to Catalan beaches (NW Mediterranean). *Natural Hazards and Earth System Sciences*, 11(2):475–484.

Boudouresque, C. and Jeudy de Grissac, A. (1983). L'herbier à posidonia oceanica en méditerranée: les interactions entre la plante et le sédiment. *Journal de Recherche Océanographique*, 8(2-3):99–122.

Boudouresque, C.-F., Bernard, G., Bonhomme, P., Charbonnel, E., Diviacco, G., Meinesz, A., Pergent, G., Pergent-Martini, C., Ruitton, S., and Tunesi, L. (2012). Protection and conservation of Posidonia oceanica meadows. RAMOGE and RAC/SPA.

Boudouresque, C. F., Pergent, G., Pergent-Martini, C., Ruitton, S., Thibaut, T., and Verlaque, M. (2015). The necromass of the posidonia oceanica seagrass meadow: fate, role, ecosystem services and vulnerability. *Hydrobiologia*, 781(1):25–42.

Bowen, A. J. and Guza, R. T. (1978). Edge waves and surf beat. *Journal of Geophysical Research: Oceans*, 83(C4):1913–1920.

Brambilla, W. (2014). *Caratterizzazione morfodinamica della spiaggia del Poetto.* PhD thesis, Università degli Studi di Cagliari.

Brambilla, W., van Rooijen, A., Simeone, S., Ibba, A., and DeMuro, S. (2016). Field observations, video monitoring and numerical modeling at poetto beach, Italy. *Journal of Coastal Research*, 75(sp1):825–829.

Buia, M. and Mazzella, L. (1991). Reproductive phenology of the mediterranean seagrasses posidonia oceanica (l.) delile, cymodocea nodosa (ucria) aschers., and zostera noltii hornem. *Aquatic Botany*, 40(4):343–362.

Camus, P., Mendez, F. J., Medina, R., and Cofiño, A. S. (2011). Analysis of clustering and selection algorithms for the study of multivariate wave climate. *Coastal Engineering*, 58(6):453–462.

Carlson, L. H. and Godfrey, P. J. (1989). Human impact management in a coastal recreation and natural area. *Biological Conservation*, 49(2):141–156.

Carrier, G. and Greenspan, H. (1958). Water waves of finite amplitude on a sloping beach. *Journal of Fluid Mechanics*, 4(1):97–109.

Chardón-Maldonado, P., Pintado-Patiño, J. C., and Puleo, J. A. (2016). Advances in swash-zone research: Small-scale hydrodynamic and sediment transport processes. *Coastal Engineering*, 115:8–25.

Church, J., Clark, P., Cazenave, A., Gregory, J., Jevrejeva, S., Levermann, A., Merrifield, M., Milne, G., Nerem, R., Nunn, P., Payne, A., Pfeffer, W., Stammer, D., and Unnikrishnan, A. (2014). Sea Level Change. In: Climate Change 2013: The Physical Science Basis. Contribution of Working Group I to the Fifth Assessment Report of the Intergovernmental Panel on Climate Change [Stocker, T.F., D. Qin, G.-K. Plattner, M. Tignor, S.K. Allen, J. Boschung, A. Nauels, Y. Xia, V. Bex and P.M. Midgley (eds.)]. Cambridge University Press, Cambridge, United Kingdom and New York, NY, USA.

Coco, G., Huntley, D., and O'Hare, T. (2000). Investigation of a self-organization model for beach cusp formation and development. *Journal of Geophysical Research: Oceans*, 105(C9):21991–22002.

Coco, G., Huntley, D., and O'Hare, T. (2001). Regularity and randomness in the formation of beach cusps. *Marine Geology*, 178(1-4):1–9.

Coco, G. and Murray, A. B. (2007). Patterns in the sand: From forcing templates to self-organization. *Geomorphology*, 91(3-4):271–290.

Coco, G., O'Hare, T. J., and Huntley, D. A. (1999). Beach cusps: a comparison of data and theories for their formation. *Journal of Coastal Research*, 15(3):741–749.

Cohn, N. and Ruggiero, P. (2016). The influence of seasonal to interannual nearshore profile variability on extreme water levels: Modeling wave runup on dissipative beaches. *Coastal Engineering*, 115(2):79–92.

Cowell, P. and Thom, B. (1994). *Morphodynamics of coastal evolution*. Cambridge University Press, Cambridge, United Kingdom and New York, NY, USA.

Cowell, P. J., Hanslow, D. J., and Meleo, J. F. (1999). *Handbook of Beach and Shoreface Morphodynamics*, chapter The shoreface. John Wiley and Sons, New York, NY, USA.

Cox, N., Dunkin, L. M., and Irish, J. L. (2013). An empirical model for infragravity swash on barred beaches. *Coastal Engineering*, 81:44–50.

Da Silva, C. P. (2002). Beach carrying capacity assessment: how important is it. *Journal of Coastal Research*, 36:190–197.

Davies, J. L. (1977). *Geographical variation in coastal development*, volume 4. Longman Publishing Group.

Davis Jr, R. A. and Hayes, M. O. (1984). What is a wave-dominated coast? 39:313–329.

De Falco, G., Molinaroli, E., Baroli, M., and Bellaciccob, S. (2003). Grain size and compositional trends of sediments from Posidonia oceanica meadows to beach shore, Sardinia, western Mediterranean. *Estuarine, Coastal and Shelf Science*, 58(2):299–309.

De Falco, G., Simeone, S., and Baroli, M. (2008). Management of beach-cast Posidonia oceanica seagrass on the island of Sardinia (Italy, Western Mediterranean). *Journal of Coastal Research*, 24(sp3):69–75.

De Muro, S., Ibba, A., Simeone, S., Buosi, C., and Brambilla, W. (2017a). An integrated sea-land approach for mapping geomorphological and sedimentological features in an urban microtidal wave-dominated beach: a case study from S Sardinia, western Mediterranean. *Journal of Maps*, 13(2):822–835.

De Muro, S., Porta, M., Passarella, M., and Ibba, A. (2016). Geomorphology of four wave-dominated microtidal Mediterranean beach systems with Posidonia oceanica meadow: A case study of the Northern Sardinia coast. *Journal of Maps*, 13(2):74–85.

De Muro, S., Porta, M., Pusceddu, N., Frongia, P., Passarella, M., Ruju, A., Buosi, C., and Ibba, A. (2018). Geomorphological processes of a mediterranean urbanized beach (sardinia, gulf of cagliari). *Journal of Maps*, 14(2):114–122.

De Muro, S., Pusceddu, N., Buosi, C., and Ibba, A. (2017b). Morphodynamics of a Mediterranean microtidal wave-dominated beach: forms, processes and insights for coastal management. *Journal of Maps*, 13(2):26–36.

Demuro, S. and De Falco, G. (2010). *Manuale per la gestione delle spiagge. Studi, indagini ed esperienze sulle spiagge sarde e corse*, volume 1. Univeristy Press, CUEC Editrice, Cagliari, Italy.

Demuro, S. and De Falco, G. (2015). *Manuale di buone pratiche per lo studio, il monitoraggio e la gestione delle spiagge della Sardegna. Handbook of best practices for the study monitoring and management of Sardinian beaches*. Univeristy Press, CUEC Editrice, Cagliari, Italy.

Dickson, M. E. and Perry, G. L. (2016). Identifying the controls on coastal cliff landslides using machine-learning approaches. *Environmental Modelling and Software*, 76:117–127.

Dietterich, T. (1995). Overfitting and undercomputing in machine learning. *ACM Computing Surveys*, 27(3):326–327.

Domingos, P. (2012). A few useful things to know about machine learning. *Communications of the ACM*, 55(10):78–87.

Duarte, C. M. (1991). Seagrass depth limits. *Aquatic botany*, 40(4):363–377.

Duarte, C. M. (2004). How can beaches be managed with respect to seagrass litter. In *European seagrasses: an introduction to monitoring and management*. The MandMS project.

Duarte, C. M., Middelburg, J. J., and Caraco, N. (2004). Major role of marine vegetation on the oceanic carbon cycle. *Biogeosciences Discussions*, 1(1):659–679.

Eastwood, D. and Carter, R. (1981). The irish dune consumer. *Journal of Leisure Research*, 13(4):273–281.

EC (1992). Council Directive 92/43/EC on the conservation of natural habitats and of wild fauna and flora. Official Journal of the European Communities, L 206, 22/07/1992.

Elfrink, B. and Baldock, T. (2002). Hydrodynamics and sediment transport in the swash zone: a review and perspectives. *Coastal Engineering*, 45(3-4):149–167.

EPC (2000). EU Water Framework Directive. Directive 2000/60/EC of the European Parliament and of the Council. Official Journal (OJ L 327) on 22/12/2000.

EPC (2008). Marine Strategy Framework Directive. Directive 2008/56/EC of the European Parliament and of the Council. Official Journal of the European Communities, N L 164/19, on 17/06/2008.

EU (2007). An Integrated Maritime Policy for the European Union, COM 574.

EU (2012). Blue Growth: Opportunities for Marine and Maritime Sustainable Growth, COM 494.

EU (2014). Directive 2014/89/EU, Establishing a Framework for Maritime Spatial Planning. European Union, Commission of the European Communities, Official Journal of the European Union, L 257.

Farris, A. S. and List, J. H. (2007). Shoreline change as a proxy for subaerial beach volume change. *Journal of Coastal Research*, 23(3):740–748.

Fonseca, M. S. and Cahalan, J. A. (1992). A preliminary evaluation of wave attenuation by four species of seagrass. *Estuarine, Coastal and Shelf Science*, 35(6):565–576.

Galelli, S., Humphrey, G. B., Maier, H. R., Castelletti, A., Dandy, G. C., and Gibbs, M. S. (2014). An evaluation framework for input variable selection algorithms for environmental data-driven models. *Environmental Modelling and Software*, 62:33–51.

Gallagher, B. (1971). Generation of surf beat by non-linear wave interactions. *Journal of Fluid Mechanics*, 49(1):1–20.

Galvin, C. (1972). Wave breaking in shallow water. In *Waves on beaches and resulting sediment transport*. Academic Press.

Goldstein, E. B. and Coco, G. (2014). A machine learning approach for the prediction of settling velocity. *Water Resources Research*, 50(4):3595–3601.

Goldstein, E. B., Coco, G., and Murray, A. B. (2013). Prediction of wave ripple characteristics using genetic programming. *Continental Shelf Research*, 71:1–15.

Gómez-Pujol, L., Orfila, A., Álvarez-Ellacuría, A., Terrados, J., and Tintoré, J. (2013). Posidonia oceanica beach-cast litter in mediterranean beaches: a coastal videomonitoring study. *Journal of Coastal Research*, 65(sp2):1768–1773.

Gourlay, M. R. (1968). Beach and dune erosion tests. Delft Hydraulics Laboratories. Report No M0935/0936.

Green, E. P. (2003). *World atlas of seagrasses*. Univ of California Press.

Guannel, G., Ruggiero, P., Faries, J., Arkema, K., Pinsky, M., Gelfenbaum, G., Guerry, A., and Kim, C.-K. (2015). Integrated modeling framework to quantify the coastal protection services supplied by vegetation. *Journal of Geophysical Research: Oceans*, 120(1):324–345.

Guedes, R., Bryan, K. R., and Coco, G. (2013). Observations of wave energy fluxes and swash motions on a low-sloping, dissipative beach. *Journal of Geophysical Research: Oceans*, 118(7):3651–3669.

Guedes, R. M., Bryan, K. R., and Coco, G. (2012). Observations of alongshore variability of swash motions on an intermediate beach. *Continental Shelf Research*, 48:61–74.

Guedes, R. M. C., Bryan, K. R., Coco, G., and Holman, R. (2011). The effects of tides on swash statistics on an intermediate beach. *Journal of Geophysical Research: Oceans*, 116(C4).

Guza, R. and Feddersen, F. (2012). Effect of wave frequency and directional spread on shoreline runup. *Geophysical Research Letters*, 39(11).

Guza, R. and Thornton, E. B. (1982). Swash oscillations on a natural beach. *Journal of Geophysical Research: Oceans*, 87(C1):483–491.

Guza, R. and Thornton, E. B. (1985). Observations of surf beat. *Journal of Geophysical Research: Oceans*, 90(C2):3161–3172.

Guza, R. T. and Bowen, A. J. (1976). Resonant interactions for waves breaking. on a beach. *Coastal Engineering Proceedings*, 1(15).

Guza, R. T. and Inman, D. L. (1975). Edge waves and beach cusps. *Journal of Geophysical Research*, 80(21):2997–3012.

Halpern, B. S., Walbridge, S., Selkoe, K. A., Kappel, C. V., Micheli, F., D'agrosa, C., Bruno, J. F., Casey, K. S., Ebert, C., Fox, H. E., et al. (2008). A global map of human impact on marine ecosystems. *Science*, 319(5865):948–952.

Hardisty, J. (1986). A morphodynamic model for beach gradients. *Earth Surface Processes and Landforms*, 11(3):327–333.

Hayes, M. O. and Boothroyd, J. C. (1969). Storms as modifying agents in the coastal environment. *SEPM Eastern Section Field Trip Guidebook*, 12:245–265.

Hemminga, M. A. and Duarte, C. M. (2000). *Seagrass ecology*. Cambridge University Press.

Hoegh-Guldberg, O., Cai, R., Poloczanska, E., Brewer, P., Sundby, S., Hilmi, K., Fabry, V., , and Jung, S. (2014). The Ocean. In: Climate Change 2014: Impacts, Adaptation, and Vulnerability. Part B: Regional Aspects. Contribution of Working Group II to the Fifth Assessment Report of the Intergovernmental Panel on Climate Change [Barros, V.R., C.B. Field, D.J. Dokken, M.D. Mastrandrea, K.J. Mach, T.E. Bilir, M. Chatterjee, K.L. Ebi, Y.O. Estrada, R.C. Genova, B. Girma, E.S. Kissel, A.N. Levy, S. MacCracken, P.R. Mastrandrea, and L.L. White (eds.)]. Cambridge University Press, Cambridge, United Kingdom and New York, NY, USA.

Holland, K., Raubenheimer, B., Guza, R., and Holman, R. A. (1995). Runup kinematics on a natural beach. *Journal of Geophysical Research: Oceans*, 100(C3):4985–4993.

Holland, K. T. (1995). *Foreshore Dynamics: Swash Motions and Topographic Interactions on Natural.* PhD thesis, Oreg. State Univ., Corvallis.

Holland, K. T., Holman, R. A., Lippmann, T. C., Stanley, J., and Plant, N. (1997). Practical use of video imagery in nearshore oceanographic field studies. *IEEE Journal of oceanic engineering*, 22(1):81–92.

Holman, R., Huntley, D., and Bowen, A. (1978). Infragravity waves in storm conditions. *Coastal Engineering*. 268–284.

Holman, R. and Sallenger, A. (1985). Setup and swash on a natural beach. *Journal of Geophysical Research: Oceans*, 90(C1):945–953.

Holman, R. A. (1986). Extreme value statistics for wave run-up on a natural beach. *Coastal Engineering*, 9:527–544.

Holman, R. A. and Guza, R. (1984). Measuring run-up on a natural beach. *Coastal Engineering*, 8(2):129–140.

Hughes, M. G., Aagaard, T., Baldock, T. E., and Power, H. E. (2014). Spectral signatures for swash on reflective, intermediate and dissipative beaches. *Marine Geology*, 355:88–97.

Hughes, M. G. and Baldock, T. E. (2004). Eulerian flow velocities in the swash zone: field data and model predictions. *Journal of Geophysical Research: Oceans*, 109(C08009):1–11.

Hunt, I. A. (1959). Design of sea-walls and breakwaters. *Transactions of the American Society of Civil Engineers*, 126(4):542–570.

Huntley, D. (2013). Waves. In *Treatise on Geomorphology*. Academic Press.

Infantes, E., Orfila, A., Simarro, G., Terrados, J., Luhar, M., and Nepf, H. (2012). Effect of a seagrass (posidonia oceanica) meadow on wave propagation. *Marine Ecology Progress Series*, 456:63–72.

Infantes, E., Terrados, J., Orfila, A., Cañellas, B., and Álvarez-Ellacuria, A. (2009). Wave energy and the upper depth limit distribution of posidonia oceanica. *Botanica Marina*, 52(5):419–427.

IPCC (2014). Climate Change 2014: Synthesis Report. Contribution of Working Groups I, II and III to the Fifth Assessment Report of the Intergovernmental Panel on Climate Change [Core Writing Team, R.K. Pachauri and L.A. Meyer (eds.)]. IPCC, Geneva, Switzerland.

Iribarren, C. and Nogales, C. (1949). Protection des ports, paper presented at xviith international navigation congress, permanent int. *Assoc. of Navig. Congr., Lisbon, Portugal*.

Jean-Yves Bouguet (2018). Camera Calibration Toolbox for Matlab. Last access: June 2018. `http://www.vision.caltech.edu/bouguetj/calib_doc/`.

Jeudy de Grissac, A. (1984). Effets des herbiers à Posidonia oceanica sur la dynamique marine et la sédimentologie littorale. In *International Workshop Posidonia oceanica Beds*, volume 1, pages 437–443. GIS Posidonie publ.

Jeudy de Grissac, A. and Audoly, G. (1985). Etude préliminaire des banquettes de feuilles mortes de posidonia oceanica de la region de marseille (france). *Rapp. Comm. Int. Mer. Medit*, 29(5).

John, B. M., Shirlal, K. G., Rao, S., and Rajasekaran, C. (2016). Effect of artificial seagrass on wave attenuation and wave run-up. *The International Journal of Ocean and Climate Systems*, 7(1):14–19.

John, B. M., Vignesh, R. A., Shirlal, K. G., and Rao, S. (2018). Experimental study on role of emergent artificial coastal vegetation in controlling wave run up. In *Hydrologic Modeling*, pages 535–542. Springer.

Kamphuis, J. W. (1991). Alongshore sediment transport rate. *Journal of Waterway, Port, Coastal, and Ocean Engineering*, 117(6):624–640.

Karambas, T. V. and Koutitas, C. (2002). Surf and swash zone morphology evolution induced by nonlinear waves. *Journal of Waterway, Port, Coastal, and Ocean Engineering*, 128(3):102–113.

Kazeminezhad, M. H. and Etemad-Shahidi, A. (2015). A new method for the prediction of wave runup on vertical piles. *Coastal Engineering*, 98:55–64.

Knaapen, M. and Hulscher, S. J. (2002). Regeneration of sand waves after dredging. *Coastal Engineering*, 46(4):277–289.

Komar, P. D. (1998). *Beach processes and sedimentation*. Prentice-Hall.

Komar, P. D. (2018). *Handbook of Coastal Processes and Erosion*. CRC Press.

Koza, J. R. (1994). Genetic programming as a means for programming computers by natural selection. *Statistics and Computing*, 4(2):87–112.

Larson, M. and Kraus, N. C. (1994). Temporal and spatial scales of beach profile change, duck, north carolina. *Marine Geology*, 117(1-4):75–94.

Loder, N., Irish, J. L., Cialone, M., and Wamsley, T. (2009). Sensitivity of hurricane surge to morphological parameters of coastal wetlands. *Estuarine, Coastal and Shelf Science*, 84(4):625–636.

Longuet-Higgins, M. S. and Stewart, R. (1962). Radiation stress and mass transport in gravity waves, with application to surf beats. *Journal of Fluid Mechanics*, 13(4):481–504.

Longuet-Higgins, M. S. and Stewart, R. (1964). Radiation stresses in water waves; a physical discussion, with applications. In *Deep Sea Research and Oceanographic Abstracts*, volume 11, pages 529–562. Elsevier.

Lotze, H. K., Lenihan, H. S., Bourque, B. J., Bradbury, R. H., Cooke, R. G., Kay, M. C., Kidwell, S. M., Kirby, M. X., Peterson, C. H., and Jackson, J. B. (2006). Depletion, degradation, and recovery potential of estuaries and coastal seas. *Science*, 312(5781):1806–1809.

Luhar, M., Coutu, S., Infantes, E., Fox, S., and Nepf, H. (2010). Wave-induced velocities inside a model seagrass bed. *Journal of Geophysical Research: Oceans*, 115(C12).

Luhar, M., Infantes, E., Orfila, A., Terrados, J., and Nepf, H. M. (2013). Field observations of wave-induced streaming through a submerged seagrass (posidonia oceanica) meadow. *Journal of Geophysical Research: Oceans*, 118(4):1955–1968.

Masselink, G. and Hughes, M. (1998). Field investigation of sediment transport in the swash zone. *Continental Shelf Research*, 18(10):1179–1199.

Masselink, G., Hughes, M., and Knight, J. (2012a). *Introduction to Coastal Processes and Geomorphology, Second Edition*. London: Routledge.

Masselink, G., Hughes, M., and Knight, J. (2012b). *Introduction to Coastal Processes and Geomorphology, Second Edition*, chapter Future Coasts. London: Routledge.

Masselink, G., Hughes, M., and Knight, J. (2012c). *Introduction to Coastal Processes and Geomorphology, Second Edition*, chapter Coasts and Climate. London: Routledge.

Masselink, G. and Puleo, J. A. (2006). Swash-zone morphodynamics. *Continental Shelf Research*, 26(5):661–680.

Masselink, G. and Short, A. D. (1993). The effect of tide range on beach morphodynamics and morphology: a conceptual beach model. *Journal of Coastal Research*, 9(3):785–800.

Mateo, M.-Á., Sanchez-Lizaso, J.-L., and Romero, J. (2003). Posidonia oceanica banquettes: a preliminary assessment of the relevance for meadow carbon and nutrients budget. *Estuarine, Coastal and Shelf Science*, 56(1):85–90.

Maza, M., Lara, J., Losada, I., Ondiviela, B., Trinogga, J., and Bouma, T. (2015). Large-scale 3-d experiments of wave and current interaction with real vegetation. part 2: experimental analysis. *Coastal Engineering*, 106:73–86.

McCowan, J. (1894). XXXIX. On the Highest Wave of Permanent Type. *The London, Edinburgh, and Dublin Philosophical Magazine and Journal of Science*, 38(233):351–358.

Michael, H. and Ian, T. (1999). *Handbook of Beach and Shoreface Morphodynamics*, chapter The beach face. John Wiley and Sons, New York, NY, USA.

Miche, M. (1951). Le pouvoir réfléchissant des ouvrages maritimes exposés à l'action de la houle. *Annales de Ponts et Chaussées*, 121:285–319.

Möller, I., Kudella, M., Rupprecht, F., Spencer, T., Paul, M., Van Wesenbeeck, B. K., Wolters, G., Jensen, K., Bouma, T. J., Miranda-Lange, M., et al. (2014). Wave attenuation over coastal salt marshes under storm surge conditions. *Nature Geoscience*, 7(10):727731.

Munk, W. (1949). Surf beats. *EOS, Transactions American Geophysical Union*, 30(6):849–854.

Munk, W. H. and Traylor, M. A. (1947). Refraction of ocean waves: a process linking underwater topography to beach erosion. *The Journal of Geology*, 55(1):1–26.

Nelson, R. and Gonsalves, J. (1992). Surf zone transformation of wave height to water depth ratios. *Coastal Engineering*, 17(1-2):49–70.

Nicolae Lerma, A., Pedreros, R., and Senechal, N. (2016). Wave set-up and run-up variability on a complex barred beach during highly dissipative storm conditions. *Journal of Coastal Research*, 75(sp1):882–886.

Niedoroda, A. and Swift, D. (1991). Shoreface processes. *Handbook of coastal and ocean engineering*, 2:736–769.

Nordstrom, K. F. (1980). Cyclic and seasonal beach response: a comparison of ocean-side and bayside beaches. *Physical Geography*, 1(2):177–196.

Nordstrom, K. F. (2013). Developed Coasts. In *Treatise on geomorphology*. Academic Press.

Nordstrom, K. F. and Jackson, N. L. (2012). Physical processes and landforms on beaches in short fetch environments in estuaries, small lakes and reservoirs: A review. *Earth-Science Reviews*, 111(1-2):232–247.

Nurse, L., McLean, R., Agard, J., Briguglio, L., Duvat-Magnan, V., Pelesikoti, N., Tompkins, E., and Webb, A. (2014). Small islands. In: Climate Change 2014: Impacts, Adaptation, and Vulnerability. Part B: Regional Aspects. Contribution of Working Group II to the Fifth Assessment Report of the Intergovernmental Panel on Climate Change [Barros, V.R., C.B. Field, D.J. Dokken, M.D. Mastrandrea, K.J. Mach, T.E. Bilir, M. Chatterjee, K.L. Ebi, Y.O. Estrada, R.C. Genova, B. Girma, E.S. Kissel, A.N. Levy, S. MacCracken, P.R. Mastrandrea, and L.L. White (eds.)]. Cambridge University Press, Cambridge, United Kingdom and New York, NY, USA.

Olden, J., Lawler, J., and Poff, N. (2008). Machine Learning Methods Without Tears: A Primer for Ecologists. *The Quarterly Review of Biology*.

Oldham, C., McMahon, K., Brown, E., Bosserelle, C., and Lavery, P. (2014). A preliminary exploration of the physical properties of seagrass wrack that affect its offshore transport, deposition, and retention on a beach. *Limnology and Oceanography: Fluids and Environments*, 4(1):120–135.

Ondiviela, B., Losada, I. J., Lara, J. L., Maza, M., Galván, C., Bouma, T. J., and van Belzen, J. (2014). The role of seagrasses in coastal protection in a changing climate. *Coastal Engineering*, 87:158–168.

Osborne, P. D. and Rooker, G. A. (1997). Surf zone and swash zone sediment dynamics on high energy beaches: West auckland, new zealand. In *Coastal Dynamics' 97*, pages 814–823. ASCE.

ONeill, M., Vanneschi, L., Gustafson, S., and Banzhaf, W. (2010). Open issues in genetic programming. *Genetic Programming and Evolvable Machines*, 11(3-4):339–363.

Pape, L., Ruessink, B. G., Wiering, M. A., and Turner, I. L. (2007). Recurrent neural network modeling of nearshore sandbar behavior. *Neural Networks*, 20(4):509–518.

Passarella, M., De Muro, S., Ruju, A., and Coco, G. (2018a). An Assessment of Swash Excursion Predictors using Field Observations. In Proceedings of the 15th International Coastal Symposium (ICS2018). *Journal of Coastal Research*, Special Issue 85:1036–1040.

Passarella, M., Goldstein, E., De Muro, S., and Coco, G. (2018b). The use of genetic programming to develop a predictor of swash excursion on sandy beaches. *Natural Hazards and Earth System Sciences*, 18(2).

Perini, L., Calabrese, L., Salerno, G., Ciavola, P., and Armaroli, C. (2016). Evaluation of coastal vulnerability to flooding: comparison of two different methodologies adopted by the Emilia-Romagna region (Italy). *Natural Hazards and Earth System Sciences*, 16(1):181.

Poate, T. G., McCall, R. T., and Masselink, G. (2016). A new parameterisation for runup on gravel beaches. *Coastal Engineering*, 117:176–190.

Puleo, J., Beach, R., Holman, R. A., and Allen, J. (2000). Swash zone sediment suspension and transport and the importance of bore-generated turbulence. *Journal of Geophysical Research: Oceans*, 105(C7):17021–17044.

Puleo, J. A. and Torres-Freyermuth, A. (2016). The second international workshop on swash-zone processes. *Coastal Engineering*, 115:1–7.

Raubenheimer, B. and Guza, R. (1996). Observations and predictions of run-up. *Journal of Geophysical Research: Oceans*, 101(C10):25575–25587.

Reid, P. C., Fischer, A. C., Lewis-Brown, E., Meredith, M. P., Sparrow, M., Andersson, A. J., Antia, A., Bates, N. R., Bathmann, U., Beaugrand, G., Brix, H., Dye, S., Edwards, M., Furevik, T., Gangstø, R., Hátún, H., Hopcroft, R. R., Kendall, M., Kasten, S., Keeling, R., Le Quéré, C., Mackenzie, F. T., Malin, G., Mauritzen, C., Ólafsson, J., Paull, C., Rignot, E., Shimada, K., Vogt, M., Wallace, C., Wang, Z., and Washington, R. (2009). Chapter 1 Impacts of the Oceans on Climate Change. *Advances in Marine Biology*, 56:1–150.

Rhein, M., Rintoul, S., Aoki, S., Campos, E., Chambers, D., Feely, R., Gulev, S., Johnson, G., Josey, S., Kostianoy, A., Mauritzen, C., Roemmich, D., Talley, L., and

Wang, F. (2013). Observations: Ocean. In: Climate Change 2013: The Physical Science Basis. Contribution of Working Group I to the Fifth Assessment Report of the Intergovernmental Panel on Climate Change [Stocker, T.F., D. Qin, G.-K. Plattner, M. Tignor, S.K. Allen, J. Boschung, A. Nauels, Y. Xia, V. Bex and P.M. Midgley (eds.)]. Cambridge University Press, Cambridge, United Kingdom and New York, NY, USA.

Roelvink, D. (2011). A guide to modeling coastal morphology. In *Advances in Coastal and Ocean Engineering*, volume 12. World Scientific Publishing Co. Pte. Ltd. Singapore.

Ruessink, B. G., Kleinhans, M. G., and Van Den Beukel, P. G. L. (1998). Observations of swash under highly dissipative conditions. *Journal of Geophysical Research*, 103(C2):3111–3118.

Ruggiero, P., Holman, R. A., and Beach, R. (2004). Wave run-up on a high-energy dissipative beach. *Journal of Geophysical Research: Oceans*, 109(C06025):1–12.

Ruggiero, P., Komar, P. D., Mcdougal, W. G., Marra, J. J., and Beach, R. A. (2001). Wave runup, extreme water levels and the erosion of properties backing beaches. *Journal of Coastal Research*, 17(2):407–419.

Ruju, A., Ibba, A., Porta, M., Buosi, C., Passarella, M., and De Muro, S. (2018). The role of hydrodynamic forcing, sediment transport processes and bottom substratum in the shoreward development of posidonia oceanica meadow. *Estuarine, Coastal and Shelf Science*, 212:63–72.

Russell, P. E. (1993). Mechanisms for beach erosion during storms. *Continental Shelf Research*, 13(11):1243–1265.

Schmidt, M. and Lipson, H. (2009). Distilling free-form natural laws from experimental data. *Science*, 324(5923):81–85.

Schmidt, M. and Lipson, H. (2018). Eureqa (Version 1.24.0 (build 9367) [Software]: Last access: May 2018. `https://www.nutonian.com/products/eureqa/`.

Senechal, N., Coco, G., Bryan, K. R., and Holman, R. A. (2011). Wave runup during extreme storm conditions. *Journal of Geophysical Research: Oceans*, 116(C7):1–13.

Serafin, K. A. and Ruggiero, P. (2014). Simulating extreme total water levels using a time-dependent, extreme value approach. *Journal of Geophysical Research: Oceans*, 119(9):6305–6329.

Serafin, K. A., Ruggiero, P., and Stockdon, H. F. (2017). The relative contribution of waves, tides, and nontidal residuals to extreme total water levels on us west coast sandy beaches. *Geophysical Research Letters*, 44(4):1839–1847.

Short, A. (1985). Rip-current type, spacing and persistence, narrabeen beach, australia. *Marine geology*, 65(1-2):47–71.

Short, A. (2012). Coastal processes and beaches. *Nature Education Knowledge*, 3(10):15.

Short, A. D. (1999a). *Handbook of beach and shoreface morphodynamics*. John Wiley and Sons, New York, NY, USA.

Short, A. D. (1999b). *Handbook of beach and shoreface morphodynamics*, chapter Wave-Dominated Beaches. John Wiley and Sons, New York, NY, USA.

Short, A. D. (2006). Australian Beach SystemsNature and Distribution. *Journal of Coastal Research*, 22(1):11–27.

Short, A. D. and Jackson, D. W. (2013). Beach Morphodynamics. In *Treatise on Geomorphology*. Academic Press.

Short, A. D. and Woodroffe, C. D. (2009). *The coast of Australia*. Cambridge University Press.

Short, F., Carruthers, T., Dennison, W., and Waycott, M. (2007). Global seagrass distribution and diversity: a bioregional model. *Journal of Experimental Marine Biology and Ecology*, 350(1-2):3–20.

Silva, C. d., Alves, F., and Rocha, R. (2007). The management of beach carrying capacity: The case of northern Portugal. *Journal of Coastal Research*, 50:135–139.

Simeone, S. (2008). *Posidonia oceanica banquettes removal: sedimentological, geomorphological and ecological implications.* PhD thesis, Università degli studi della Tuscia-Viterbo.

Simeone, S. and De Falco, G. (2012). Morphology and composition of beach-cast posidonia oceanica litter on beaches with different exposures. *Geomorphology*, 151:224–233.

Simeone, S. and De Falco, G. (2013). Posidonia oceanica banquette removal: sedimentological, geomorphological and ecological implications. In Proceedings of the 12th International Coastal Symposium (ICS2013). *Journal of Coastal Research*, 65:1045–1050.

Simeone, S., De Muro, S., and De Falco, G. (2013). Seagrass berm deposition on a mediterranean embayed beach. *Estuarine, Coastal and Shelf Science*, 135:171–181.

Smith, E. R., Wang, P., and Zhang, J. (2003). Evaluation of the CERC formula using large-scale model data. Technical report, Engineer Research and Development Center Coastal and Hydraulics Laboratory,Vicksburg, MS.

Stephen, J. (2017). Marine Spatial Planning Assessing net benefits and improving effectiveness. Technical report, The Organisation for Economic Co-operation and Development (OECD).

Sterman, J. D. (2000). *Business dynamics: systems thinking and modeling for a complex world*. McGraw-Hill Education,Jeffrey J. Shelstad.

Stewart, R. H. (2008). *Introduction to physical oceanography*. University Press of Florida.

Stockdon, H. F., Holman, R. A., Howd, P. A., and Sallenger, A. H. (2006). Empirical parameterization of setup, swash, and runup. *Coastal Engineering*, 53(7):573–588.

Stockdon, H. F., Sallenger Jr, A. H., Holman, R. A., and Howd, P. A. (2007). A simple model for the spatially-variable coastal response to hurricanes. *Marine Geology*, 238(1-4):1–20.

Svendsen, I. A. (2006). *Introduction to nearshore hydrodynamics*, volume 24. World Scientific.

Symonds, G., Huntley, D. A., and Bowen, A. J. (1982). Two-dimensional surf beat: Long wave generation by a time-varying breakpoint. *Journal of Geophysical Research: Oceans*, 87(C1):492–498.

Taborda, R. and Silva, A. (2012). Cosmos: A lightweight coastal video monitoring system. *Computers and geosciences*, 49:248–255.

Tecchiato, S., Buosi, C., Ibba, A., Ryan, D. A., and De Muro, S. (2016). A comparison of geomorphic settings, sediment facies and benthic habitats of two carbonate systems of western mediterranean sea and south western australia: Implications for coastal management. *Journal of Coastal Research*, 75(sp1):562–566.

Temmerman, S., Meire, P., Bouma, T. J., Herman, P. M., Ysebaert, T., and De Vriend, H. J. (2013). Ecosystem-based coastal defence in the face of global change. *Nature*, 504:79–83.

Tinoco, R., Goldstein, E., and Coco, G. (2015). A data-driven approach to develop physically sound predictors: Application to depth-averaged velocities on flows through submerged arrays of rigid cylinders. *Water Resources Research*, 51(2):1247–1263.

Tucker, M. (1950). Surf beats: sea waves of 1 to 5 min. period. *Proc. R. Soc. Lond. A*, 202(1071):565–573.

UNESCO (2018). Marine Spatial Planning Around the Globe. Last access: June 2018. `http://msp.ioc-unesco.org/world2018`.

Vacchi, M., De Falco, G., Simeone, S., Montefalcone, M., Morri, C., Ferrari, M., and Bianchi, C. N. (2017). Biogeomorphology of the Mediterranean Posidonia oceanica seagrass meadows. *Earth Surface Processes and Landforms*, 42(1):42–54.

Vacchi, M., Montefalcone, M., Bianchi, C. N., Morri, C., and Ferrari, M. (2010). The influence of coastal dynamics on the upper limit of the posidonia oceanica meadow. *Marine Ecology*, 31(4):546–554.

Van Rooijen, A., McCall, R., Van Thiel de Vries, J., Van Dongeren, A., Reniers, A., and Roelvink, J. (2016). Modeling the effect of wave-vegetation interaction on wave setup. *Journal of Geophysical Research: Oceans*, 121(6):4341–4359.

Vassallo, P., Paoli, C., Rovere, A., Montefalcone, M., Morri, C., and Bianchi, C. N. (2013). The value of the seagrass posidonia oceanica: A natural capital assessment. *Marine pollution bulletin*, 75(1-2):157–167.

Vousdoukas, M., Velegrakis, A., Dimou, K., Zervakis, V., and Conley, D. (2009). Wave run-up observations in microtidal, sediment-starved pocket beaches of the eastern mediterranean. *Journal of Marine Systems*, 78:S37–S47.

Vousdoukas, M. I., Ferreira, P. M., Almeida, L. P., Dodet, G., Psaros, F., Andriolo, U., Taborda, R., Silva, A. N., Ruano, A., and Ferreira, Ó. M. (2011). Performance of intertidal topography video monitoring of a meso-tidal reflective beach in South Portugal. *Ocean Dynamics*, 61(10):1521–1540.

Vousdoukas, M. I., Wziatek, D., and Almeida, L. P. (2012). Coastal vulnerability assessment based on video wave run-up observations at a mesotidal, steep-sloped beach. *Ocean Dynamics*, 62(1):123–137.

Wainwright, J. and Mulligan, M. (2012). *Environmental modelling: finding simplicity in complexity*. John Wiley and Sons.

Waldrop, M. M. (1993). *Complexity: The emerging science at the edge of order and chaos*. Simon and Schuster.

Waycott, M., Duarte, C. M., Carruthers, T. J., Orth, R. J., Dennison, W. C., Olyarnik, S., Calladine, A., Fourqurean, J. W., Heck, K. L., Hughes, A. R., et al. (2009). Accelerating loss of seagrasses across the globe threatens coastal ecosystems. *Proceedings of the National Academy of Sciences*, 106(30):12377–12381.

Werner, B. and Fink, T. (1993). Beach cusps as self-organized patterns. *Science*, 260(5110):968–971.

Wiedemann, A. M. (1984). *The ecology of Pacific Northwest coastal sand dunes: a community profile*. Citeseer.

WMO (1998). *Guide to Wave analysis and forecasting.* World Meteorological Organization Publications.

Wong, P., Losada, I., Gattuso, J.-P., Hinkel, J., Khattabi, A., McInnes, K., Saito, Y., and Sallenger, A. (2014). Coastal systems and low-lying areas. In: Climate Change 2014: Impacts, Adaptation, and Vulnerability. Part A: Global and Sectoral Aspects. Contribution of Working Group II to the Fifth Assessment Report of the Intergovernmental Panel on Climate Change [Field, C.B., V.R. Barros, D.J. Dokken, K.J. Mach, M.D. Mastrandrea, T.E. Bilir, M. Chatterjee, K.L. Ebi, Y.O. Estrada, R.C. Genova, B. Girma, E.S. Kissel, A.N. Levy, S. MacCracken, P.R. Mastrandrea, and L.L. White (eds.)]. Cambridge University Press, Cambridge, United Kingdom and New York, NY, USA.

Woodroffe, C. D. (2002). *Coasts: form, process and evolution*. Cambridge University Press.

Wright, L. and Short, A. D. (1984). Morphodynamic variability of surf zones and beaches: a synthesis. *Marine geology*, 56(1-4):93–118.

Wright, L. and Thom, B. (1977). Coastal depositional landforms: a morphodynamic approach. *Progress in Physical Geography*, 1(3):412–459.

Yates, M. and Cozannet, G. L. (2012). Brief communication "Evaluating European Coastal Evolution using Bayesian Networks". *Natural Hazards and Earth System Sciences*, 12(4):1173–1177.

LIST OF PUBLICATIONS

PEER REVIEWED INTERNATIONAL JOURNALS

1. De Muro, S., Porta, M., Passarella, M., and Ibba, A. (2016). Geomorphology of four wave-dominated microtidal Mediterranean beach systems with Posidonia oceanica meadow: A case study of the Northern Sardinia coast. *Journal of Maps*, 13(2):74–85.

2. De Muro, S., Porta, M., Pusceddu, N., Frongia, P., Passarella, M., Ruju, A., Buosi, C., and Ibba, A. (2018). Geomorphological processes of a Mediterranean urbanized beach (Sardinia, Gulf of Cagliari). *Journal of Maps*, 14(2):114–122.

3. Passarella, M., De Muro, S., Ruju, A., and Coco, G. (2018a). An Assessment of Swash Excursion Predictors using Field Observations. In Proceedings of the 15th International Coastal Symposium (ICS2018). *Journal of Coastal Research*, Special Issue 85:1036–1040.

4. Passarella, M., Goldstein, E., De Muro, S., and Coco, G. (2018b). The use of genetic programming to develop a predictor of swash excursion on sandy beaches. *Natural Hazards and Earth System Sciences*, 18(2):8, 599–611.

PAPERS, POSTERS AND ABSTRACTS, AT INTERNATIONAL CONFERENCES

1. Ruju A., Passarella M., Trogu D., Ibba A., and De Muro S. (2018, May). Assessing the performance of an operational wave system within a Mediterranean beach monitoring programme. Proceedings of the 7th International Conference on the Application of Physical Modelling in Coastal and Port Engineering and Science (Coastlab18).

2. De Muro S., Ruju A., Buosi C., Porta, M., Passarella M., and Ibba A. (2017, April). Interaction between Posidonia oceanica meadows upper limit and hydro-

dynamics of four Mediterranean beaches. EGU General Assembly 2017. Geophysical Research Abstracts, 19.

3. DeMuro S., Frongia P., Pusceddu N., Passarella M., Buosi C., and Ibba A. (2016, August). Effects of anthropic development in an urban beach of south Sardinia (Italy, western Mediterranean) evaluated using hydrodynamic models, run-up and DSAS indices. 35th International Geological Conference, August-September 2016 South Africa.

4. De Muro S., Pusceddu N., Frongia P., Buosi C., Passarella, M., and Ibba A. (2016, April). Human impact, geomorphological and bio-environmental indicators for mapping and monitoring of a Mediterranean urban-beach with Posidonia oceanica (Gulf of Cagliari-Sardinia). EGU General Assembly 2016, abstract in Geophysical Research Abstracts, 18.

5. De Muro S., Buosi C., Pusceddu N., Frongia P., Passarella, M., and Ibba A. (2016, April). Geomorphology and anthropogenic impact including military constraints in a microtidal wave-dominated embayment in south western Sardinia (Porto Pino beach, SCI ITB040025, Mediterranean Sea). Implications for beach management. EGU General Assembly 2016, abstract in Geophysical Research Abstracts, 18.